DEVELOPING INTEGRATED DNA MOLECULAR CIRCUITS

by

ANDREA CAROLINA BARDALES
M.S. University of Central Florida, 2023
B.S. Universidad Nacional Autónoma de Honduras del Valle de Sula, 2014

A dissertation submitted in partial fulfillment of the requirements
for the degree of Doctor of Philosophy
in the Department of Chemistry
in the College of Sciences
at the University of Central Florida
Orlando, Florida

Fall Term
2024

Major Professor: Dmitry M. Kolpashchikov

ABSTRACT

Due to nucleic acid's programmability, it is possible to realize DNA structures with computing functions, and thus a new generation of molecular computers is evolving to solve biological and medical problems. There is evidence that genetic heredity diseases and cancer can be the result of genetic heterogeneity, thus there is a need for diagnostics and therapeutic tools with multiplex and smart components to compute all the molecular drivers. DNA molecular computers mimics electronic computers by programming synthetic nucleic acids to perform similarly to central processing units. Considering how the evolution of integrated circuits made possible the revolution of silicon-based computers, integrated DNA molecular circuits can be developed to allow modular designing and scale to complex DNA nano-processors. This dissertation covers the development of four-way junction (4J) DNA logic gates that can be wired to result in functionally complete gates, and their immobilization on a modular DNA board that serves as a scaffold for logic gate integration, fast signal processing, and cascading. Connecting 4J DNA logic gates YES and NOT resulted in OR, NAND, and IMPLY logic circuits; the three circuits can operate under the input of miRNAs, either oncogenic or/and tumor-suppressors, and give two possible diagnoses: healthy or cancerous. The DNA board can expand as the DNA circuit grows in the number of integrated 4J units. Signal propagation across a wired of 4J YES logic gates showed signal completion in < 3 min, accounting for a signal propagation rate of 4.5 nm/min and that up to 6 units can be cascaded before the signal dissipates. Lastly, an approach to chemically ligate all oligonucleotide components of the DNA molecular device is presented, in which we also found a route for the bioconjugation of 5' to 5' and 3' to 3' oligonucleotides.

Desde un salón de clase en San Francisco de los Valles, Santa Barbara, ante la carencia de recursos institucionales, aquella pequeña estudiante repetía por tercera vez segundo grado buscando con pasión el conocimiento. Sin un título en papel membretado o ceremonia despampanante, ella educo a ingenieros y licenciados. Fue también la enfermera de médicos y consejera de doctores. Esta disertación que completa el título académico más alto que un estudiante puede obtener es dedicado a Vilma Aminta Martinez. Por su esmero y compasión al formar a quien es hoy una candidata a doctorado. Tus enseñanzas han quedado impregnadas en esta, tu ultima pupila.

ACKNOWLEDGMENTS

I am truly grateful to Dr. Dmitry Kolpashchikov whose encouragement and support allow me to pursue a doctorate degree. Throughout this journey, his mentorship nurtured in me the curiosity and creativity of a researcher while challenging me to think as a chemist. There might not be enough words to convey my gratitude for his welcoming me as a mentee at a time when I could barely communicate in this foreign language.

I would also like to thank Dr. Yulia Gerasimova for her invaluable guidance and embrace me as one of her students. To Dr. Jonathan Caranto, I'm grateful for providing access to his research facility and instrumentation, and to Yuri L. Lyubchenko and Alexander Lushnikov for AFM imaging and analysis performed at the Nanoimaging Core Facility, University of Nebraska Medical Center. My deepest appreciation to each of my fellow graduate students, and research colleagues, especially Edwin Barahona, Viktor Smirnov, Brittany Mueller, and Santra's lab members for their support and friendship. I also want to thank each of the undergraduate students whom I have had the fortune to serve as a research mentor and see their growth as researchers, especially Quynh Vo, Ryan Mills, and Katherine Taylor for their extensive collaboration and camaraderie through these years.

I would like to thank and acknowledge the immeasurable contribution of my family here in USA and Honduras whose no frontiers stopped them from being there in times of need and for believing in me and reminding me that those with a strong will, can reach the stars.

I would also like to thank the UCF College of Science, College of Graduate Studies, Chemistry Department, and American Chemical Society whose funds helped my professional development and to the National Science Foundation for providing the funding that made this

research dissertation possible. The research findings reported were supported by the National Science Foundation through the CCF: Software and Hardware Foundations under Cooperative Agreements SHF-1907824 and SHF-2226021.

TABLE OF CONTENTS

LIST OF FIGURES

LIST OF TABLES

LIST OF ABBREVIATIONS

1-CNI	1-cyanoimidazole
4J	Four-way junction
A	Adenosine
bp	Base pair
C	Cytidine
CGP	Contacted gate pitch
DNA	Deoxyribonucleic acid
DNA IC	DNA integrated circuit
dsDNA	double-stranded DNA
DX-tile	Double crossover tile
F	Fluorophore
G	Guanosine
Q	Quencher
MB	Molecular beacon
nt	Nucleotide
RNA	Ribonucleic acid

ssDNA	single-stranded DNA
T	Thymidine
U	Uridine

CHAPTER ONE: INTRODUCTION

1.1 DNA Molecular Computers for Smart Analysis of Biomarkers

Biotechnological tools oriented toward nucleic acid biomarkers have attracted attention of the scientific community, thus leading to increasing efforts in their development.[1–3] On the path toward personalized medicine, multiple nucleic acid sequences must be analyzed for precise diagnosis and proper treatment. Such nucleic acid sequences become inputs in the decision-making of molecular devices that produce a diagnostic and/or therapeutic output. These inputs can undergo complex algorithms (similar to those executed by electronic computers) for their analysis. Although electronic computers are made from semiconductors, other materials can be used to build computers.[4,5] Individual molecules and atoms have been proposed as building units for molecular computers.[5–7] Stojanovic and colleagues reported the first nucleic acid Boolean logic operators[8] and a half adder using RNA-cleaving deoxyribozymes[9] which marked the beginning of an era of DNA computational devices mimicking semiconductor computers.[10–14] Thus, efforts have been made to build molecular computers out of DNA since it is a compatible material for directly

computing nucleic acid biomarkers.[15–21] By using the principles of digital computing, DNA molecular computers are capable of multiplex parallel recognition of biomarkers.[17]

To develop DNA molecular computers, it is necessary to understand the foundation of modern computers. Computers are arrays of logic gates (transistors in electronic computers) connected in a particular order to complete specific logical tasks (Figure 1A). Therefore, a logic gate is the most basic unit within any computer. The different arrangements and connectivity of logic gates allow computers to execute various tasks of arbitrary complexity. In digital computing, these logic gates follow Boolean algebra, a binary system where variables are defined with only two possible values - 0 (False, Low, Off) or 1 (True, High, On). Boolean logic is the most implemented in electronic and molecular computing because of its simplicity and robustness.[22,23]

Boolean logic gates (e.g. YES, NOT, OR, AND, IMPLY, and NAND Figure 1A) can accept and process the digital values of multiple inputs but produce only a single output. Each Boolean logic has a predetermined input(s) yielding a specific output set, defined by truth tables (Figure 1B). For example, the truth table of OR logic dictates output is digital 1 when either or both inputs are digital 1; in NAND's logic, output is digital 0 only when both inputs are digital 1, and for IMPLY's logic the output digital 0 is obtained only in a specific input value combination (Figure 1B). In Boolean algebra, OR, IMPLY and NAND logic are important to construct more complex computational circuits. A circuit is a set of logic gates purposely connected to achieve a desired output (Fig. 1A). For example, in electronic computers, the circuits are realized by connecting each logic gate and integrating them on boards made out of semiconductor materials (Figure 1A); where the circuits direct the flow of electrons based on the programmed Boolean logic. The digital value of a circuit's output is dictated by the combination of values of the multiple inputs (Figure 1B),

enabling output computing based on particular input combinations, a quality needed for personalized medicine.

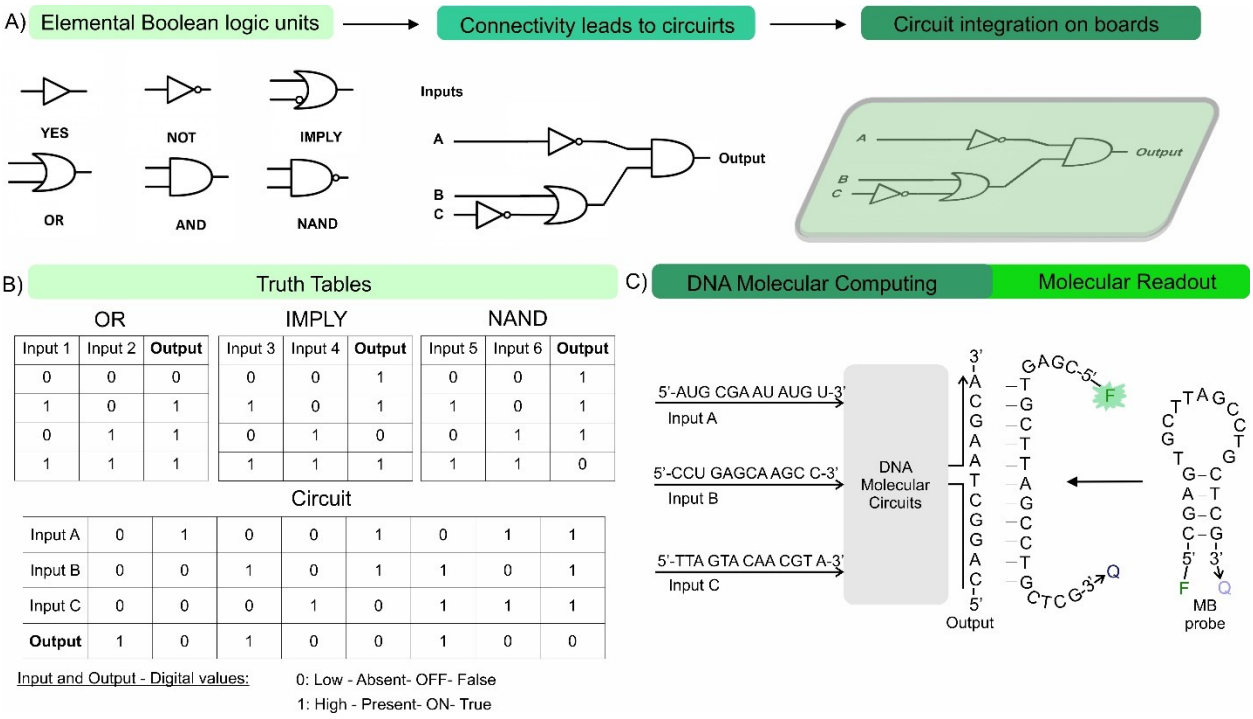

Figure 1. General concepts of computation. A): Evolution pathway followed by electronic computers; starting from representatives of Boolean logic units (symbols indicated), their connectivity leading to circuits, and circuit integration in boards (silicon-based motherboards). B): Truth tables of an OR, IMPLY, and NAND Boolean logic and the circuit made of NOT and OR gates connected to an AND gate, as depicted in panel A. C) DNA molecular computing shows the intake of different nucleic acid sequences (DNA and/or RNA) as inputs to yield a new nucleic acid sequence as output after inputs are processed by DNA molecular circuits. Molecular readout scheme shows a molecular beacon (MB) probe recognizing the output sequence via Watson-Crick interactions and producing a fluorescence readout due to the concomitant conformational change (unfolding of the MB native hairpin-like conformation).

Building DNA logic gates and circuits is possible due to predictability of Watson-Crick base-pairing, where adenosine (A) pairs with thymidine (T), and guanosine (G) pairs with cytidine (C).[24] This predictable base-pairing is used to program Boolean logic functions that operate

through the association and dissociation of DNA fragments.[17] The intrinsic coding feature of nucleic acids and precise base pairing allows for the designing of nucleotide sequences that are capable of completing logic operations[8–14,25,26] and that respond to external inputs according to Boolean functions (AND, OR, NOT, etc.).[27,28] More complex logic gates like Feynman and Fredkin, which involve reversible computation,[29–31] adders,[28] subtractors,[32] multipliers,[33] and square roots[34] performing arithmetic logic operations (ALU), solving puzzles, and encrypting information have been reported. Many of these computational building blocks have been designed to work through interactions with enzymes and other proteins, nanoparticles, and quantum dots.[35] These developments suggest that DNA can be programmed to perform similarly to the central processing units (CPU) of electronic computers and serve as building material of molecular computer hardware, a function different from the natural role of DNA as a storage of genetic information.

Approaches focusing in the development of DNA computer's elementary components and toolbox, computing mechanisms, Boolean operators, arithmetic functions and coupling with non-DNA components have been compiled in reviews and books.[25,35–41] This dissertation focuses on yet another important trend in developing DNA computers—integrating DNA logic units in communicating chains by tethering them to DNA scaffolds (DNA board), named as an all-DNA integrated circuit (DNA IC).

1.2 Advantages of DNA Molecular Circuits.

Even though the industry of electronic computers pitches their semiconductor transistors in nanometer scale, the distance between gates (also contacted gate pitch, CGP) limits

miniaturization as it has reached physical limitations.[41–44] Thus, efforts in further miniaturization inspired exploring new computing materials beyond semiconductor technology including molecules like nucleic acids.

DNA computers might not be at the stage of ultra-fast data processing; however, it circumvents the physical barriers of electronic computers.[38,41] In perspective, a ssDNA gate inherently possesses a gate width of ~1 nm and the lowest CGP currently reported is 5 nm,[45,46] meanwhile the smallest Si-transistor has a 2-fold increase in both gate length and CGP (Figure 2, top). The reduction of CGP is desired because it allows for an increase in gate density. For instance, Intel's 0.1 billion transistors can fit in 1 mm^2,[44] while 40 billion DNA gates could fit in the same area. This is a potential 400 times improvement in transistor density, suggesting the vast room for highly dense DNA nano-circuits. The manufacturing of DNA ICs depends on chemical synthesis and assembly strategies. Although this could be considered expensive and work intensive, the cost per unit should be by far more affordable since billions of DNA computational units can be assembled at once in a small reaction volume.[41] However, the material phase and the interface between DNA ICs and user differs from electronic computers, making both technologies neither competitive nor compatible with each other.

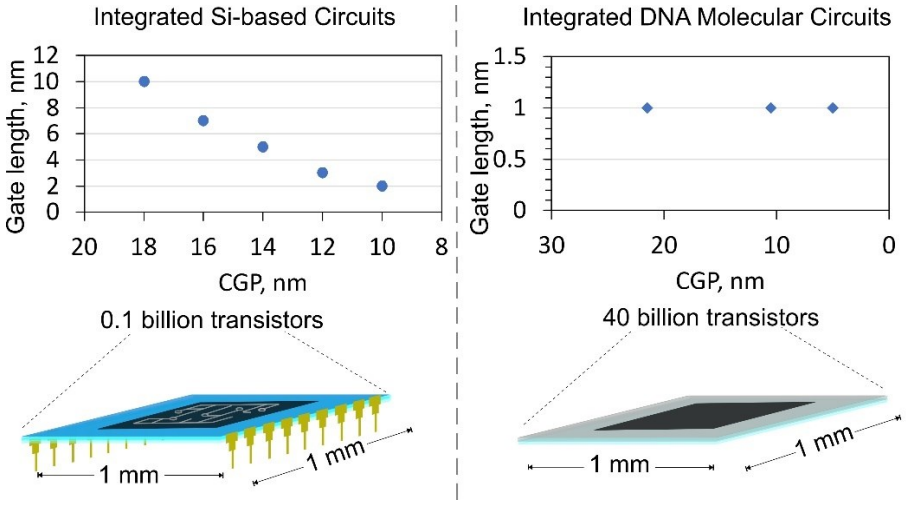

Figure 2. DNA IC in analogy to Si-based IC. Top graphs illustrate the typical CGP values associated with the gate length for Si-based[42] and DNA-based ICs.[45,47,48] Bottom schematics show the number of transistors capable of being integrated on a 1mm^2 chip.

DNA molecular computing holds the potential for being biocompatible. Thus, it has been envisioned for biological and medical purposes.[35,49] Nonetheless, general purpose DNA molecular computing for digital data storage has been developed showing robust data fidelity after retrieval.[50,51] This feature is expected, considering that DNA is nature's material for data preservation and transmission. In cell-free media, DNA molecular computers have shown their biosensing capabilities for multiplex diagnostics.[52–55] *In vitro*, DNA logic gates have been proposed for bioimaging, controlled drug delivery, and other theranostic approaches.[56–58]

1.3 Scaling up Integrated DNA Molecular Circuits (Mimicking a Si-chip).

Even though DNA logic gates can identify as inputs a myriad of biomolecules (ions,[59] small molecules,[60] nucleic acids,[28] and peptides[58]) as well as non-molecular stimulus (temperature,[61] electromagnetic force,[62] and pH[63]), input and output homogeneity are necessary among each logic gate for their intercommunication. DNA allows for homogeneity by using DNA sequences as

inputs and outputs, which interact with the DNA logic gates by formation and/or dissociation of base pairs. As a result, multiple DNA logic gate motifs have been developed, which operate through the association/dissociation of hairpins, four-way junctions (4J), strand displacement reactions (SDR), RNA/DNA enzyme, and tweezers. (Figure 3).[8,12–14,25,46,64–68]

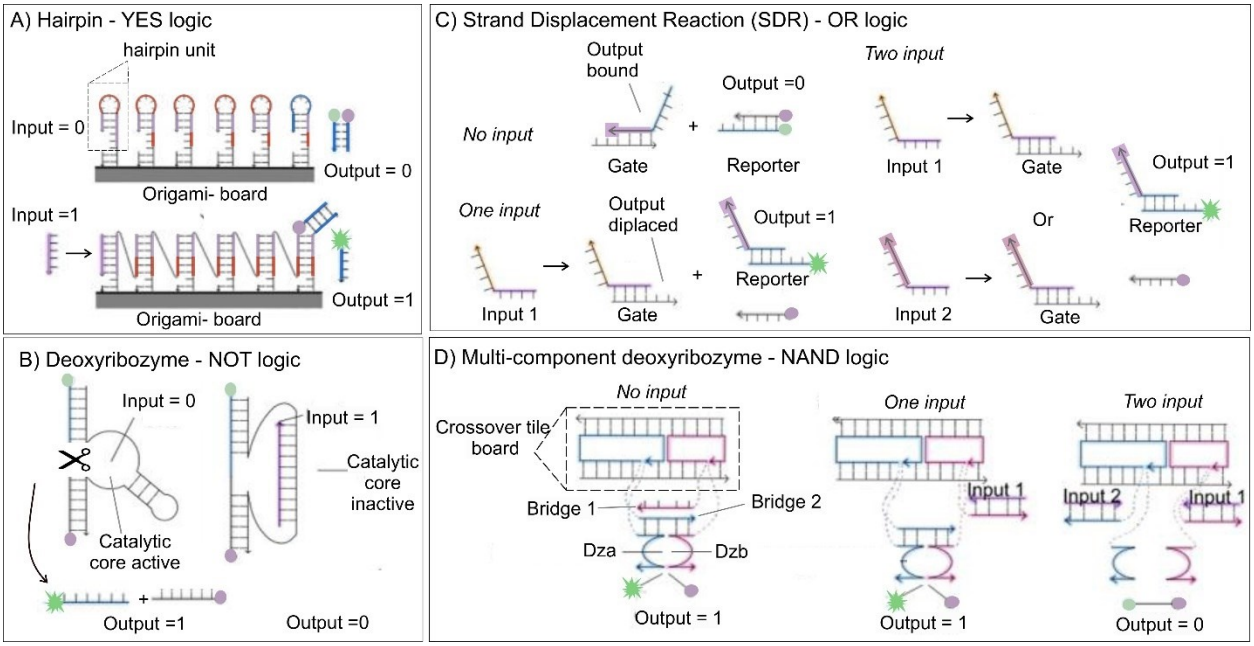

Figure 3. DNA logic gate motifs using fluorescence reporters. High fluorescence is correlated to high output signal (1) and low fluorescence to low output signal (0). Purple dots represent molecular quenchers, green dots-quenched fluorophore, and green stars- fluorescent fluorophores. a) Cascade of 6 hairpin YES gates localized on DNA origami board; each YES unit remains as a hairpin in the absence of input, upon input addition (pink ssDNA) the first YES unit opens its stem and communicates with a toehold (red) from a YES unit neighbor, this triggers a chain reaction until a quencher tagged ssDNA is displaced from its fluorophore tagged complement, redrawn from ref. [47]. b) Deoxyribozyme NOT gate in bulk; in the absence of input the catalytic core actively cleaves a substrate into two fragments, one tagged with a fluorophore and the second with a quencher. Input (pink ssDNA) forms a duplex that inhibits the catalytic core from substrate cleavage, redrawn from ref. [8]. c) SDR OR gate in bulk; No input scheme shows Gate holding the Output (pink-blue ssDNA). Adding input 1 (orange-pink) or input 2 (magenta-pink) displaces the bound Output out of the Gate, and Output displaces quencher-tagged ssDNA from its fluorophore-tagged complement, redrawn from ref [69]. d) Multicomponent deoxyribozyme-NAND gate localized on crossover tile board; No input scheme shows Bridge 2 holding the deoxyribozyme ssDNA components (Dza and Dzb), which allows catalytic core integrity for

substrate cleavage into two fragments. Input 1 binds to Bridge 1; however, Bridge 2 keeps the catalytic core integrity, vice versa if input 2 is added. When Bridge 1 and Bridge 2 are bound to Input 1 and Input 2, the catalytic core falls apart into Dza and Dzb fragments inhibiting substrate cleavage (Two input scheme), redrawn from ref [66].

1.3.1 Free diffusion vs Spatial Localization of DNA Molecular Circuits.

The first DNA circuitries were realized with all gate components freely diffusing in aqueous solutions (bulk circuits).[8–14,69] Nonetheless, scaling up integrated gates in bulk circuits i) slows response down to hours, ii) requires unique gate sequences to avoid crosstalk, and iii) increases signal leakage and unwanted interactions. Therefore, the design complexity of DNA circuits operating in bulk increases proportionally to the number of communicating gates, since the use of repeating elements must be excluded. This requirement leads to overpopulation of computing components, which increases potential undesired crosstalk and inhibitory interactions.

Table 1 compares the performance of bulk circuits capable of processing ALU. To overcome the mentioned obstacles, common approaches include fuel DNA components and enzymes (to speed up the processes),[70] inhibitory components (to avoid signal leakage),[13,47,69,71] and gate and input libraries (to reduce design complexity).[72] Although, they are useful features, another alternative for addressing the aforementioned problems is anchoring the DNA logic gates to a scaffold.[47,73,74] Remarkably, at the cellular level, spatial localization accelerates the interaction between components that are closer to each other and reduces nonspecific crosstalk between them.[75–77] This paradigm has been extrapolated to catalysis, electronic computers and now molecular computing.

Table 1. High performance bulk DNA circuitry.

Gate motif	Computation				Outcome	Ref
	Max # gates[a]	Operator	t_f, min[b]	$t_{1/2}$, min[c]		
SDR/canvas switching circuits	2	YES	< 10	< 3	Fast and scalable computations by routing DNA logic gates in grid	[34]
	3	3-bit input voting	< 12	~ 3		
	3	Full added	< 10	< 3		
	2	Square root	ND	< 10		
Polymerase mediated SDR	2	XOR	~ 10	~ 4-6	Developed a ALU using a polymerase mediated strand displacement	[70]
	4	Full adder	~ 20	~ 10		
	3	Multiplexer	~12	~ 5		
	7	1-bit ALU	~20	~ 5-10		

ND: Not determined. [a] Maximum number of cascaded gates.[b] Full processing time to reach plateau. [c] Half processing time.

1.3.2 DNA boards for DNA Molecular Circuits.

Although multiple materials have been proposed as scaffolds to spatially localized DNA logic gates (e.g. beads,[37] cell surfaces,[61,78] microarray chips,[39] droplets[79], polymers,[80] and Au films[81]), molecular structures made out of DNA (DNA boards) can be used. DNA is a molecule that can construct scaffolds and structural templates aiding chemical reactions and bio-molecule characterization, the last was demonstrated by Ned Seeman.[82,83]

All-DNA computers allow i) greater biocompatibility, (ii) simplicity in circuit layout since DNA logic units can be precisely localized in DNA boards by hybridization and iii) customization to increase computer performance. The advantages of incorporating DNA boards over bulk circuitry are: i) ability to closely hold multiple DNA logic processing units,[84] ii) flexibility in spatial arrangement of the integrated units,[47] iii) reusability of functional sequences since localization gives circuit orthogonality,[46,85] iv) isolation of computing elements as one unit,[50] v) facilitate cell uptake and vi) relative stability to nuclease degradation.[86,87]

Paul Rothemund's work lighted a pathway to construct large DNA scaffolds of different shapes, a technique named DNA origami.[88] At first glance DNA origami offers a large surface area for the anchoring of molecules, thus becoming a widely used DNA board.[89,90] The limitation of DNA origami is the yield of the targeted DNA nanostructure, where the moderate (~83-90%) of staple incorporation has been reported.[45,47,85] Thus, incomplete incorporation of structural strands can further compromise gate incorporation and circuit performance. Additionally, scaling up to multi-origami, assembly although possible,[91] might physically hinder intra and inter circuitry processes due to the improper alignment, bending or breaks.[92,93] One way to circumvent the limitations carried from DNA-origami boards is the use of small 2D tiles. Our lab explored the use of crossover tiles[66,94] and integrated up to 3 DNA logic gates (Table 2). However, when scaling up in the integration of more logic units, such DNA boards were prone to bend and misplace the DNA logic units from optimal intercommunication. This was possibly due to the torsional effects and rigidity conferred from the multiple crossover points (Figure 3D and Figure 4D).[66,94]

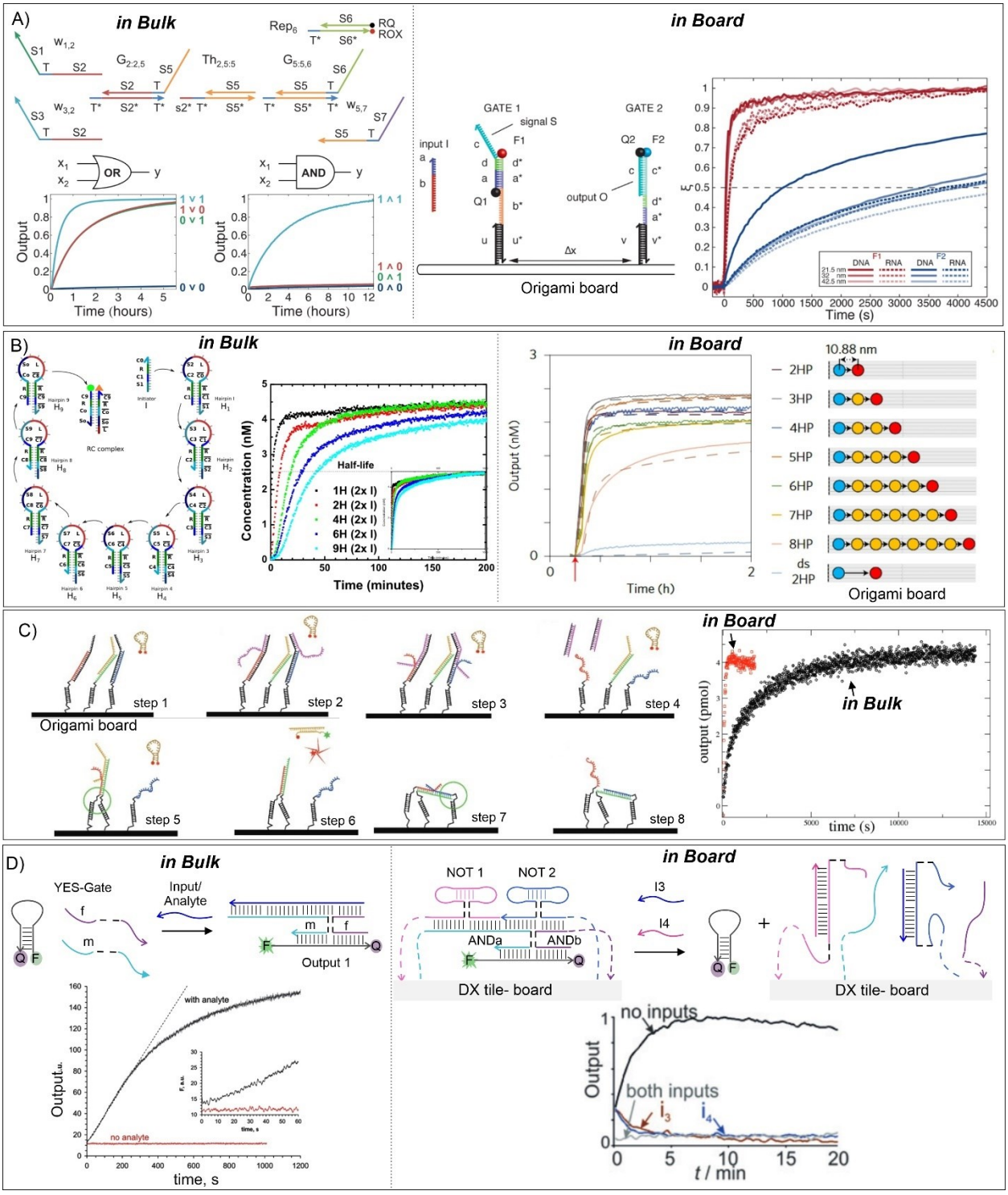

Figure 4. Kinetics comparison of DNA logic gates diffusing in solution (in bulk) vs spatially localized in DNA boards. Intercommunication of different types of DNA logic gate motif are displayed. Left panels show in bulk: a) Seesaw, b) Hairpin, c) SDR, d) 4J in bulk, reproduced with permission from [69], [64], [45], [149] respectively. Copyright 2011, The American Association

for the Advancement of Science. Copyright 2017, IOP Publishing Ltd and Deutsche Physikalische Gesellschaft. Copyright 2009, Royal Society of Chemistry. Copyright 2013, Elsevier. Right panels show localized a) Seesaw, b) Hairpin (represented by coloured dots), c) SDR, d) 4J in DNA substrates, reproduced with permission from [48], [47], [45], [94]. Copyright 2014, American Chemical Society. Copyright 2017, Springer Nature. Copyright 2009, Royal Society of Chemistry. Copyright 2016, Wiley-VCH.

Another proposed alternative is using 3D DNA boards[27,28,95,96] which are mostly used *in vitro* studies. These 3D DNA boards (e.g. tetrahedrons, pyramids and cubes),[97,98] also known as three-dimensional framework nucleic acids (FNA) exhibit unique biophysical properties. For instance, after their injection into mice, ssDNA had a half-life of ~15 min, increasing to ~35 min for a tetrahedral DNA.[87] Thus, DNA tetrahedra has a longer half-life than ssDNA in an intracellular environment. In addition, DNA tetrahedrons can be easily taken up by cells.[86]

The ability to produce an easily detectable output signal at low concentrations is important in intracellular sensing of biological compounds. Yang et al. proposed an entropy-driven aggregation of DNA tetrahedron circuits that led to amplification of the output fluorescence signal and improved LOD from nM to fM range.[96]Therefore, further exploration of *in vitro* DNA ICs can be done using these 3D DNA substrates.

1.3.3 Integrated DNA Molecular Circuits (DNA ICs) and Their Performance.

Is it possible to integrate DNA logic gates in long communicating chains like Si-based transistors are integrated on a Si chip? Two research groups theoretically explored the feasibility and performance of cascading DNA hairpin-gates tethered to an origami board (Table 2).[84,85] Although gate motif and board were in essence similar, the two studies differed in the following

aspects: i) addition of untethered components for gate processing and readout; ii) different spatial configurations of gate wiring; iii) probabilistic and kinetic simulations of circuit performance. Dalchau et al. exemplified faster kinetics of DNA ICs predicting completion times of minutes instead of hours as their equivalent bulk circuits. They evaluated 10 elemental YES gates connected in series with a 50% completion time ($t_{1/2}$) of approximately 3.5 min, while shorter times were predicted for cascades with reduced number of gates[85] (Table 2). This work emphasized the need for models that comprehensively reflect the molecular behavior of localized gates to properly evaluate the kinetic behavior of such circuits. In another approach, Stefanovic and coworkers studied the cascading of molecular spider nanostructures to build DNA ICs.[99] They simulated kinetic behavior and developed an algorithm generating the spatial configuration of the integrated gates on DNA boards. Their work shows the importance of DNA ICs layout to avoid signal impedance and unwanted interactions.

Table 2. DNA circuits localized on DNA board.

DNA board	Gate motif	Computation				Outcome	Ref
		Max # gates[a]	Operator	t_f, min[b]	$t_{1/2}$, min[c]		
Theoretical works							
Origami	Hairpin	3 2-YES 2-AND	YES AND Half adder	~ 480 ND ND	~ 180 ND ND	Spatial localization of DNA hairpin	[84]

DNA board	Gate motif	Computation				Outcome	Ref
		Max # gates[a]	Operator	t_f, min[b]	$t_{1/2}$, min[c]		
		4-AND 1-OR	Full adder	ND	ND	for circuit designing	
Origami	Hairpin	10 2 2 3-(AND - OR)	10-YES OR-AND AND-OR Square root (4-bit number)	ND ~ 2 ~ 2 ~ 1.5-3	~ 3.5 ~ 0.5-0.8 ~ 0.5-0.7 ~ 0.7-1	Development of a method for the probabilistic analysis of localized hybridization circuits	85
			Experimental works				
Origami 90x60 nm	SDR	2-YES	4th degree fan-out	~ 4-8	ND	Signal amplification	45
Origami	Hairpin	8 2-AND 3-AND	YES 3-bit input AND 6-bit input AND	~ 40 ~ 20 ~ 40	< 10 < 6 ~ 12	Increased processing speed of hairpin chain reactions	47

DNA board	Gate motif	Computation				Outcome	Ref
		Max # gates[a]	Operator	t_f, min[b]	$t_{1/2}$, min[c]		
		OR-AND	Dual rail XNOR	~ 15-30	< 8		
Origami 65x90 nm	SDR	2	YES	ND	~ 17	Reduced processing time	[48]
DNA crossover (X) tile	4WJ	AND-2-NOT AND-NOT	NOR INHIBIT	~ 5 ~ 40	~ 1 ~ 8	Reusable array of communicating gates	[94]

ND: Not determined. [a] Maximum number of cascaded gates.[b] Full processing time to reach plateau. [c] Half processing time.

Experimental works showed that DNA circuit performance can be influenced by the spatial distancing of gates within the DNA board. Simmel and coworkers proposed 21.5 nm distance between seesaw (strand displacement-based) gates to avoid signal leakage in the absence of input.[48] Chatterjee et al. separated them by 10.88 nm; however, such 2-fold reduction was allowed by a self-protected motif (hairpin) leading to minimal signal leakage.[47] Lastly, Elezgaray and coworkers distanced each gate by 5 nm with the use of diffusible protector strands[45] or G-quadruplex[46] (Fig 5a), this being the smaller CGP reported. Therefore, far distanced gates have

suboptimal communication, while closely distanced gates require additional components to minimize leakage.

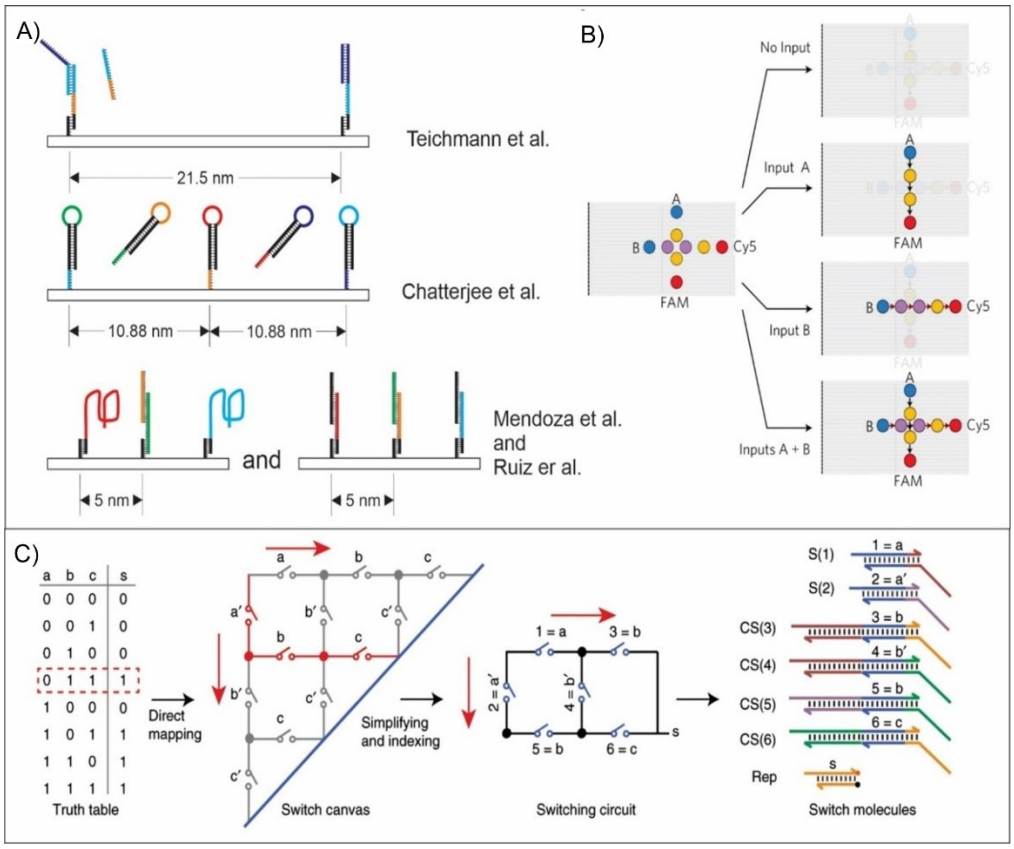

Figure 5. Possible layouts of DNA logic gates on DNA boards a) Distance between gates on origami board, top: seesaw (SDR) middle: hairpins, bottom: G-quadruplex or using of diffusible protector strands, redrawn with permission from [48], [47], [45], [46]. Copyright 2014, American Chemical Society. Copyright 2017, Springer Nature. Copyright 2009, Royal Society of Chemistry. Copyright 2016, American Chemical Society. b) DNA hairpin on origami board layout in a communication crossover fashion for signal transmission under different Input combinations. Reproduced with permission from [47]. Copyright 2017, Springer Nature. c) The mapping of signal transmission on DNA-based switching circuits used in the design of bulk circuits in a grid pattern. Reproduced with permission from [34]. Copyright 2020, Fei Wang et al.

The largest wire experimentally tested had 8 YES hairpin gates arranged in a linear cascade with a CGP of 10.88 nm (Figure 4B, right) and produced an output with a $t_{1/2}$ < 10 min (Table 2). In comparison to its bulk counterpart (composed of 9 YES hairpin gates) with a $t_{1/2}$ ~42 min[64], localization on a DNA board showed a 4-fold improvement in signal transmission time. Additionally, the result suggests that 50% of the DNA ICs had released their output in < 10 min, accounting for the signal transmission rate of < 0.76 nm/min. However, an 8-layered YES wire is a simple system. The increase in the number of connected units on the DNA board in such a fashion expectedly increased the circuit processing time, a similar behavior observed in bulk circuitry.[45,47,48,66,84,85,94]

To speed up signal transmission, approaches such as dual rail input/output (different molecules encode bit-0 and bit-1),[50] and circuit parallelism (independent circuits in simultaneous operation)[47,81] have been suggested. Alternatively, signal can be relayed in different types of arrangement. One example is DNA circuits arranged in a grid pattern, proposed by Wang et al.[34] which reduced the processing time of bulk circuitry (Figure 5C and Table 1). On a DNA board, Chatterjee et al. demonstrated the communication of DNA hairpins in a crossover fashion (Figure 5B). However, using this arrangement for the wiring of more than 8 units was not explored.

In summary, current localized single to multi-layered DNA circuits propagate signal in the range of 1-40 min. This operation time is an improvement on those circuits in bulk which operate at a scale of hours when enzyme-free (Figure 4). DNA boards allow diverse gate localization and arrangement.[45,47] Additionally, localization enables reducing functional input concentration from 100 nM to 2 nM,[47] allows modular combination of logic gates into various circuits, isolation and storage of computing elements[50] and gate reusability, which reduces the population of computing

components. On the other hand, signal dissipation has been observed when connecting their logic gates in series, which could be the result of improper assembly of the units and/or the physical limits of the wiring.

1.4 Biological Applications of DNA ICs.

Due to its biocompatibility, DNA logic gates find the following bio-applications: intracellular molecular sensing,[28,59,100,101] gene regulation,[96] triggering cell death,[58] subcellular imaging,[100,102,103] and cell-surface recognition.[104] Various biological analytes (ATP,[28,59,100,102] protons,[28,100,102] metal cations,[28,59,101] miRNA,[96] ssDNA and mRNA,[28,95,100] membrane proteins,[58,104]) have been used as inputs for DNA logic gates. Aptamers, i-motif, MSO sequence, G-quadruplex, DNAzymes, toe hold domains and hairpins were used as sensitive modules of DNA logic gates. However, integration of logic gates as circuits into a single DNA board have not been used in an intracellular environment yet. Instead, our literature study has revealed two distinct architectural approaches: i) the integration of DNA logic gates within a single DNA board, where gate-to-gate communication occurred, is absent *in vitro* studies; [28,58,59,100–105] and ii) the interaction and regulatory behavior of DNA logic gates localized on separate DNA boards has been proposed.[96,106]

1.5 Perspective of Integrated DNA Molecular Circuits

Initial DNA circuits executed computational tasks with all the components in bulk. With the scaling up in the chain of intercommunicating units, this approach faced the problems of slow communication rates, non-specific crosstalk, signal dissipation, and overpopulation of computing

components. To overcome the problems, the field is evolving to restraining the freedom of the diffusing components. Among a variety of proposed platforms for logic gate localization are DNA boards. DNA boards offer the advantage of higher biocompatibility, circuits performing as one computing unit, increased nuclease resistance, increased space for high density circuitry, and ease of DNA ICs isolation. Although, different 2D and 3D DNA board architectures have been proposed, they require *in silico* modeling to minimize and avoid misassembling and communication hindrance. The use of DNA boards introduces assembly efficiency, an important parameter in the manufacturing of DNA ICs, where the incorporation of structural and logic gate oligonucleotides into the target DNA nanostructure can compromise circuit performance. Alternatively, the covalent crosslinking of the DNA board during or after assembly[107,108] is an avenue that can be explored to reduce partially assembled structures and disassembly from aging. Another relevant parameter is the distance between intercommunicating gates (CGP) which can be precisely adjusted on DNA boards. Similarly, CGP is a deterministic factor to Si-based circuits in achieving maximum logic gate density and efficient communication between gates.

DNA ICs are proven to speed up output response and have been able to detect lower concentrations of inputs in comparison to the same ICs performing in bulk. However, the integration of more than 8 DNA logic units on DNA boards has not been achieved yet, as increasing the number of intercommunicating gates seem to face similar challenges as in bulk. As the number of gates increases in the communicating chain, signal dissipation and slow signal processing rates are unavoidable even within a DNA board. To mitigate these limitations, signal amplification or transient storage of outputs for later relay to new circuit units are needed—the last showing the relevance of compartmentalization of computing elements for their isolation as a DNA IC.

Alternatively, integration of DNA circuits arranged in grid pattern could significantly speed up DNA ICs as in DNA bulk circuit. Although Boolean logic is commonly pursued, non-Boolean circuits/connections, like logic switches could potentially allow for flexibility in gate wiring and increase density of the DNA ICs. The layout of logic units can affect not only speed but circuit growth and length since localization strings could impede the ability to expand the number of interconnected units. In this regard, the ability to design highly scalable DNA logic circuits is an important aspect to evolve from performing a few numbers of computations to general-purpose computing and automatization.

Circuit designing and analysis software has been used for the planning and wiring of DNA logic circuits *in silico*, which helps to speed up experimental testing and performance troubleshooting. However, such software packages are limited to specific types of DNA gate motifs, limiting their use to less conventional computing nanostructures. Thus, developing a universal software applicable for broader range of DNA gate motifs, substrates, and wiring is needed. Although delivery of DNA logic units into cells has been reported, no intercommunication of logic gates on DNA substrates as a DNA ICs has been applied in cells up to date. Therefore, we find it important to fill this gap to show the relevance of the integrated DNA circuits to i*n vivo* applications.

1.6 Dissertation Scope

This chapter looks at the state of the art in developing DNA ICs and provides an outlook on the advantages of spatial localization of DNA computing units on DNA boards as well as the need for better design strategies and architectures to advance the technology. Due to the limitations

of current DNA board architectures, a new 2D DNA board for the localization of DNA computational units is proposed in this work. This DNA board is considered to provide the following features: i) adjustable size based on the number of computing units anchored, ii) reduced number of constituents to minimize misassembling, iii) connectivity with one or more DNA board modules, and iv) spatial orientation of the computing units. None of these features have been attributed to previously proposed DNA board systems.

The general goal of this dissertation is to establish modular units of DNA logic gates and DNA boards to allow the scalable and versatile fabrication of DNA ICs, and it aims to provide the fundamental principles for the construction of high-complexity DNA circuitry. To accomplish this, we investigated the following research questions:

i) is it possible to construct functionally complete Boolean logic functions from non-Boolean connectivity of elemental gates/switches with YES and NOT logic?

ii) Can a DNA board expand as the number of computing units it anchors increases? How many computing units can we cascade on the DNA board before the signal dissipates? Will it be possible to achieve connectivity of multiple DNA board modules?

iii) Is it possible to reduce computation times down to seconds and minimize the computation slow down when increasing the density of the DNA ICs?

iv) Can we provide an affordable chemical ligation method for the covalent crosslinking of all the DNA ICs components to consolidate them as a whole unit and minimize disassembly from aging?

Our attempts to answer each of the research questions are highlighted in each chapter. Chapter Two focuses on answering research question i) by investigating the use of elemental Boolean YES and NOT logic to construct functionally complete " universal" Boolean NAND and IMPLY logic. This chapter introduces the novel DNA board for the spatial localization of a combination of up to two DNA four-way (4J) YES and NOT logic gates. Furthermore, based on the outcomes of this investigation, the development of a DNA computation education kit to teach the fundamental principles of this technology is also included.

Chapter Three is oriented towards research question ii) where the designing principles of the novel DNA board are highlighted to allow customizable size according to its anchored computation units. This chapter also includes the results of cascading five 4J YES gates in two different DNA board modules and the later integration of both modules into a cascade of up to ten 4J YES gates to explore the signal propagation and dissipation borderline of this computation units.

Chapter Four focuses on research question iii) where a new molecular readout reporter system is proposed for the translation of the output sequence of a DNA IC into a fluorescence readout. This reporter system aims to minimize its kinetic contribution to the computation time response of a DNA IC cascading four 4J YES gates. Furthermore, we attempt to provide a quantitative measurement of the response time and time delay between inter-gate cascading units.

Research question iv) is investigated in Chapter Five by firstly exploring the use of 1-cyanoimidazole and a divalent metal cation for the chemical ligation of two DNA oligonucleotides in aqueous solution. This chapter shows the use of a DX-tile template to achieve the 5' to 5' and 3' to 3' non-conventional ligation of two oligonucleotides using the aforementioned chemical

reaction. From the understanding and optimization of these condensation reagents, we investigated the suitability of this reaction in the covalent crosslinking of DNA IC components.

Lastly, Chapter Six discusses and summarizes the major outcomes achieved from each chapter and reviews the answers provided to each of the research questions investigated in this dissertation.

CHAPTER TWO: TWO LEVEL FUNCTIONALLY COMPLETE LOGIC CIRCUITS FROM MODULAR INTEGRATION OF YES AND NOT LOGIC GATES

2.1 Introduction

In our DNA molecular computing designs,[109,110] inputs and outputs correspond to nucleic acid sequences. We have been developing DNA logic gates connected to each other via DNA four-way junction (4J) structures (Figure 6) .[94,109] These 4J gates recognize the nucleic acid sequences as inputs and produce a new sequence by bringing two oligonucleotide fragments into proximity, which is the output of the 4J gates (Figure 6C). The new output sequence can be conveniently detected by a molecular beacon (MB) probe—a fluorophore—and a quencher-labelled DNA hairpin.[111] In the absence of a complementary output, MB is in a hairpin conformation, which keeps the fluorophore near the quencher, ensuring low fluorescence. Upon the binding of MB to its complement, it stretches and distances the fluorophore from the quencher, enhancing the fluorescence signal (Figure 6C). Therefore, MB helps in transducing the nucleic acid output to a fluorescence signal, and easily monitoring the molecular computing readout. These change in

fluorescence from the opening/closing of the MB probe can be correlated to the binary response (0 and 1) as in digital computing.

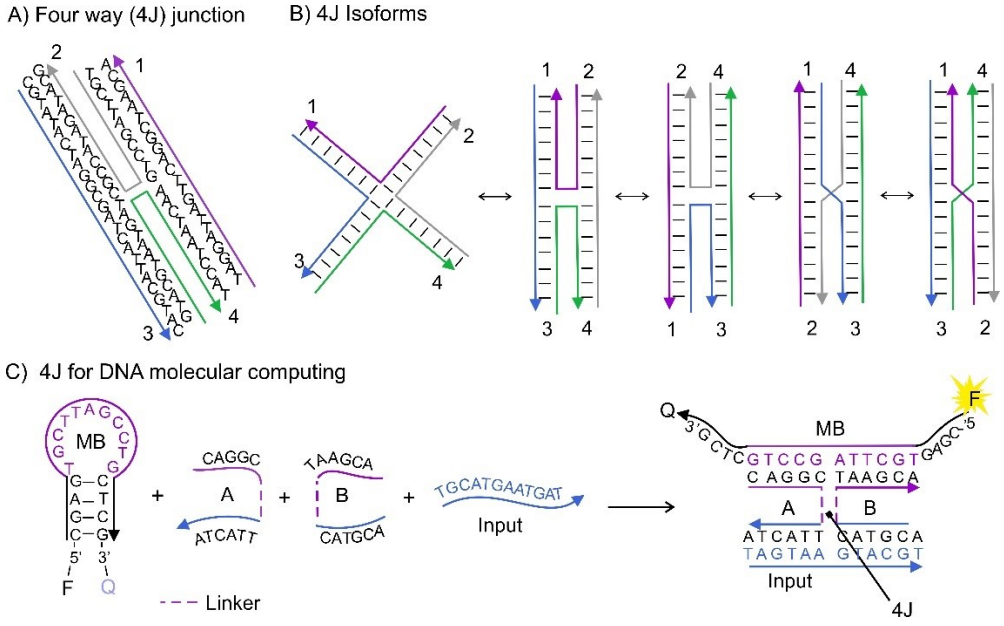

Figure 6. Structure of DNA four-way junction (4J). A) Schemes shows the hybridization of four strands of DNA into a 4J due to the crossover complementarity of strands 2 and 4 towards strands 1 and 3. B) Different conformations of 4J have been reported due to the twisting at their point of convection or by strand shifted migration; redrawn from ref [113] and [114]. C) For DNA molecular computing, a nucleic acid input binds to the complementary fragments (blue) of crossover strands A and B by bringing the together purple fragments of A and B results the an output sequence is made and it is recognized by a molecular beacon probe (MB); redrawn from ref [111]. Arrows represent single-stranded DNA which arrowheads indicate 3' ends. Polyethylene glycol linkers are represented by dashed lines F and Q correspond to fluorophore and quencher tags, respectively.

Due to the different conformations a DNA 4J can adopt[112,113], we introduced covalent polyethylene glycol linkers in between the input binding and output fragments of the crossover strands A and B. The separation of the nucleic acid sequences by these linkers prevents strand

migration into a conformation that could place MB's fluorophore and quenchers back in proximity (Figure 6B).

The simplest Boolean logic gates are YES and NOT. YES produces a high output in the presence of the input and a low output in its absence (Figure 7A). NOT is the inverter of YES logic (Figure 7A). Inspired by the 4J structure a 4J YES and 4J NOT Boolean logic gates were realized and their functional mechanism is illustrated in Figure 7. The 4J YES gate is composed of two DNA strands (A and B) that are bridged by a nucleic acid input to make the output sequence and triggering the opening of MB_1.[114,115] In the 4J NOT gate, strands A' and B' are brought together by a DNA "bridge" which forms the output sequence that hybridizes with the MB_2 probe in the absence of input. In this setting, the 4J NOT gate follows the NOT logic truth table by giving a functional output sequence (output 1) for input 0 (absence/low). The addition of the nucleic acid input sequesters the bridge fragment from a 4J NOT gate leading to the separation of the two output (green) fragments, which results in the dissociation of the MB_2 probe. This causes MB_2 to fold itself as a hairpin and to exhibit low fluorescence (Output 0).

The connectivity of 4J YES and NOT logic gate can be achieved by rationally designing the output sequence of the downstream gate as an alternative input of an upstream 4J YES or 4J NOT gate as shown in Figure 7B. We reported that a connected 4J YES and 4J NOT and two connected 4J NOT gates can lead to functionally complete IMPLY or NAND gates, respectively.[114] To facilitate communication between these gates, we spatially localized them on a DNA scaffold, named here DNA board, which is composed of four strands: Rail 1, Rail 2, Staple 1, and Staple 2 (Figure 7C). The DNA board is a molecular structure assembled in aqueous solution where it provides spatial localization of two 4J Boolean logic gates for their integration into DNA circuits

The DNA board contains a single-stranded (ss)DNA section that serves as a flexible hybridization board for the integration of multiple DNA logic units, which allows for DNA circuits to be built.

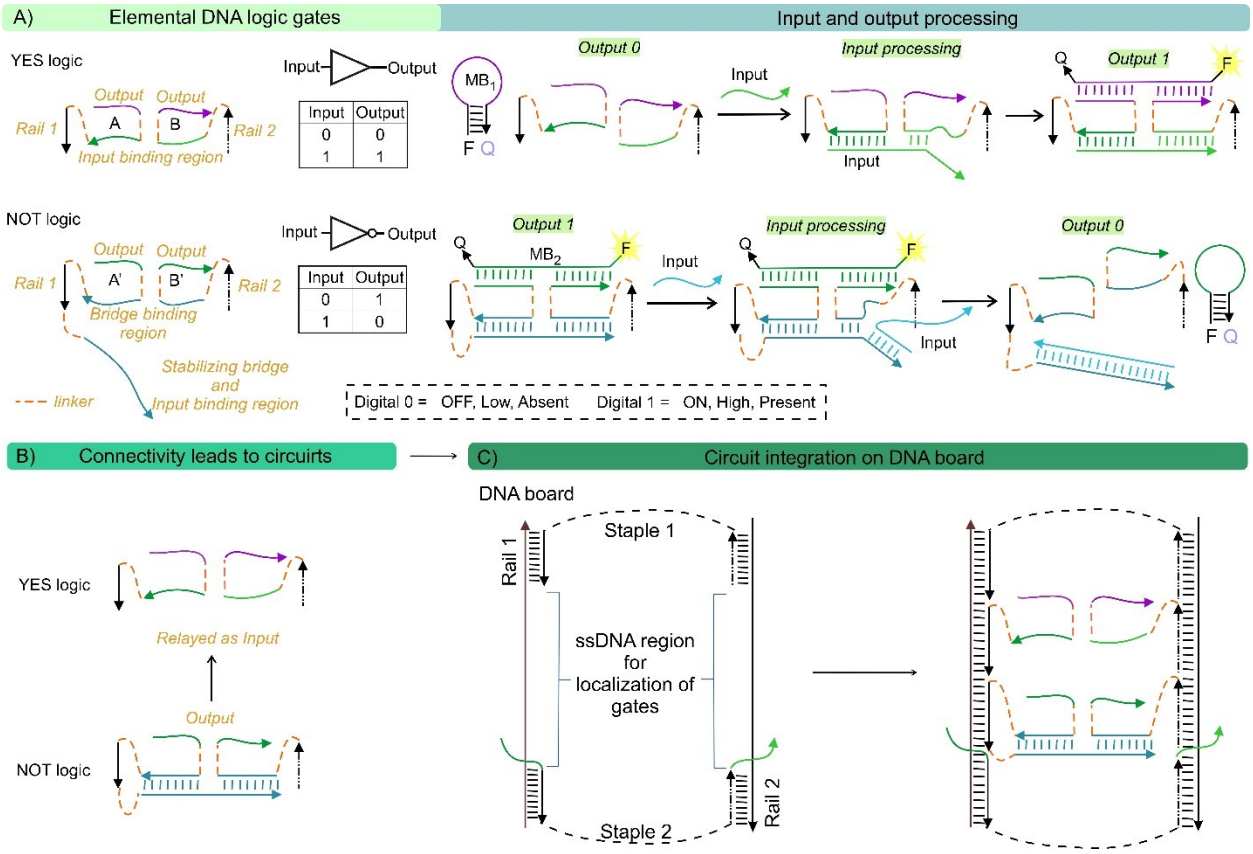

Figure 7. Molecular insight of the components of the DNA molecular circuits: A) Elemental DNA 4J YES and NOT logic gates. In the 4J YES gate, the input strand bridges strands A and B by binding to their green fragments, thus bringing the purple fragments in proximity to make an output sequence that is sensed by the MB probe (MB_1). In the 4J NOT gate, the output sequence (green fragments) is formed in the absence of the input strand due to bridging of strands A' and B' via complementarity of their blue fragments with the stabilizing bridge fragment (cyan). The input strand sequesters the bridge fragment from the bridge-binding fragments of strands A' and B'. Thereby causing separation of A' and B' and decomposition of the output into two fragments (green). B) The connectivity of 4J YES and NOT gates is achieved by relaying the output sequence of the downstream NOT gate as an input for the upstream YES gate, which results in a DNA molecular circuit. C) DNA board (left) is a four-stranded DNA nanostructure that allows spatial localization for connectivity of the individual YES and NOT logic gates (right). Arrows represent single DNA strands where arrowheads indicate the 3' ends. Stacked lines represent base pairs and dashed lines indicate an oligomeric linker.

2.2 Materials and Methods

2.2.1 Materials

DNase/protease-free water was purchased from Fisher Scientific Inc. (Pittsburg, PA) and used for all buffers and oligonucleotide stock solutions. MgCl2 (1 M solution) was purchased from Thermo Scientific (Waltham, MA), 1M Tris-HCl pH 7.4 buffer from KD Medical (Columbia, MD), and Triton X100 from Sigma-Aldrich (Burlington, MA). All oligonucleotides were custom-made by Integrated DNA Technologies, Inc. (Coralville, IA), and their stock solutions were prepared by resuspension in water and stored at – 20°C until use. The concentrations of the oligonucleotides' stocks were determined from the Beer-Lambert equation, for which absorbance at 260 nm was measured with a Thermo Scientific Nanodrop One UV-Vis Spectrophotometer, while the corresponding extinction coefficients were determined using OligoAnalyzer 3.1 software (Integrated DNA Technologies, Inc.). Fluorescence assays were performed with Perkin Elmer LS 55 Fluorescence Spectrometer, Deuterium Lamp. Gel electrophoresis experiments were performed using BioRad electrophoresis equipment (Hercules, CA), and visualized using BioRad Gel Doc XR+.

Table 3. Oligonucleotides used in Chapter Two studies.

Name	Sequences
DNA Board	
Rail 1*	CCT ATC GTG TT TTG TCG CTGA CCA TC GTA TCG CTT CGT CTATG
Rail 2*	CTGAG TGAAT GAG CT CTA CA C TGC AGT ACC AC CGT TAG TCA
Staple 1*	ATTCA CTCAG /iSp18//iSp18/ CATAG ACG AAG

Name	Sequences
Staple 2*	GACA AA CAC GAT AGG TTTTTT TTTTTT TGA CTA ACG GT CCAG
Staple 2-OR	AA CAC GAT AGG TTTTTT TTTTTT TGA CTA ACG GT
Blck A_1	CGA TAC GAT GG
Blck B_1	TGT AGA GCTC
Blck A_2	TCAG CGA CAA
Blck A_2	GGT ACT GCA G
YES 1	
A_1*	TC TAT TG /iSp9/A GAC AAT GTA GC/iSp9/CGATAC GATGG
B_1*	AGTAG AGCTC/iSp9/GAAAC CCA GC/iSp9/ TAT GTT AACG
A_1	CT TTG TTC/iSp18/A GAC AAT GTA GC/iSp18/CGATAC GATGG
B_1	AGTAG AGCTC/iSp18/GAAAC CCA GC/iSp9/ GAT G ATT CC
NOT 2	
A_2*	TA CAT TGTC T/iSp9/GGT GAAC C/iSp9/TCAG CGA CAA
B_2*	TG TTG CTC/iSp9/GCT GGG
Bridge*	AGGG GTT CAC CGA GCA ACA TTC/iSp9/GGT ACT GCA G
NOT 3	
A_3*	CT TTG TTC/iSp9/A GAC AAT G/iSp9/CGATAC GATGG/iSp9/ AAATC TAC ATT GTCT GC TGG GTTTC
B_3*	AGTAG AGCTC/iSp9/AAC CCA GC/iSp9/GAT G ATT CC
YES 4	
A_4*	TC TAT TG/iSp9/TCT GATAAGCTA/iSp9/CGATAC GATGG

Name	Sequences
B_4*	AGTAG AGCTC/iSp9/TCAA CAT CAG/iSp9/TAT GTT AACG
YES 5	
A_5*	TTA TCA GA/iSp9/A GAC AAT GTA GC/iSp9/TCAG CGA CAA
B_5*	GGT ACT GCA G/iSp9/GAAAC CCA GC/iSp9/CTG ATG TT
MB Probes	
MB_1	/56-TAMN/ CCT GG AATCATC GAACAAAG CA CAG CC AGG /3BHQ2/
MB_2	/56-FAM/ CCAGG CCCAGC AGACAATGTA CCT GG/3BHQ1/
MB NAND*	FAM- CCTGG AATCATCGAACAAAG CA CAG CCAGG -BHQ1
MB OR/IMPLY*	FAM-CGCG TTA ACA TA CAA TAG AT CGCG-BHQ1
Inputs	
hsa-miR-21-5p (Input 4)*	/5Phos/rUrArGrCrUrUrArUrCrArGrArCrUrGrArUrGrUrUrGrA
hsa-miR-221-3p (Input 1)*	/5Phos/rArGrCrUrArCrArUrUrGrUrCrUrGrCrUrGrGrGrUrUrUrC
hsa-miR-409-3p (Input 2)*	/5Phos/rGrArArUrGrUrUrGrCrUrCrGrGrUrGrArArCrCrCrCrU
Input 3*	GAAAC CCAGCAGACAAT GTA GC

* Oligonucleotides were used specifically on *J. Chem Educ*. (2024) manuscript corresponding to the development of the education kit. Each sequence is entered as 5'→ 3'; iSp9 and iSp18 are oligoethylene glycol spacers 9 and 18 from Integrated DNA Technologies (IDT); FAM and BHQ1 correspond to 6-carboxyfluorescein and 3'Black Hole Quencher-1 respectively; /5'-phos/

represents a 5’ terminal phosphate group and r indicates ribonucleotide. Extinction coefficients were obtained from OligoAnalizer online calculator OligoAnalyzer from IDT website.

2.2.2 Assembly of DNA logic gates with DNA board

All DNA oligonucleotides corresponding to the DNA logic gates and DNA board intended for assembly into the target DNA logic circuit were mixed at 200 nM in equimolar ratios in a buffer mix containing 100 mM Tris-HCl at pH 7.4, 100 mM MgCl2, 0.06 % Triton X100; followed by vortex and centrifuged to make sure all the solution was dragged down. The samples were annealed by placing them in a water bath at 95 ℃ for 2 min and slowly cooling down to 22 ℃ within 8 h.

2.2.3 Fluorescence assays and data analysis

After assembly, a master mix solution was prepared containing molecular beacon (MB) probe solution and the DNA assembly. From this master mix, aliquots were dispensed in individual microcentrifuge tubes for the addition of the different inputs, followed by incubation at room temperature (22-25 ℃) for 20 min. The fluorescence emission was read from those samples, containing 100 nM DNA logic gate assembly, 50 nM MB probe (12.5 nM for YES 1 and IMPLY), 100-200 nM input, 50 mM Tris-HCl at pH 7.4, 50 mM MgCl2, 0.03 % Triton X100.

Average and standard deviations were calculated from three independent samples. To normalize the fluorescence response of each output signal, we subtracted the average fluorescence response of a MB only solution. Each graph plots the average fluorescence difference *(ΔF): fluorescence output signal – fluorescence MB signal*; Error bars represent the standard deviation from three independent samples.

2.2.4 Gel electrophoresis

Native gels were prepared at 8 % acrylamide (19:1 acrylamide:bisacrylamide) and contained 50 mM MgCl2 . Gels were run at constant voltage (95V) for 75 min. Samples were prepared using a 6 ×Cyan/Yellow loading dye (TrackItTM, Thermofisher). TBE buffer (89 mM Tris Base, 89 mM boric acid, and 2 mM EDTA) was used as the running buffer. Denaturing gels were prepared to contain 8 M urea and 12 % acrylamide (19:1 acryla-mide: bisacrylamide). Samples were prepared using a 2X denaturing loading buffer (85 % Formamide, TBE, and traces of Bromophenol blue and Xylene Cyanol). Gels were run at constant voltage (150V) and 65 ℃ for 1 h and 30 min. Gel-Red was used as a staining dye for the visualization of DNA bands.

2.2.5 Gel extraction of DNA assemblies

150 pmol of the DNA assembly was loaded into a Native gel. For gel extraction, gels were run at constant voltage (100 V) and 22 ℃ for 1 h 30 min. The target band was identified and cut with a scalpel blade, followed by thinly crushed, soaked in 1 mL DNA grade water, and incubated under shake (120 rpm) at 37℃ for up to 24 h. Supernatant was filtered using a X-Spin Coastar filter. From the collected supernatant, DNA was precipitated by adding a 2-fold volume 2 % LiClO4 – acetone solution and separated from the supernatant by centrifugation at 10,000 RPM for 3 min (step repeated with pure acetone). DNA pellet was dried under vacuum for 30-60 min and then resuspended with DNA-grade water.

2.3 Results and Discussion

2.3.1 4J YES and 4J NOT logic gate units

We optimized the performance of individual 4J YES 1 and 4J NOT 2 on the DNA board structure to achieve the correct digital response. Input 1 and Input 2 are the DNA sequences corresponding to hsa-miR-221-3p and hsa-miR-409-3p, respectively. Input 1 is recognized by YES 1, while Input 2 is recognized by NOT 2. Upon input recognition, YES 1 combines A_1 and B_1, giving an output sequence of a total of 18 nucleotides (nt) long. Conversely, NOT 2 dissociates its output sequence (17 nt) upon input binding to the bridge strand. When only YES 1 was assembled on the DNA board, blocker strands blck A_2 and blck B_2 were added to cover the empty ssDNA regions on both Rail strands (Figure 8A). Similarly, when only NOT 2 was assembled on the DNA board, blck A_1 and B_1 were added (Figure 8C). We observed signal enhancement for YES 1 and signal reduction for NOT 2, as expected, in the presence of the input strand (Figure 8B and D).

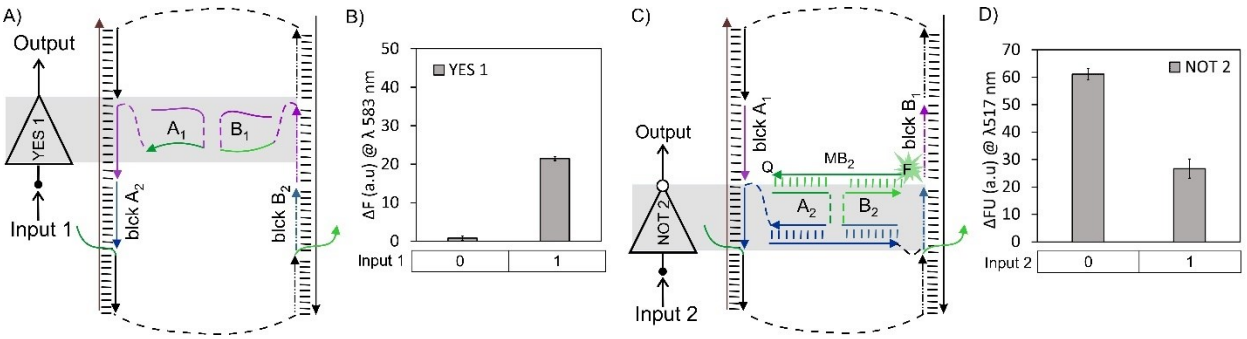

Figure 8. Functionally complete 4J gates integrated on DNA board. The 4J YES 1 A) and NOT 2 gates C) on the DNA board, both in the absence of input; ssDNA blocker strands (blck A_1, A_2, B_1 and B_2) fill the Rail fragments lacking the gates. Fluorescence response of 4J YES 1 B) and 4J NOT 2 D), respectively.

In DNA molecular computing, the development of individual logic gates has been thoroughly addressed. However, achieving complex molecular circuits is still in its infancy. A set of AND, OR, and NOT gates is a well-known functionally complete set in digital computers.[22] This set has attracted attention because of its universality—the ability to achieve any other logic functions by integrating multiple units of this limited set.[116] This modular and scalable approach enables the easy design and cost-efficient manufacturing of computational circuits. IMPLY and NAND are 'universal' (or functionally complete) gates: each of them is sufficient to build semiconductor circuits of arbitrary complexity.[117] operations.[118,119] In digital computing, neither the combination of YES and NOT gates, nor NOT gates alone, have ever been reported to comprise a functionally complete set of gates like IMPLY and NAND.

2.3.2 IMPLY Logic Circuit (4J YES + 4J NOT)

The IMPLY logic produces a low output only when the conditional set (Input 1: low, and Input 2: high) is true (Figure 9A). Lately, IMPLY has attracted attention for its use in 'memristive' switches, memory resistors that perform logic. We integrated both YES 1 and NOT 2 gates on the DNA board such that the output of NOT 2 served as an input for YES 1, as shown in Figure 9A. In this arrangement, the system was expected to perform as a two-input IMPLY logic circuit producing high output (measured as high fluorescence of MB_1) in all input combinations except when only Input 2 complementary to NOT 2 gate was present (Figure 9E). The fluorescence assays show the correct digital response of the IMPLY logic circuit (Figure 9B-C). An experimental threshold (red dashed line in Figure 9B) for the differentiation of digital 1 and digital 0 output

signal of the IMPLY unit was established following the concept of the limit of detection and corresponded to the average signal of YES 1-output 0 plus three times its standard deviation (SD).

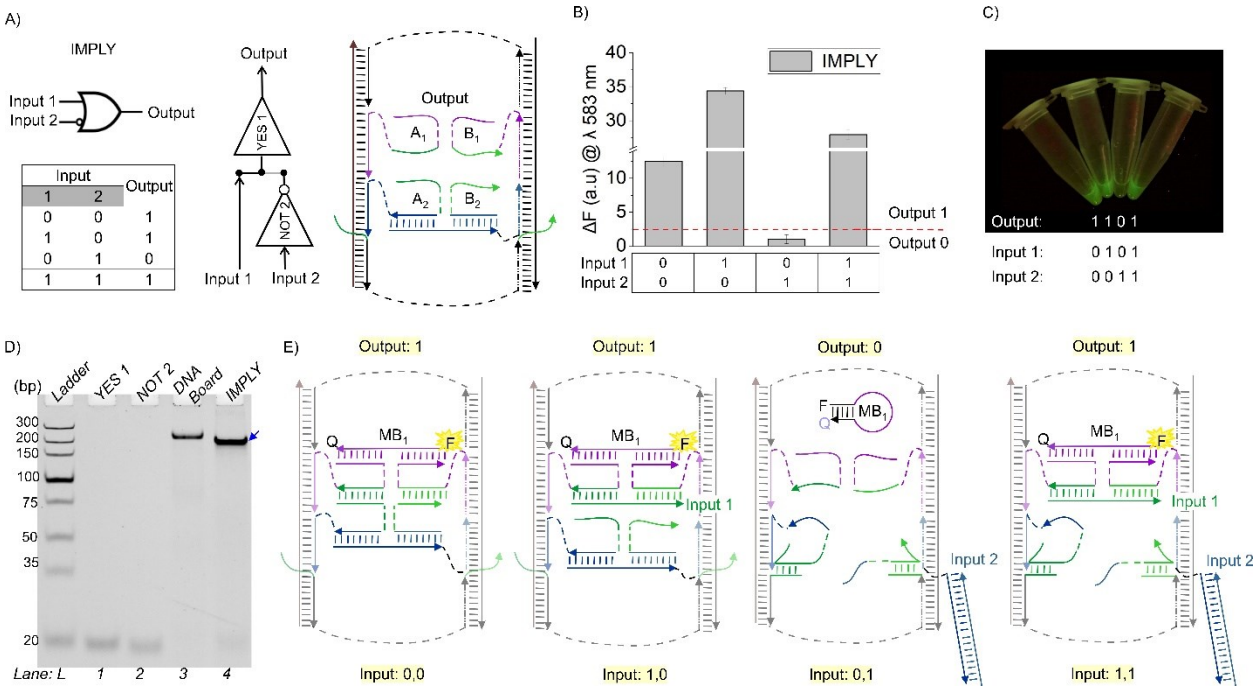

Figure 9. YES 1 + NOT 2 = IMPLY. A) IMPLY truth table (left) Localization and connectivity of YES 1 and NOT 2 on the DNA board (right). B) Fluorescence of IMPLY upon excitation at 555 nm. Red dashed line represents an experimental threshold, which was calculated as the average fluorescence of YES 1's output 0 plus three standard deviations. C) Visual fluorescence of IMPLY. D) 8% native PAGE–50 mM MgCl2 results. Ladder: dsDNA markers with their length, in base pairs, indicated to the left, YES 1: gate strands (A1 + B1), NOT 2 gate strands: (A2 + B2 + Bridge), DNA board and IMPLY full assembly: (YES 1 + NOT 2 + DNA board). The blue arrow indicates the fully assembled IMPLY gate nanostructure. E) Molecular structural changes in the IMPLY nanostructure for the four Input 1/Input 2 combinations: digital inputs 0, 0; 1, 0; 0, 1; 1, 1.

We also assessed the full assembly of the YES 1 and NOT 2 gates on the DNA board through gel electrophoresis (Figure 9D). Lane 4 shows faster mobility of the IMPLY unit than that of the DNA board alone. This can be explained by the higher overall negative charge of the 'loaded' DNA board nanostructure, which has a comparable electrodynamic volume with that of the

unloaded DNA board. To prove that the major band in Lane 4 contained all the expected strands, we cut this band out of the gel, eluted its content, and analyzed the content using denaturing gel electrophoresis (Figure 10A). For mobility reference, individual ssDNA components were added from Lane 2 to 10. Lane 11 shows the four DNA bands corresponding to the mobility of the DNA board components: Rail 1, Rail 2, Staple 1, and Staple 2. The IMPLY full assembly was loaded to Lane 12, which shows six DNA bands corresponding to the overlapping mobility of the components of the DNA board, YES 1 (A_1 + B_1) and NOT 2 (A_2 + B_2 + bridge). The IMPLY assembly after gel extraction was loaded in Lane 13, which shows five DNA bands corresponding to the components of the DNA board, YES 1 and NOT 2's A_2 and bridge. B_2 is not observed in Lane 13 (Figure 10A, blue arrowhead), and since this strand is detached from the DNA board, we consider that under non-equilibrium conditions like those of gel electrophoresis, B_2 is prone to dissociation from the major assembly and was lost from the IMPLY full assembly during gel extraction.

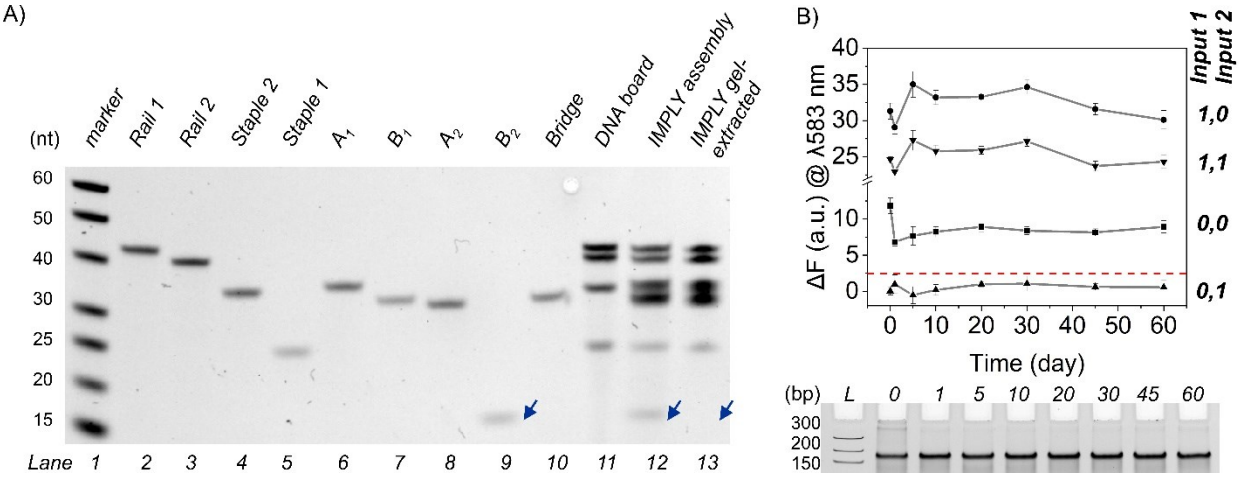

Figure 10. dPAGE analysis of full IMPLY assembly and shelf-life. A) 12% dPAGE–8 M urea results. Lane 1: ssDNA markers with their lengths, in nucleotides, indicated; 2–10: individual ssDNA components of the IMPLY assembly; 11: DNA board; 12: IMPLY assembly before PAGE

extraction. 13: IMPLY assembly after PAGE extraction. Blue arrowheads indicate the mobility of B_2. B) Fluorescence readout for up to two months of storage at 25℃ and native-PAGE assay showing IMPLY assembly stability.

A shelf-life assay of the IMPLY assembly was performed by running fluorescence assays at different time points for up to two months (Figure 10B). A master mix of the IMPLY assembly was prepared as listed in Materials and Methods Section 2.2.2 and stored on the bench at room temperature (~ 25 ℃). Aliquots of this master mix were taken to prepare the different samples containing any of the four possible input combinations and to perform a gel electrophoresis assay (Figure 10B). Both fluorescence and electrophoresis results suggest that the assembly has a robust performance for up to two months from its preparation without requiring freezing or special storage conditions.

2.3.3 NAND Logic Circuit (4J NOT + 4J NOT)

NAND Boolean logic produces a low output only when both inputs (Input 2 and Input 3) are high (Figure 11C). To create a universal NAND function, we loaded the DNA board with two NOT gates (NOT 2 + NOT 3). NOT 3 recognizes Input 3 (a 22 nt long ssDNA). For later connectivity with NOT 2, NOT 3 was designed to assemble in the same ssDNA region as YES 1 on the DNA board. Additionally, the NOT 3 output sequence is also recognized by MB_1. To test the individual response of NOT 3 on the DNA board, blck A_2 and blck B_2 were added as replacements for NOT 2 strands (A_2 and B_2) to maintain the rigidity of the DNA board. NOT 3 alone showed a 3-fold reduction when Input 3 was added (Figure 11B), demonstrating the digital NOT behavior of this gate.

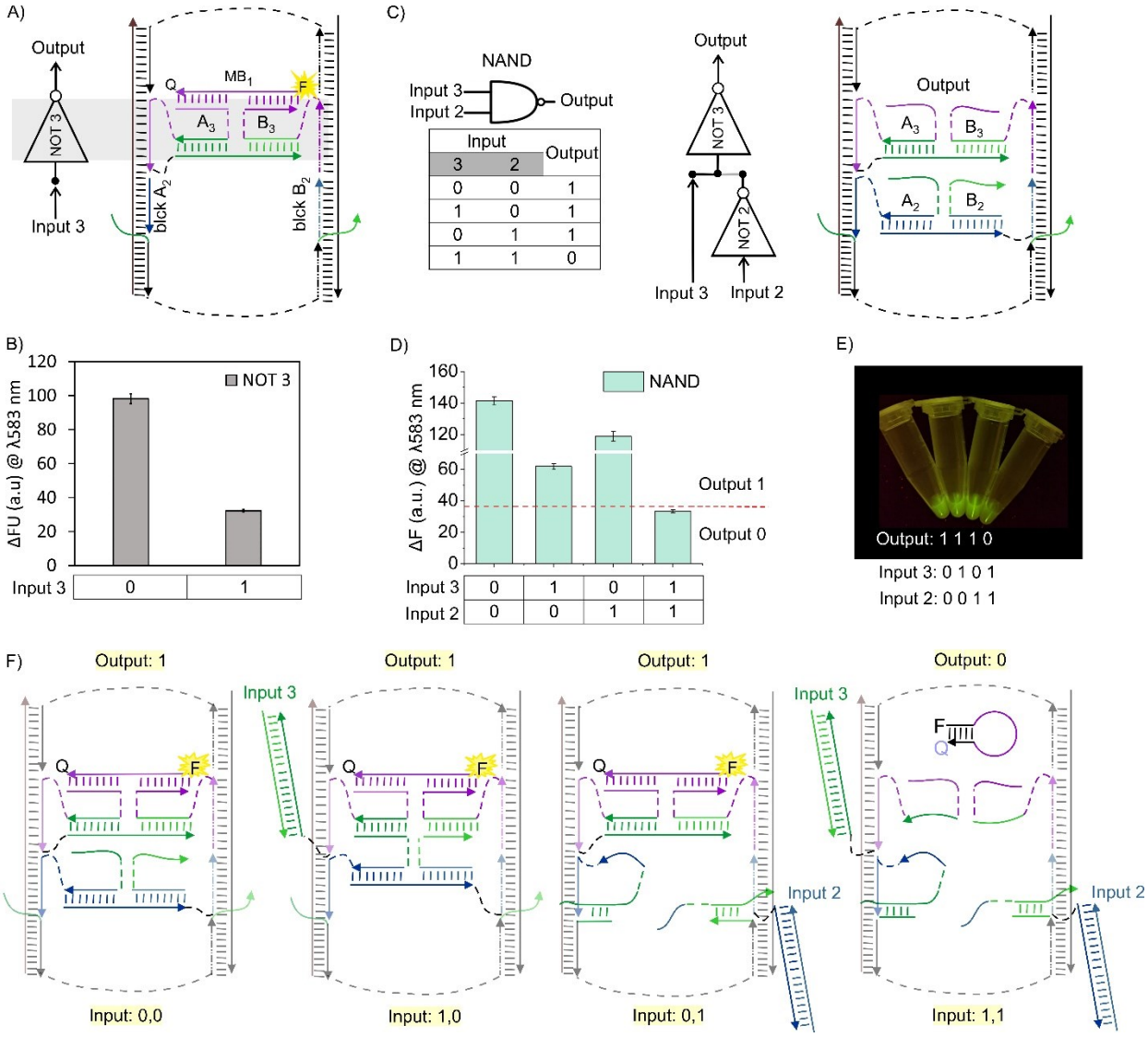

Figure 11. NOT 2 + NOT 3 = NAND. A) The 4J NOT 3 gate on DNA board; left: in the absence of input; ssDNA blocker strands blck A_2, and B_2 hybridized to ssDNA board area lacking gates. B) The 4J NOT 3 fluorescence response after exciting at λ: 555 nm. C) NAND truth table (left); schematic representation of localization and connectivity of NOT 2 and NOT 3 (right). D) Fluorescence response of NAND upon excitation at 555 nm. Red dashed line represents an experimental threshold, which was calculated as the average fluorescence of NAND's output 0 plus three standard deviations. E) Visual fluorescence of NAND. F) Molecular structural changes in the NAND nanostructure for the four Input 3 / Input 2 combinations: digital inputs 0,0; 1,0; 0,1; 1,1.

By connecting NOT 3 with NOT 2, we obtained a two-input NAND Boolean function, which is another functionally complete logic gate (Figure 11C). We performed similar fluorescence and gel electrophoresis assays as for the IMPLY logic unit. NAND fluorescence assays show the correct digital response as expected based on its truth table (Figure 11C-E). Gel electrophoresis also revealed a faster mobility band corresponding to the full NAND assembly (Figure 12A, Lane 4) as compared to the unloaded DNA board (Figure 12A, Lane 3). To prove that the major band (shown by a blue arrowhead) in Lane 4 contained all NAND expected strands, we performed a similar procedure as for the IMPLY assembly, by cutting and eluting this band out of the gel and analyzing its content via denaturing gel electrophoresis (Figure 12C).

Denaturing gel electrophoresis (dPAGE) allows for the imaging of the individual constituents of DNA assemblies. After gel extraction, the NAND assembly was loaded into Lane 13, which shows seven DNA bands corresponding to the components of the DNA board, NOT 2's A_2 and bridge, and NOT 3. B_2 is not observed in Lane 13 (Figure 12C, blue arrowhead) since this strand is detached from the DNA board. Therefore, in non-equilibrium conditions like those of gel electrophoresis, B_2 is prone to dissociation from the major assembly during gel extraction; a similar result was observed for the extraction of the IMPLY assembly (Figure 10A). A master mix of the NAND assembly was prepared as listed in Materials and Methods section 2.2.2 and stored on the bench at room temperature (~ 25 ℃) for shelf-life assays. Aliquots of this master mix were taken to prepare the different samples containing any of the four possible input combinations and to get assembly stability over time through gel electrophoresis (Figure 12B). Both fluorescence and gel electrophoresis assays show a robust performance and stability of the NAND logic circuit, even though the output when both inputs are digital 1 overpassed the experimental threshold (red dashed line Figure 12B) twice, the response of the NAND logic circuit followed its Boolean truth table.

From the Native-PAGE image (Figure 12B bottom), we observed that annealing is necessary to avoid undesired associations and/or construct aggregates.

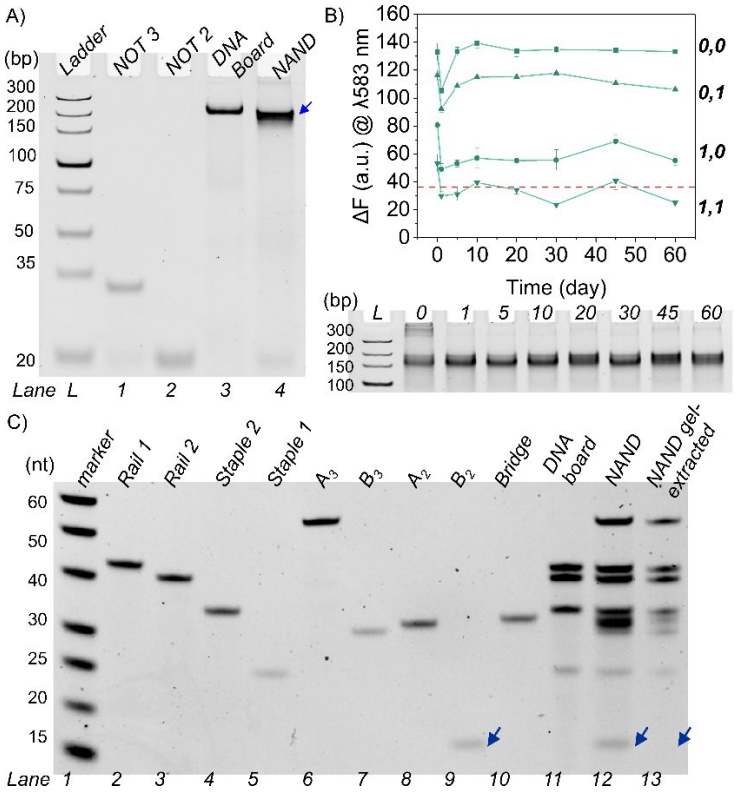

Figure 12. NAND Full assembly and shelf-life. A) 8% native PAGE–50 mM $MgCl_2$.Lane L: dsDNA markers with their length, in base pairs, indicated, 1: NOT 3 gate strands (A_3 + B_3), 2: NOT 2 gate strands (A_2 + B_2 + Bridge), 3: DNA board only, 4: NAND full assembly (NOT 2 + NOT 3 + DNA board). B) Fluorescence readout of NAND assembly stored at 25 ℃ for up to two months and its native-PAGE assay showing NAND assembly stability .C) 12% dPAGE–8 M urea after NAND assembly gel extraction. Lane 1: ssDNA markers with their lengths, in nucleotides, specified; 2–10: individual ssDNA components of the NAND assembly; 11: DNA board; 12: NAND assembly before PAGE extraction. 13: NAND assembly after PAGE extraction. Blue arrowheads indicate the mobility of B_2.

2.3.4 OR Logic circuit (4J YES + 4J YES)

We developed a OR logic circuit by exploiting the connectivity of two 4J YES logic gate modules. In OR Boolean logic, digital output 0 is achieved when either one or both inputs are digital 1 (Figure 13A, left). Integrating both 4J YES gates (YES 4 + YES 5) on the DNA board allows their optimal connectivity through nucleic acid relayed binding where the output sequence of YES 5 binds as input to YES 4 (Figure 13A, right). In this arrangement, the DNA nanostructure is expected to perform as a two-bit OR logic circuit where the output sequence is produced due to the direct binding of input 4 to YES 4 or due to the relayed output of YES 5 when input 1 is bound. When both inputs are added to the solution, the output digital 1 value can be produced due to the coexistence of any of two molecular-input binding events (Figure 13C middle and right). Gel electrophoresis shows that full assembly of the OR logic circuit results in a slower mobility than the DNA board alone due to the increased molecular weight (Figure 13B).

The fluorescence assays show the correct digital response of the OR logic circuit (Figure 13D-E). An experimental threshold (red dashed line in Figure 13D) for the differentiation of output digital 1 and digital 0 was established based on the average signal of YES 4-output 0 plus three times its standard deviation. Similarly to IMPLY and NAND logic circuits, we evaluated the stability of the OR logic circuit assembly for up to two months. Figure 13F shows the robust performance of the OR assembly under the different input combinations.

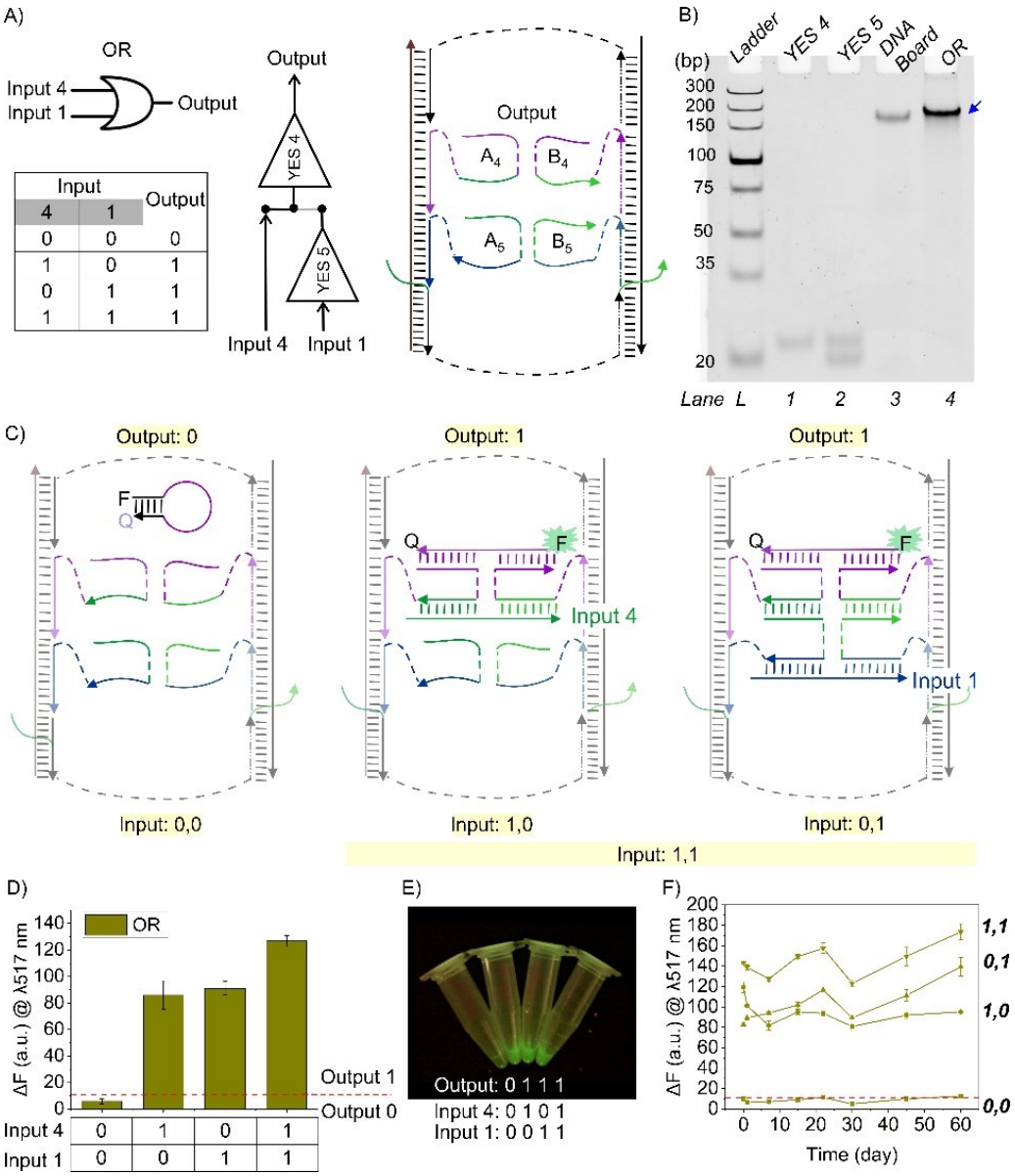

Figure 13. YES 4 + YES 5 = OR. A) OR truth table (left) Localization and connectivity of YES 4 and YES 5 on the DNA board (right). B) 8% native PAGE–50 mM MgCl2 results. Ladder: dsDNA markers with their length, in base pairs, indicated to the left, YES 4: gate strands (A_4 + B_4), YES 5 gate strands: (A_5 + B_5), DNA board and OR full assembly: (YES 4 + YES 5 + DNA board). The blue arrow indicates the fully assembled OR logic circuit. C) Molecular structural changes in the OR nanostructure for the four Input 1/Input 2 combinations: digital inputs 0, 0; 1, 0; 0, 1; 1, 1. D) Fluorescence of OR upon excitation at 485 nm. Red dashed line represents an experimental threshold, which was calculated as the average fluorescence of YES 4's output 0 plus three standard deviations. E) Visual fluorescence of OR. F) Fluorescence readout of OR assembly stored at 25 ℃ for up to two months.

2.3.5 Developing an education kit to promote the technology

Pioneering research, such as DNA nanotechnology, recombinant DNA, and CRISPR, is contributing to the transformation of biology-related disciplines.[120] Therefore, increased exposure of students to vanguard science is becoming a part of academic curriculums in high school and undergraduate programs.[120,121] Following this effort, forefront scientific approaches are framed for their introduction in teaching laboratory experiments allowing students to learn the competent concepts and technical skills.[122–126] For biochemistry and molecular biology students, early engagement in understanding cutting-edge technologies can motivate and increase their preparation for later graduate studies and research.[127,128] Therefore, we developed and implemented a laboratory experiment that introduces basic concepts for building DNA molecular computers and their potential implications for cancer diagnostics.

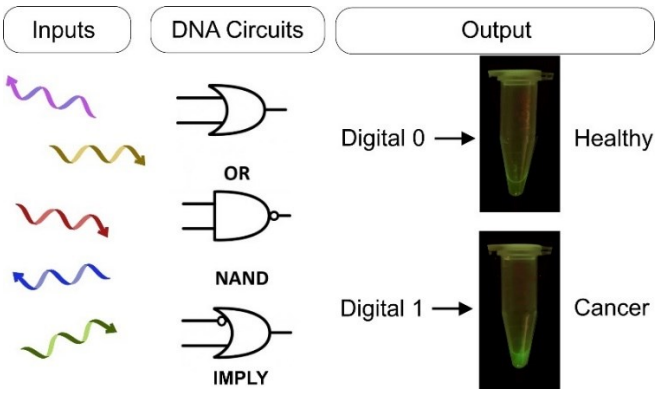

Figure 14. DNA molecular circuits for microRNA-based diagnostics. microRNAs are recognized as inputs by the DNA molecular circuits OR, NAND, and IMPLY where their analysis results in two possible outputs: Digital 0 (miRNA(s) correspond to a healthy condition) or Digital 1 (microRNA(s) correspond to a cancerous condition). The output readout for all DNA circuits is done through fluorescence intensities, where low fluorescence (Digital 0) and high fluorescence (Digital 1).

The laboratory experience consisted of four activities (1- Pre-test, 2- Lecture, 3- Experimental work, and 4- Post-test), which aimed at constructing the OR, IMPLY, and NAND Boolean logic circuits (sections 2.2-2.3) and using them to classify mixtures of microRNA biomarkers as indicators of healthy or cancerous conditions (Figure 14). The laboratory activity provides students with a learning experience on DNA molecular computing which is a multidisciplinary technology. Table 4 lists the specific learning objectives and outcomes.

To emphasize the relevance of DNA molecular computing as a biomedical tool, the DNA circuits were designed to recognize as inputs microRNAs (miRs) correlated with the diagnosis of hepatocellular carcinoma (HCC), one of the most common types of liver cancer.[129] This practical relevance is an important component of the learning experience,[130] that provides students with an outlook on the real-world application of the topic/skills learned.[131,132] miRs are non-coding RNA of a short length (18-25 nucleotides) lacking secondary structures in their mature form.[133] miRs have been found to regulate processes like RNA gene expression/silencing and as signaling molecules of intercell communication. In their mature form, they can be found either in the cellular matrix or circulating in plasma.[133,134] These features make them attractive candidates as biomarkers in the diagnosis of diseases. In cancer, more than one miR can be abnormally overexpressed and/or underexpressed. The precision of the diagnosis can be improved by considering as many miRs as possible.[134] However, analyzing multiple miRs (each with different aberrant expression levels) can be a challenging task. We selected miRs whose over and underexpression have been correlated with the development, tumor growth, and metastasis of HCC.[129,135,136] The following synthetic miR HCC markers were given to the students: hsa-miR-221-3p (Input 1), hsa-miR-409-3p (Input 2), hsa-miR-21-5p (Input 4), and the DNA complement of hsa-miR-221-3p (Input 3).

Table 4. Learning objectives and outcomes.

Objectives	-To learn the concepts of Boolean logic gates, molecular computing, DNA logic gates, MB probe, miR, and molecular diagnosis of hepatocellular carcinoma. -To predict the output of DNA logic circuits based on their Boolean truth table. -To construct DNA logic circuits with OR, NAND, and IMPLY Boolean logic. -To use DNA logic circuits to classify mixtures of miR markers as indicators of cancerous or healthy conditions. -To understand the principles of fluorescence-based MB probes.
Outcomes	-Students will be able to describe and apply the key concepts of Boolean logic gates, molecular computing, DNA logic gates, MB probe, miR, and molecular diagnosis of hepatocellular carcinoma. -Students will be able to interpret Boolean truth tables and predict their output. -Students will gain the technical skills to construct, test, and report the readout of DNA logic circuits. -Students will be able to discriminate between a cancerous or healthy condition based on the response of DNA logic circuits to the mixtures of miR markers. -Students will be able to explain fluorescence phenomena based on the states of MB probes.

The OR logic circuit was designed to recognize the selected overexpressed miR, while NAND logic circuit could identify an underexpressed miR. IMPLY logic circuit could bind to one overexpressed and one underexpressed miR. During the lecture (SI, lecture slides), we introduced miRs biological background and how digital values could be assigned to their under and over-

expression during testing with each DNA logic circuit. To simplify interpretation of the DNA circuits' response, the sample was classified as "cancerous" state if the miR input(s) triggered a high fluorescence signal. Conversely, low fluorescence indicated a "healthy" state. The fluorescent readout was either visually observed by using a blue-LED flashlight and UV/Blue light blocking goggles or measured with a spectrofluorometer. All the materials students needed were packed in individual kits as shown in Figure 15A and C. To improve the visual detection experience, a fluorometric box made out of black cardstock paper was provided to hold the different input combination samples for simultaneous irradiation and visualization (Figure 15B).

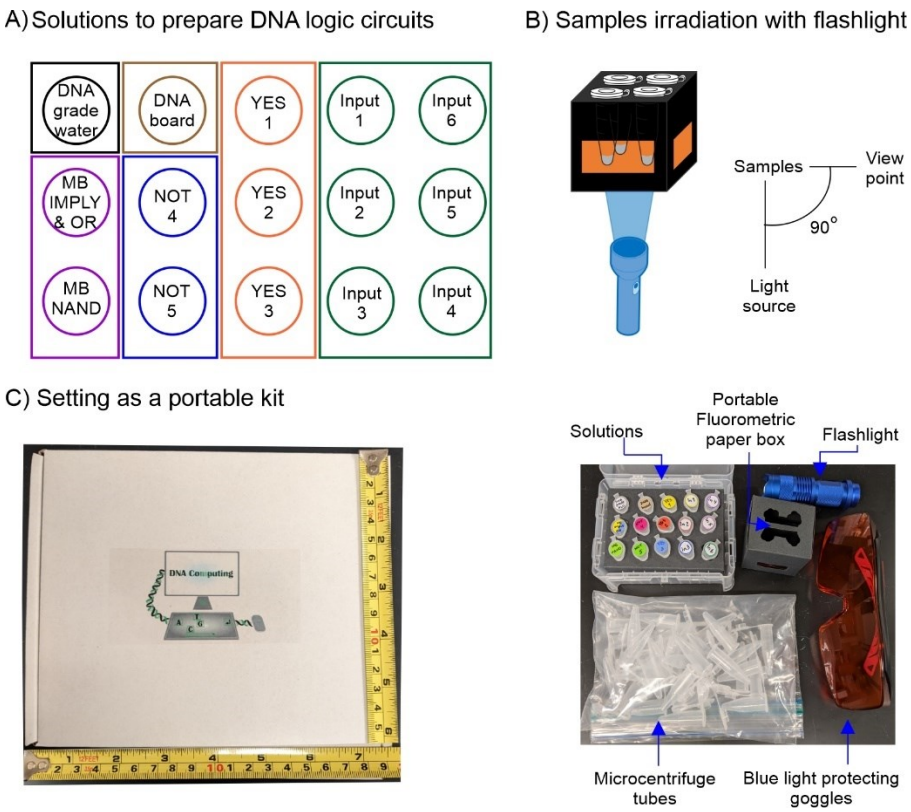

Figure 15. Setting up the materials and reagents. A) Arrangement of 15 different microcentrifuge tubes (represented by circles) filled with solutions needed for constructing and testing the three DNA logic circuits: one tube with DNA grade water (black), one tube containing assembled DNA board (brown), three tubes with different YES gates (orange), two tubes with different NOT gates

(blue), two tubes with the MB probe solutions to report the output of IMPLY/OR circuit and NAND circuit (purple), and six tubes containing individual inputs (green). B) A tube-holder box made of black cardstock paper for holding samples containing four different input combinations of one DNA logic circuit. The samples are irradiated with a blue LED flashlight for output visualization at a 90-degree angle. C) All necessary materials and reagents can be conveniently packaged into a 19x16x8 cm box as a portable education kit for the DNA molecular computing activity.

The student assessment in achieving the learning objectives was done under IRB-approved protocol (IRB ID: 00006043). The laboratory experience was offered twice with a total of 9 volunteers (4-5 volunteers per session). The population of volunteers consisted of undergraduate students from chemistry, biochemistry, biotechnology, and biomedical sciences programs in their freshman to senior academic levels and current members of research laboratories from our institution. The recruitment was done by extending a formal invitation directly to the students or indirectly through the research laboratory advisors. Each session was scheduled based on the most voted meeting time by students who accepted the invitation. The volunteers participated as active learners and simultaneously shared their thoughts and recommendations for improving the learning experience.

Due to the two methods for fluorescence detection, students in the first session used a spectrofluorometer, and students in the second session used a hand-held lamp. We observed the spectrofluorometer challenged the students to numerically discriminate digital output 0 from digital output 1 since the fluorescence intensity values were variable. Therefore, we specified that digital output 0 would be at least 3-fold lower than digital output 1 The group that used a hand-held lamp had less struggle assigning the digital values to the fluorescence intensities. However, to ensure the effectiveness of this method, we provided a fluorometric box made of black cardstock

(Figure 15B). Students acknowledged that this tool was helpful during the data collection and interpretation steps.

From the first session, 4 of 5 volunteers successfully constructed and tested all DNA logic circuits (Figure 16, left). The pre and post-tests gave an average score of 69% and 82%, respectively (Figure 16, right), showing a 13% increase. The pre-test high average score showed that students from this session had a degree of familiarity with the concepts. From the post-test scores, we observed that students' knowledge level was normalized after the laboratory class. From the second session, 2 of 4 students successfully constructed and tested all DNA logic circuits while at least one of the DNA logic circuits failed for the other 2 students (Figure 16, left panel). Nonetheless, the students with incorrectly responding DNA logic circuits readily identified or suggested an explanation for the corrupted readout, which gave insights into students' understanding of the taught concepts to discriminate erroneous data. The average scores for the pre- and post-tests were 45% and 64%, respectively (Figure 16, right), showing a 19% increase. The pre-test low average score showed that students were less familiar with the concepts than students from the first session. Students achieved scores equal to or above the pre-test average score and the highest score of 90% in the post-test. From this session, students mostly engaged in asking questions about challenges in developing the technology and its usage with actual patients. Overall, students determined which inputs would trigger a readout interpreted as "cancerous" or "healthy". However, students overlooked using the terms underexpression or overexpression when asked about the miRs expression level based on the DNA logic circuit response.

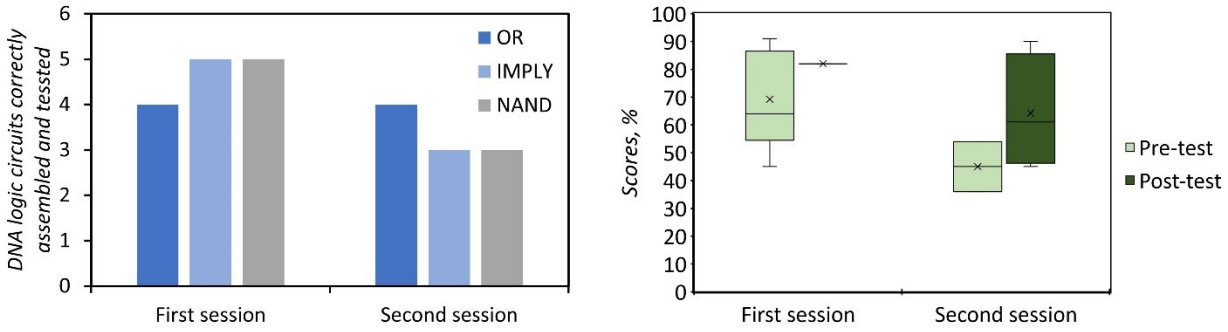

Figure 16. Students' experimental and theoretical outcomes of the laboratory activity. The left panel shows the number of DNA logic circuits correctly assembled and tested in the experiment by a total of 5 students in the first session and a total of 4 students in the second session. The right panel shows the pre- and post-test scores achieved by students in both sessions.

The achievement of the learning objectives and outcomes was assessed based on students' communication with the instructor, ability to correctly assemble and test the DNA logic circuits, the assessment of students' conclusions, and students' performance on the pre-test and post-test. Most students gained knowledge of the concepts taught and predicted the expected outputs for the DNA logic circuits based on their truth tables. Most students succeeded in experimentally constructing and testing the DNA logic circuits and correctly correlated the fluorescence readout with the diagnostic outcome. Regardless of the fluorescence detection method, students correctly described the principles of MB probes, such as MB probe conformational states based on fluorescence intensity and were exposed to spectrofluorometry concepts such as incident light, wavelength selection, and light filters.

2.4 Conclusions

One common paradigm in developing a molecular computer follows the path established by the semiconductor computer technology. This includes designing a functionally complete sets

of Boolean logic gates, connecting them in circuits by integrating into a common platform, powering using (bio)chemical reactions, and achieving an easily readable signal for convenient communication with a human operator.[47,94] Applications of such computational systems in controlling gene expression and in diagnosing infectious diseases and cancer have been envisioned.[49,137–140] Thus, computers made of molecules can be explored for the application of well-developed computational living systems.

This study demonstrates that molecular (DNA) computational systems may offer opportunities unrealized in electronics. Indeed, an electronic set of YES and NOT gates has never been considered as a complete set of Boolean gates. In this work, we demonstrated for the first time that YES and NOT gates, or two NOT gates made of DNA, can be connected in a circuit that fulfills functionally complete gates, IMPLY and NAND. This was possible because the 4J YES 1 gate in IMPLY and 4J NOT 3 in the NAND gate recognized either the oligonucleotide input or the outputs of the downstream gates; the coexistence of these two distinct modules is a feature that is absent in the majority of other devices that fulfill the function of Boolean logic gates.

4J YES, and NOT gates preserved their Boolean truth table by binding to only one input at a time either an input externally added to the DNA circuit, or an input relayed from the downstream gate (Figure 9,11, and 13). Since both IMPLY and NAND functions are sufficient to make a circuit of arbitrary complexity, we concluded that singleton {NOT} and doubleton {YES; NOT} gates can act as functionally complete sets in DNA-integrated computational circuits.

Therefore, we can conclude that two DNA 4J gates with YES and NOT Boolean functions can be connected to make IMPLY, while two NOT gates can make a NAND function. Theoretically, a computational circuit of any complexity can be built only from this set of DNA

logic gates. This opens a route to building computational circuits of arbitrary complexity from simple YES and NOT DNA logic gates. This modular connectivity could ease the burden of developing new architectures when realizing new Boolean circuitries. Therefore, while developing molecular logic gates, we should look for opportunities that are unexpected from our experience with electronic computers.

Furthermore, the educational kit allowed students to follow the progress of building DNA molecular circuits from individual DNA logic gates and to be familiar with new non-conventional avenues in constructing DNA molecular circuits as we discussed above. The experiment is versatile and can be implemented in different classroom settings by offering visual observation or quantitative measurement of the fluorescence readout. It uses non-toxic and inexpensive reagents. Although the two-session pilot testing was performed with a few student volunteers, they yielded positive feedback and proved it to be an engaging experiment driving students' curiosity to know more about this novel technology.

CHAPTER THREE: MODULAR DNA BOARD FOR MULTILEVEL LOGIC CIRCUITS

3.1 Introduction

In the pathway of scaling up the complexity of integrated DNA circuits (DNA ICs), the number of cascading 4J DNA logic units achieving effective communication is an important parameter. In Chapter One section 1.3, we introduced the challenges of increasing the number of cascading logic computing units and the limitations faced by currently available DNA scaffolding systems reported in the literature. One of the challenges of cascading 4J DNA logic units is their low stability (Figure 17A-B) which can be attributed to the high entropy penalty, weak binding strength, and the multiple junctions across the cascading units. Therefore, their spatial localization on a DNA board aids in increasing the local concentration of the 4J logic gate components and stabilizing the cascading junctions of the multiple 4J units. In chapter two, we introduced the DNA board as a nanostructure made from assembling four single strands of DNA (Rail 1, Rail 2, Staple 1, and Staple 2) with a ssDNA region to anchor two 4J DNA logic gates. This DNA board is a novel nanostructure developed under the scope of this dissertation as an alternative scaffolding system that is considered to provide the following features: i) adjustable size based on the number of computing units anchored, ii) reduced number of constituents to minimize misassembling, iii) connectivity with one or more DNA board modules, and iv) directed spatial orientation of the computing units. Each of these features has not been attributed to previously proposed DNA board systems.

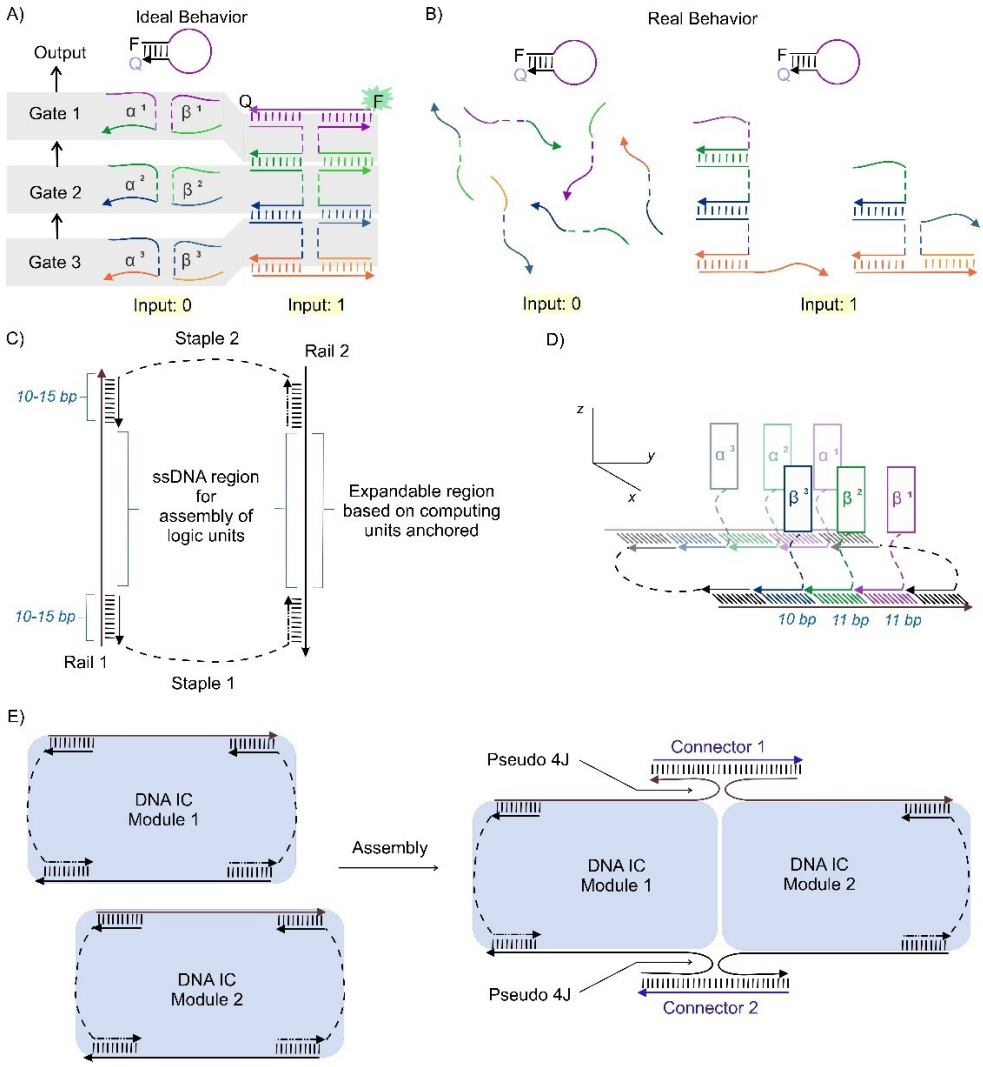

Figure 17. Scaling up of 4J DNA molecular circuits. Scheme in A) shows a desired "ideal" structural assembly when cascading multiple 4J DNA gates each composed of two fragments: α and β (left side) that are free in solution when input is 0. When input equals 1 the binding of each complementary fragment is triggered resulting in a cascade of 4Js. However, the arrangement of each 4J gate component into such ordered nanostructure faces limitations, and B) shows a more realistic scenario of incomplete cascading structures. C) Our proposed DNA board is composed of rail 1 and rail 2 assembled with staples 1 and 2 by complementary binding of 10 -15 bp. The ssDNA region located at the center of the DNA board is designed for the localization of computing components and its length can be customized to the number of computing components. D).A 3D representation of the DNA board localizing three 4J logic gates shows that a 4J component (α and β) anchored to the rails must perform one B-DNA helical turn for parallel alignment with the other 4J components. E) scheme shows how different DNA board modules can be integrated into a new whole unit for scaling up DNA ICs.

Here we explore the expanding capacity of the DNA board for the localization of more than two 4J DNA logic gates and determine the number of computing units that can be cascaded before the signal dissipates. To allow efficient communication among 4J logic gates, the spatial localization of each complementary fragment (e.g. β^1 - β^2 and β^2 - β^3 or α^1 - α^2 and α^2 - α^3) must be aligned parallel to the z-axis in a 3D space (Figure 17D). To achieve this spatial alignment, the length of the rail binding fragment for each 4J logic gate component was purposely set to perform one B-DNA helical turn, which corresponds to 10-11 nt (Figure 17D). If the rail binding length of the 4J units is lower or higher than 10-11 nt the alignment of each cascading unit is gradually shifted to the east or west from the z-axis, thus leading to partial delocalization and their communication can be limited by steric constrains. Therefore, the overall length of the DNA board rails expands by 10 to 11 nt per 4J logic gate meant to be anchored to the rails. Here, we propose and investigate this feature of adjustable befitting length to provide a customizable DNA board.

Furthermore, we propose a structural approach for the integration of two or more DNA board modules that can facilitate the scaling up of DNA ICs from already available/constructed DNA ICs units. Inspired by the manufacturing approaches of Si-based circuits in which scaling up complexity is achieved by the integration of multiple motherboard units, here we propose the assembly of two DNA ICs modules by triggering the formation of a pseudo 4J junction by a connector ssDNA that binds the staple complementary fragments from the rails of two different DNA ICs modules (Figure 17E).

3.2 Materials and Methods

3.2.1 Materials

DNase/protease-free water was purchased from Fisher Scientific Inc. (Pittsburg, PA) and used for all buffers and oligonucleotide stock solutions. MgCl2 (1 M solution) was purchased from Thermo Scientific (Waltham, MA), 1M Tris-HCl pH 7.4 buffer from KD Medical (Columbia, MD), and Triton X100 from Sigma-Aldrich (Burlington, MA). All oligonucleotides were custom-made by Integrated DNA Technologies, Inc. (Coralville, IA), and their stock solutions were prepared by resuspension in water and stored at – 20°C until use. The concentrations of the oligonucleotides' stocks were determined from the Beer-Lambert equation, for which absorbance at 260 nm was measured with a Thermo Scientific Nanodrop One UV-Vis Spectrophotometer, while the corresponding extinction coefficients were determined using OligoAnalyzer 3.1 software (Integrated DNA Technologies, Inc.). Fluorescence assays were performed with Perkin Elmer LS 55 Fluorescence Spectrometer, Deuterium Lamp, and with Agilent Cary Eclipse Fluorescence Spectrometer, Xenon Lamp. Gel electrophoresis experiments were performed using BioRad electrophoresis equipment (Hercules, CA), and visualized using BioRad Gel Doc XR+.

Table 5. List 1 of Oligonucleotides used in Chapter Three studies.

Name	Sequences
DNA Board Module 1	
4J Rail 1	CAC TCT AGT TTA CAG/iSp9/ G ATC GTA TCA CCT ATC GTG TT TTG TCG CTGA CAC CAC CT GAC CCA TC GTA TCG CTT CCT CTATG

Name	Sequences
4J Rail 2	CTGAC TGAAT GAG CT CTA CA GA CGA CTA CAG C TGC AGT ACC AC CGT TAG TCA ACT CACT CTG /iSp9/ GT ACTT TCT ACT AAC
4J Staple 1	ATTCA GTCAG /iSp18//iSp18/ CATAG AGG AAG
4J Staple 2	CTG TAA ACT AGA CTG /iSp18//iSp18/ GTT AGT ACA AAGT AC
Blck 1A	CGA TAC GAT GG
Blck 1B	TGT AGA GCTC
Blck 2A	GTC AG GTG GTG
Blck 2B	CTG TAG TCG TC
Blck 3A	TCAG CGA CAA
Blck 3B	GGT ACT GCA G
Blck 4A	GA CAC GAT AGG
Blck 4B	TGA CTA ACG GT
Blck 5A	TGA TAC GAT C
Blck 5B	CGG AGT GAG
YES 1	
1A	TCACCTGG /iSp9/ CATGCAAG /iSp9/ CGATAC GATGG
1B	AGTAG AGCTC /iSp9/ GCCTAACA /iSp9/ ACGTACGA
YES 2	
2A	CTTGCATG /iSp9/ TCTCCATG /iSp9/ GTCAG GTGGTG
2B	CTGTA GTCGTC /iSp9/ TACCCACT /iSp9/ TGTTAGGC
YES 3	

Name	Sequences
3A	CAT GGAGA /iSp9/ AT GGT TGC /iSp9/ TCAG CGA CAA
3B	GGTAC TGCAG /iSp9/ ACG TTG GA /iSp9/ AGT GGG TA
YES 4	
4A	GCA ACC AT /iSp9/ GTCTCAG G /iSp9/ GA CAC GAT AGG
4B	TGACTA ACGGT /iSp9/ CAAGTTAGGG /iSp9/ TC CAA CGT
4vi	TGA CTA ACG GT /iSp18/ CAA GTT AGG /iSp18/ TC CAA C
YES 5	
5A	CCTGAGAC /iSp9/ TGTCAGTG /iSp9/ TGATA CGATC
5B	CGGAG TGAGT /iSp9/ CTTGTGTTG /iSp9/ CCTAACTTG
5Avi	T GAG AC /iSp9/ TG TCA GTG /iSp9/ TGA TAC GAT C
5Bvii	CGGAG TGAGT /iSp9/ CTT GTG TTG /iSp9/ CCTAACT
MB probes	
MB 1	/FAM/CCT CGT ACG TCC AGG TGA GG/BHQ1/
MB 2	/FAM/ CCGGCCTAACA CATGCAAG CCGG /BHQ1/
MB 3	/FAM/CTT GCT ACC CAC TTC TCC ATG CAA G/BHQ1/
MB 4	/FAM/ C ACG TTG GA AT GGT TGC GTG/BHQ1/
MB 5	/FAM/ CCGC A CAAGTTAGG GTCTCAGG G GCGG/BHQ1/
Inputs	
I 1	CTTGCATG TGTTAGGC
I 2	CAT GGA GAA G TGG GTA
I 3	GCA ACC AT TC CAA CGT

Name	Sequences
I 4	CCTGAGACCCTAACTTG
I 5	CACTGACACAACACAAG

Each sequence is entered as 5'→ 3'; iSp9 and iSp18 are oligoethylene glycol spacers 9 and 18 from Integrated DNA Technologies (IDT); FAM and BHQ1 correspond to 6-carboxyfluorescein and 3'Black Hole Quencher-1 respectively; /5'-phos/ represents a 5' terminal phosphate group and r indicates ribonucleotide. Extinction coefficients were obtained from OligoAnalizer online calculator OligoAnalyzer from IDT website. *List 2 for sequences corresponding to the second module of 4J gates and DNA board can be found in Appendix B

3.2.1 Assembly of DNA logic gates with DNA board

All DNA oligonucleotides corresponding to the DNA logic gates and DNA board intended for assembly into the target DNA logic circuit were mixed at 200 nM in equimolar ratios in a buffer mix containing 100 mM Tris-HCl at pH 7.4, 100 mM MgCl2, 0.06 % Triton X100; followed by vortex and centrifuged to make sure all the solution was dragged down. The samples were annealed by placing them in a water bath at 95 ℃ for 2 min and slowly cooling down to 22 ℃ within 8 h.

3.2.3 Fluorescence assays and data analysis

After assembly, a master mix solution was prepared containing molecular beacon (MB) probe solution and the DNA assembly. From this master mix, aliquots were dispensed in individual microcentrifuge tubes for the addition of the different inputs, followed by incubation at room temperature (22-25 ℃) for 20 min. The fluorescence emission was read at 517 nm after excitation at 485 nm. The final concentration of the reading samples was the following: 100 nM DNA logic gate assembly, 50 nM MB probe, 200 nM input, 50 mM Tris-HCl at pH 7.4, 50 mM MgCl2, 0.03 % Triton X100.

Average and standard deviations were calculated from three independent samples. To normalize the fluorescence response of each output signal, we subtracted the average fluorescence response of a MB only solution. Each graph plots the average fluorescence difference *(ΔF): fluorescence output signal – fluorescence MB signal*; Error bars represent the standard deviation from three independent samples.

3.3 Results and Discussion

3.3.1 Characterization of individual 4J gates in free diffusion vs spatially localized

To demonstrate the expanding capacity of our DNA board, we increase the length of the ssDNA inner region to localized five different 4J YES gates. This DNA board, here called 4J DNA board is also composed of four ssDNA (4J Rail 1, 4J Rail 2, 4J Staple 1, and 4J Staple 2), similar to the DNA board from Chapter Two. For later assembly with another 4J DNA board module, polyethylene glycol linkers (dashed line Figure 18C) were internally added between the binding regions for 4J Staple 2 and YES 5. Each 4J YES gate was designed with unique input binding and output-producing sequences and for inter-gate communication the output sequence of an upstream gate is relayed as input for a downstream gate (e.g. YES 5's output becomes YES 4's input). For this study, all inputs used are synthetic deoxyribo oligonucleotides whose sequences were randomly generated. Each A and B 4J YES gate component is about 14 to 16 nt of length (8 nt for input binding fragments and 6-8 nt as output producer). The fluorescence readout produced by each 4J YES gate can be determined by adding a complementary MB probe to the target gate. Figure 18 shows the fluorescence response of each 4J YES gate individually tested in free diffusion (Figure 18B) or spatially localized on the 4J DNA board (Figure 18D). From the results, we

observed a significant increase in the amplitude of fluorescence change (ΔΔF) between Output: 0 and Output: 1 samples when 4J YES gate components are spatially localized in comparison to free diffusion components.

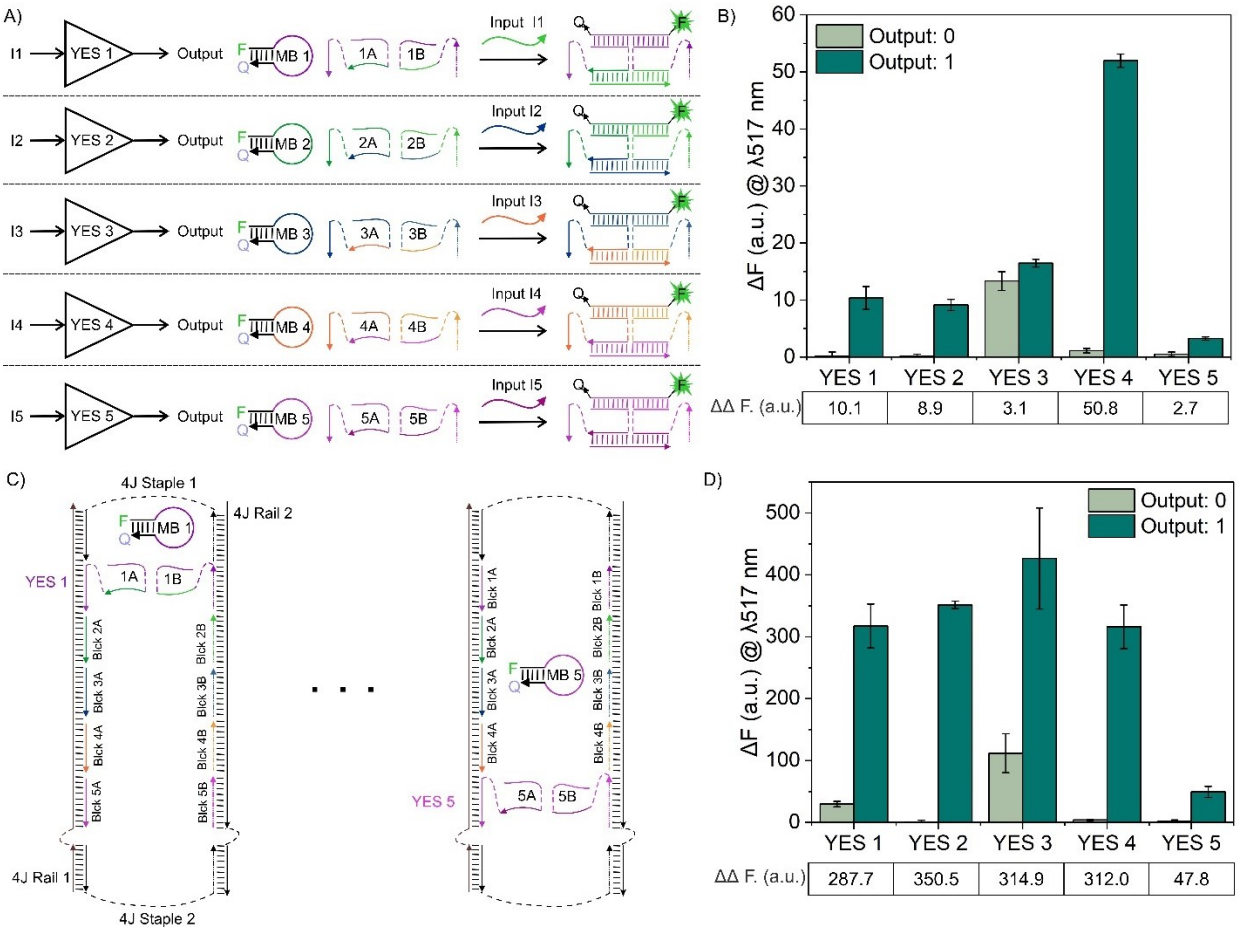

Figure 18 Fluorescence readout of individual 4J YES logic gates. A) Five different 4J logic gates were design with YES Boolean logic (left), the output sequence of each 4J YES gate requires the appropriate complementary MB probe for fluorescence readout as shown in B) where the response of free diffusion 4J YES gates were measured. C) shows a DNA board that has been expanded to allocate five 4J gate. Individual localization of each 4J gate requires the use of blocker strands (Blck 1A-5A and Blck 1B-5B) to cover the empty fragments meant for binding other gates. D) Fluorescence readout of individual 4J YES gates localized on the 4J DNA Board. Measurements were performed on LS55 Perkin Elmer instrument.

Although the same fluorophore and quencher tags were used for all MB probes, their different sequences in the loop and stem confer slightly different thermodynamics. Due to this diversity of MB probes, we observed that the ΔΔF varies among each 4J gate.

3.3.2 Cascading 4J gates free diffusion vs spatial localization

In Chapter One, we discussed that one of the major challenges in cascading DNA molecular logic gates is the signal dissipation. To determine the physical limits on wiring 4J DNA logic gates, we use the simplest of our 4J Boolean logic gates (YES). 4J YES gate is the lowest in terms of computing components and its input processing does not require any type of strand displacement reaction (Figure 7A), for these reasons we consider the 4J YES gate as an ideal candidate to determine the signal propagation borderline of 4J logic gates cascaded in series. Each upstream 4J YES gate cascades its output sequence to its neighboring downstream 4J YES gate. For example, if three 4J YES gates are localized, the external input to be added will be Input I3. When I3 binds to YES 3, it triggers the localization of 3A and 3B blue fragments making the output sequence that is relayed as input of YES 2. Once 2A and 2B green fragments approach near each other, they make the second output sequence that is relayed as input of YES 1. Lastly, 1A and 2B purple fragments are close nearby from all the cascading binding events, the strength and stability of this localization lead to stretching of the MB probe and high fluorescence readout. Figure 19A shows the gradual localization of 4J YES gates on the 4J DNA board and indicates the input to be externally added accordingly to the upstream gate. In each cascading structure, YES 1 becomes the downstream gate releasing the output sequence that will be translated into a fluorescence readout due to its complementary binding with MB1.

We tested the cascading of five 4J YES gates where each 4J component was in free diffusion and when all components were spatially localized on the 4J DNA board. Our results indicate that cascading 4J YES gates with components in free diffusion is not possible (Figure 19B) since only YES 1 achieved a significant ΔF when output: 1. Initiating a cascaded between YES 1 and YES 2 to YES 1 up to YES 5 show a ΔΔF < 0.2 a.u. On the contrary, we observed a significant fluorescence response of output: 1 from each of the cascading 4J YES gates localized on the 4J DNA board (Figure 19C).

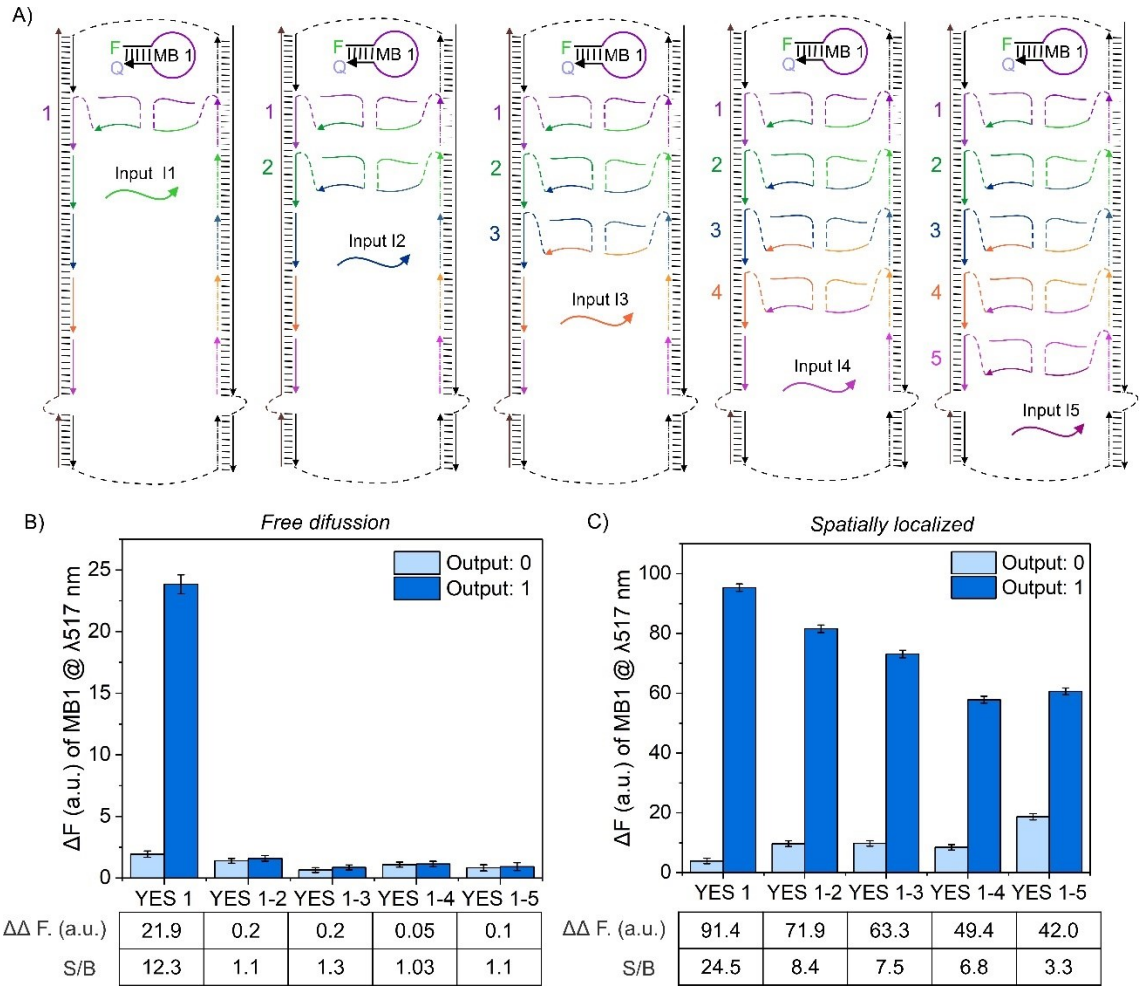

Figure 19. DNA IC Module 1 cascading five 4J YES gates. A) Scheme demonstrates the gradual localization of each 4J YES gate on the 4J DNA board to assess the strength of the signal relayed

from each unit. B) Fluorescence readout from a cascade of five 4J YES gates with free diffusion in the solution. C) Fluorescence readout from a cascade of five 4J YES gates spatially localized on the 4J DNA board. Measurements were performed on Agilent Cary Eclipse instrument

The results indicate that the 4J DNA board plays an important role in achieving effective inter-gate communication when cascading up to five 4J YES gates. In Figure 19C we observed that ΔF of output: 0 increases proportionally to the number of 4J YES gates added to the cascade. This increase in signal can be attributed to the short distance between gates (Contacted Gate Pitch, CGP) and the binding accessibility of the neighboring complementary fragments, thus resulting in signal leakage. On the other hand, ΔF of output: 1 increases disproportionally to the number of 4J YES gates added to the cascade, thus indicating signal dissipation. Both signal leakage and signal dissipation directly impact inter-gate communication and limit the scaling up of cascading units. To determine the degree of effective inter-gate communication, we employed Equation (1).

(1) $$S/B = \frac{\Delta F\ of\ Output{:}1}{\Delta F\ of\ Output{:}0} = \frac{Population\ of\ units\ with\ completed\ signal\ cascade}{Population\ of\ units\ with\ signal\ leakage}$$

Therefore, S/B correlates the degree of effective signal-propagating units with the degree of signal-leaking units and indicates the extent to which the population of signal-propagating units outnumbers the population of signal-leaking units. S/B can also be considered as a parameter to measure the degree of signal dissipation, e.g. if the number of signal-propagating units decreases S/B reduces indicating the loss of signal cascading power. Thus, if a DNA IC has a S/B=1 then 100% of its signal dissipates.

From the addition of each 4J YES gate to the cascade, we also determined the percentage of non-leaking activated DNA ICs units (ADU) using equation (2). Table 6 shows the ADU values obtained from cascading five 4J YES gates on DNA IC module 1.

(2) $$ADU = \frac{\Delta F\ of\ Output{:}\ 1 - \Delta F\ of\ Output{:}0}{\Delta F\ of\ Output{:}1} x100$$

Table 6. Percentage of non-leaking activated DNA IC units of Module 1

Cascading gates	YES 1	YES 1-2	YES 1-3	YES 1-4	YES 1-5
ADU	95.9	88.1	86.6	85.4	69.2

Figure 19C shows how S/B decreases as the number of cascading 4J YES gates increases. After the addition of the first cascading gate (YES 2), S/B reduces by 66%, this is not only due to the decrease in signal-propagating units but also due to the increase of signal-leaking units. Cascading all five 4J YES gates shows a ~5-fold increase of signal-leaking units in comparison to having only YES 1; However, for five cascading gates, the output:1's ΔF can be attributed to 69% of non-leaking DNA ICs fully completing the signal cascade up to YES 1 output:1 release. From these results, we observed that after cascading five 4J YES gates, S/B≠1 thus there is still room for increasing the number of cascading 4J YES units.

3.3.3 Integration of DNA ICs modules

To determine the signal propagation borderline of a 4J YES gate cascade and investigate the possibility of integrating two DNA IC modules, we designed a second DNA board anchoring

another set of five cascading 4J YES gates (Figure 20A). The output sequence given by the DNA IC module 2 is relayed as input of the upstream gate of module 1, resulting in a cascade of ten 4J YES gates (Figure 21).

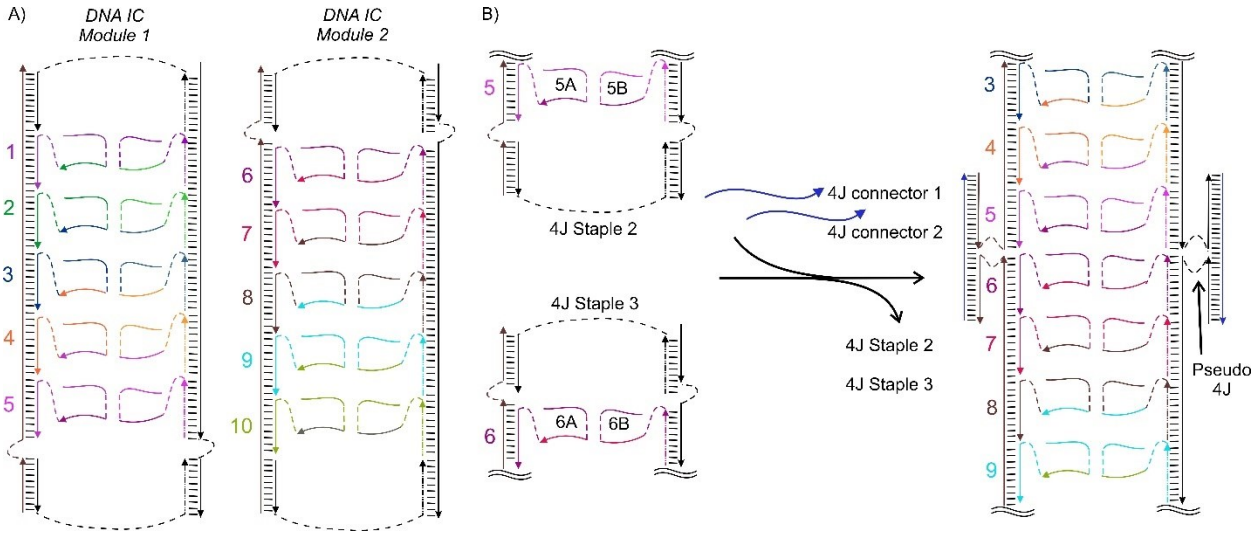

Figure 20 Connecting two DNA IC modules. A) Each DNA IC module holds five 4J YES in cascading. Module 1 holds YES 1 up to YES 5 and module 2 holds YES 6 up to YES 19. B) 4J staples 2 and 3 are replaced by 4J connectors 1 and 2 which join both DNA IC modules and the DNA IC cascade increases up to ten units.

The connectivity of the two DNA IC modules is achieved by removing the staple strands next to YES 5 and YES 6 and forming a pseudo 4J by crossover binding of a 4J connector ssDNA with the free staple binding fragments (Figure 20B). We experimentally tested the signal propagation of DNA IC module 2 (Appendix C, Figure 34) and the one from integrating ten 4J YES into a cascade (Figure 21).

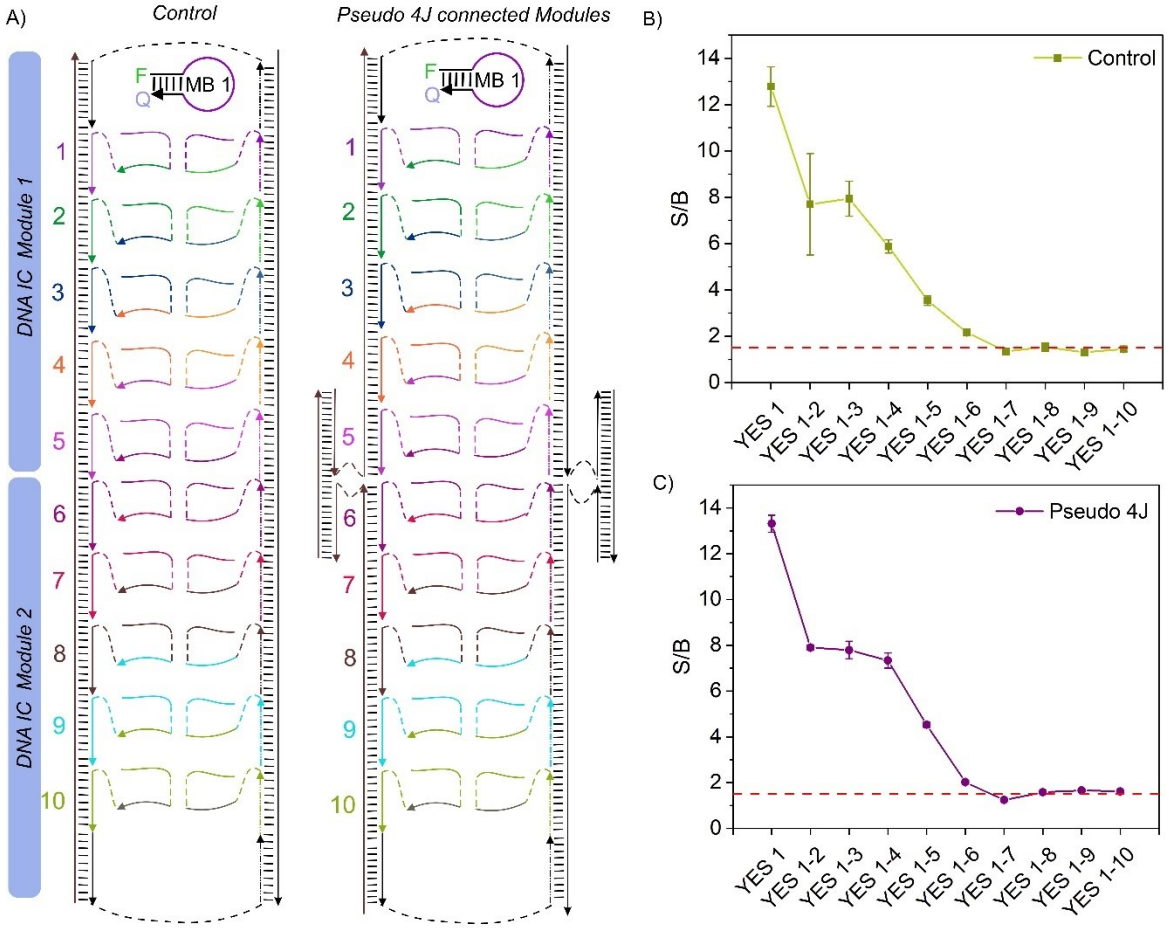

Figure 21.S/B of ten 4J YES gates cascades. A) shows DNA IC modules 1 and 2, each cascading five 4J YES gates; when integration occurs by joining each module via a pseudo 4J connection, the cascade scales up to ten 4J YES gates (left). A long DNA board was constructed as control. B) Fluorescence readout of the ten cascading 4J YES gates on a long DNA board control. C) Fluorescence readout of the ten cascading 4J YES gates on the pseudo 4J connected DNA board module 1 and module 2.

First, we integrated all ten 4J YES gates on a long DNA board to serve as a positive control when integration occurs from two different DNA board modules (Figure 21A). Figure 21B and C show the S/B profile achieved from both DNA board systems in gradually cascading 4J YES gates up to ten units. The results show that both systems have a similar S/B trace and after adding the seventh unit S/B= 1.5 remains almost constant. Therefore, we considered that in both systems the signal propagation and dissipation borderline meet after cascading seven 4J YES gates.

Interestingly, the S/B of YES 1 localized on the long DNA board was lower than the S/B achieved from the smaller DNA board holding five units (Figure 19C). However, after the addition of the YES 2 up to YES 5 the S/B profiles on Figure 21B and C match with the observed in Figure 19C. Nonetheless, the result suggests that the length of the DNA board influences the output response of the DNA IC, an influence not previously reported in the literature. From our literature review, DNA boards have been documented to influence the output achieved only in terms of the distance between gates (CGP) and not due to the size of the DNA board itself.

3.4 Conclusions

Integration of multiple 4J DNA logic gates without a DNA board is an unfavorable process attributed to the high entropy penalty, the weak binding strength of each complementary unit, and the instability of multiple junctions across the cascading units. Here, we showed that spatial localization of 4J logic gates is necessary for inter-gate communication and integration in larger circuits. Although the use of DNA boards to facilitate the integration of DNA logic units into circuits has been reported in the literature,[45,47,48,66,94] those nanostructures require a large number of ssDNA structural components that increases the probability of dis-assembly and non-incorporation, and there is no systematic region for anchoring the computing components thus limiting circuit layout. To overcome those limitations, here we proposed a novel DNA board composed of only four ssDNA components, the region for anchoring computing units is well-defined and can be expanded as necessary.

Different spatial distances for gates within a DNA board have been reported[45–48] reported to avoid signal leakage and to improve signal transmission. From those works the shortest CGP

reported corresponds to 5 nm (~ 1.5 B DNA helical turn), where diffusible protector strands and G-quadruplex minimize signal leakage from the communicating DNA gates. Here, we report a CGP of 3.4 nm (1 B-DNA helical turn), thus providing more room for increasing circuit density within a DNA board. Due to the two-component nature of the 4J gates, we minimize the spurious crosstalk of the computing units; however, in a cascade of only 4J YES gates signal leakage was still observed. To overcome that limitation, we challenged the binding strength limits of each 4J component and found that by reducing the binding affinity up to 50% (~ ΔG = -6.0 kcal/mol) signal leakage is minimized under our experimental conditions.

In this chapter, we introduced S/B as a parameter to determine the degree of signal-propagating units outnumbering the signal-leaking units. From this parameter, we observed that signal-propagating units outnumber signal-leaking units in a DNA IC cascading 4J YES gates. However, the population of signal-propagating units is dis-proportionally to the number of cascaded 4J YES gates and vice versa for signal-leaking units. Although our ten 4J YES gates wired did not reach S/B=1, it shows that after the seventh cascaded gate signal propagation and signal dissipation reached a plateau, and adding more cascading units seems to not affect this borderline.

Furthermore, we found that the output response of the 4J YES gates can be affected by the length of the DNA board based on our results from systematically expanding the size of the DNA board. We hypothesize that by increasing the length of the gate anchoring region the DNA board flexibility and torsional effects can influence the circuit performance. However, due to the modular features of this DNA board, it is possible to increase the rigidity of the nanostructure to mitigate the fluctuations in circuit performance when increasing the DNA board size.

Although cascading multiple units of 4J YES gates shown to be possible, we considered this type of inter-gate wiring not ideal in the pathway of scaling up DNA ICs. Therefore, other approaches like fan-out and signal amplification systems should be explored as alternatives for long cascades of closely localized computing units.

CHAPTER FOUR: KINETICS OF 4J DNA IC

4.1 Introduction

The spatial localization of DNA computing units on a DNA scaffold can improve circuit response and facilitate orthogonality in circuit design; thus, its use can increase DNA ICs' density. However, we found that increasing the number of integrated computing units increases the computing processing times. The slow-down in computation processes becomes a physical barrier to DNA ICs achieving optimal performance.[45,47,64] Although DNA boards can speed up the computation process of a DNA IC than its bulk counterpart, it still faces a slowdown as its circuit density increases. To speed up signal propagation from cascading units using gate motifs such as hairpins or strand displacement reactions, approaches such as dual rail input/output (different molecules encode bit-0 and bit-1),[50] and circuit parallelism (independent circuits in simultaneous operation)[47,81] have been suggested. The advantage of computing with 4J YES gates is that input and output do not require overcoming a preexisting secondary structure on the gate motif like hairpin or strand displacement reaction gates. Thus, the activation energy barrier for input binding a 4J YES gate is smaller and can lead to faster processing times. In cascading 4J YES gates, this feature can render faster kinetics than cascades built from DNA gates holding secondary structures.

The rate at which two nucleic acid (NA) fragments with Watson-crick complementary form a duplex proceeds as a second-order reaction.[141–144] This rate, also known as hybridization rate, is influenced by factors such as temperature and nucleic acid concentration.[145] The mechanism of NA hybridization has been proposed to consist of the two NA fragments: i) closing in proximity, ii) nucleating, and iii) zippering.[141–143] This mechanism applies when two NA strands are free in

solution; however, if the two complementary fragments are spatially localized near each other only the nucleation and zippering steps are involved.

DNA ICs and NA molecular devices commonly use molecular beacon (MB) probes to translate the output sequence into a visible readout. Introduced by Tyagi and Kramer,[111] MB is a single NA strand folded as a hairpin and tagged with a fluorophore and a quencher at opposite termini. MB probes are thoroughly used due to their NA sequence specificity, low background signal,[146] and easy monitoring. Although MB probes are ubiquitously employed in steady-state and kinetic experiments; they commonly face structural challenges such as multiple intramolecular secondary structures distorting their hairpin form.[147,148] Furthermore, these molecular readout systems are typically diffusing free and solution, a delocalization that can contribute to the observed computation times. Therefore, for kinetics of spatially localized NA the influence of diffusion and secondary structure of the MB and similar probes must be accounted for in NA hybridization rates.

To eliminate the kinetic contribution of an MB probe, we designed a reporter system that bounds to the DNA board, and it consists of two DNA strands: one tagged with a fluorophore (rA) and the second one (rB) tagged with a quencher (Figure 22C). rA and rB lack of any secondary structures under the experimental conditions. This reporter system was investigated on a two-cascading 4J YES gates DNA IC (module 1.2) and later used on a four-cascading 4J YES gates DNA IC (module 1.4).

4.2 Materials and Methods

4.2.1 Materials

DNase/protease-free water was purchased from Fisher Scientific Inc. (Pittsburg, PA) and used for all buffers and oligonucleotide stock solutions. MgCl2 (1 M solution) was purchased from

Thermo Scientific (Waltham, MA), 1M Tris-HCl pH 7.4 buffer from KD Medical (Columbia, MD), and Triton X100 from Sigma-Aldrich (Burlington, MA). All oligonucleotides were custom-made by Integrated DNA Technologies, Inc. (Coralville, IA), and their stock solutions were prepared by resuspension in water and stored at – 20°C until use. The concentrations of the oligonucleotides' stocks were determined from the Beer-Lambert equation, for which absorbance at 260 nm was measured with a Thermo Scientific Nanodrop One UV-Vis Spectrophotometer, while the corresponding extinction coefficients were determined using OligoAnalyzer 3.1 software (Integrated DNA Technologies, Inc.). Fluorescence assays were performed with Agilent Cary Eclipse Fluorescence Spectrometer, Xenon Lamp, and with a Applied Photophysics SX20 Stopped-Flow spectrometer incorporated with a Xenon Arc Lamp and a photodiode array for fluorescence detection.

Table 7. List of Oligonucleotides used in Chapter four studies.

Name	Sequences
DNA Board Module 1.2	
4J Rail 1.2	CCT ATC GTG TT TTG TCG CTGA CAC CAC CT GAC CCA TC GTA TCG CTT CGT CTATG
4J Rail 2.2	CTGAG TGAAT GAG CT CTA CA GA CGA CTA CAG C TGC AGT ACC AC CGT TAG TCA
4J Staple 1.2	ATTCA CTCAG /iSp18//iSp18/ CATAG ACG AAG
4J Staple 2.2	AA CAC GAT AGG/iSp18//iSp18/ TGA CTA ACG GT
DNA board Module 1.4	

Name	Sequences
4J Rail 1.4	CAC TCT AGT TTA CAG/iSp9/ G ATC GTA TCA CCT ATC GTG TT TTG TCG CTGA CAC CAC CT GAC CCA TC GTA TCG CTT CCT CTATG
4J Rail 2.4	CTGAC TGAAT GAG CT CTA CA GA CGA CTA CAG C TGC AGT ACC AC CGT TAG TCA ACT CACT CTG /iSp9/ GT ACTT TCT ACT AAC
4J Staple 1.4	ATTCA GTCAG /iSp18//iSp18/ CATAG AGG AAG
4J Staple 2.4	CTG TAA ACT AGA CTG /iSp18//iSp18/ GTT AGT ACA AAGT AC
Blck 1A	GTC AG GTG GTG
Blck 1B	CTG TAG TCG TC
Blck 2A	TCAG CGA CAA
Blck 2B	GGT ACT GCA G
Blck 3A	GA CAC GAT AGG
Blck 3B	TGA CTA ACG GT
Blck 4A	TGA TAC GAT C
Blck 4B	CGG AGT GAG
Bridge	CCT AAA ACT ACG ATT AGT AAG G
Blck 1Ab	GTC AG GTG GTG CCTTA CTA ATC
Blck 1Bb	GTA GTT TTAG G CTG TAG TCG TC
Blck 2Ab	TCAG CGA CAA CCTTA CTA ATC
Blck 2Bb	GTA GTT TTAG G GGTAC TGCAG
YES 1 and YES 1b	
1A	CTTGCATG /iSp9/ TCTCCATG /iSp9/ GTCAG GTGGTG

Name	Sequences
1B	CTGTA GTCGTC /iSp9/ TACCCACT /iSp9/ TGTTAGGC
1Ab	CTTGCATG /iSp9/ TCTCCATG /iSp9/ GTC AG GTG GTG CCTTA CTA ATC
1Bb	GTA GTT TTAG G CTG TAG TCG TC /iSp9/ TAC CCA CT /iSp9/ TGT TAG GC
YES 2 and YES 2b	
2A	CAT GGAGA /iSp9/ AT GGT TGC /iSp9/ TCAG CGA CAA
2B	GGTAC TGCAG /iSp9/ ACG TTG GA /iSp9/ AGT GGG TA
2Ab	CAT GGAGA /iSp9/ AT GGT TGC /iSp9/ TCAG CGA CAA CCTTA CTA ATC
2Bb	GTA GTT TTAG G GGTAC TGCAG /iSp9/ ACG TTG GA /iSp9/ AGT GGG TA
YES 3	
3A	GCA ACC AT /iSp9/ GTCTCAG G /iSp9/ GA CAC GAT AGG
3vi	TGA CTA ACG GT /iSp18/ CAA GTT AGG /iSp18/ TC CAA C
YES 4	
4Avi	T GAG AC /iSp9/ TG TCA GTG /iSp9/ TGA TAC GAT C
4Bvii	CGGAG TGAGT /iSp9/ CTT GTG TTG /iSp9/ CCTAACT
MB probes	
MB 1	/FAM/ CCGGCCTAACA CATGCAAG CCGG /BHQ1/

Name	Sequences
MB 1a	TGT AGA GCTC /iSp9//FAM/T CCGGCCTAACA CATGCAAG CCGG /BHQ1/
rA	/FAM/CA TGC AAG /iSp9/ CG ATA CGA TGG
rB	AGT AGA GCT C/iSp9/G CCT AAC A/BHQ1/
Inputs	
I 1	CAT GGA GAA G TGG GTA
I 2	GCA ACC AT TC CAA CGT
I 3	CCTGAGACCCTAACTTG
I 4	CACTGACACAACACAAG

Each sequence is entered as 5'→ 3'; iSp9 is oligoethylene glycol spacers 9 from Integrated DNA Technologies (IDT); FAM and BHQ1 correspond to 6-carboxyfluorescein and 3'Black Hole Quencher-1 respectively; /5'-phos/ represents a 5' terminal phosphate group and r indicates ribonucleotide. Extinction coefficients were obtained from OligoAnalizer online calculator OligoAnalyzer from IDT website.

4.2.2 Assembly of DNA logic gates with DNA board

All DNA oligonucleotides corresponding to the DNA logic gates and DNA board intended for assembly into the target DNA logic circuit were mixed at 200 nM in equimolar ratios in a buffer mix containing 100 mM Tris-HCl at pH 7.4, 100 mM MgCl2, 0.06 % Triton X100; followed by vortex and centrifuged to make sure all the solution was dragged down. The samples were annealed by placing them in a water bath at 95 ℃ for 2 min and slowly cooling down to 22 ℃ within 8 h.

4.2.3 Fluorescence kinetic measurements and data analysis

After assembly, a master mix solution was prepared containing molecular beacon (MB) probe solution and the DNA assembly. From this master mix, aliquots were dispensed in individual microcentrifuge tubes for the addition of the different inputs, followed by incubation at room temperature (22-25 °C) for 20 min. The fluorescence emission was read at 517 nm after excitation at 485 nm. The final concentration of the reading samples was the following: 100 nM DNA logic gate assembly, 50 nM MB probe and rA, 200 nM input, 50 mM Tris-HCl at pH 7.4, 50 mM MgCl2, 0.03 % Triton X100.

Average and standard deviations were calculated from three independent samples. Each graph plots the average fluorescence. The standard deviation from three independent samples are represented by a light-colored area around the line pathway. A biphasic exponential decay equation (3), where x= time, y = $F_{(x)}$, y_0= $F_{(plateau)}$, A_1 = $\Delta F_{(fast\ rate)}$, A_2= $\Delta F_{(slow\ rate)}$, t_1= time constant of fast rate, and t_2 = time constant of slow rate. From those parameters rate constants (k1 and k2) can be calculated based on equation (4), and individual half-lives based on equation (5). Equation (3) was selected based on ANOVA best fit to each of the kinetic graphs.

(3) $$y = y_0 + A_1 e^{-x/t_1} + A_2 e^{-x/t_2}$$

(4) $$k_1 = \frac{1}{t_1} \ and \ k_2 = \frac{1}{t_2}$$

(5) $$halflife = t_1 In2 \ and \ halflife_2 = t_2 In2$$

4.3 Results and Discussion

4.3.1 A localized reporter system for spatially localized 4J logic gates

First, we explored the influence of the molecular probe when i) free in diffusion, ii) attached to the DNA board, and iii) without any secondary structure to overcome. For the comparison of each system, we used a small DNA board anchoring two cascading 4J YES gates. YES 1 was designed to release the output sequence recognized by each of the probes (Figure 22). The results show that the observed computation times depend on the type of molecular probe used. The longer computation times were observed on the DNA IC using MB1 (Table 8).

The slow response of this system can be attributed to i) a higher activation energy barrier to dissociate the secondary structure of the MB's stem and ii) the kinetic contribution of diffusion. Due to these factors, YES 1 achieved a 90% increase in fluorescence signal at t ~1700 s (28 min) after input addition, also referred to as t_{90} (Table 8 and Figure 22). This computation time is comparable to the previously 4J YES gate operated in bulk.[149] From this comparison, it is important to consider that the differences in binding energies of the MB probe, input, and A and B strands might not reflect the effect on the localization of a 4J YES gate on the DNA board. When cascading two 4J gates, t_{90} is reduced by 7-fold; this speed-up can be attributed to the energy released from YES 1- YES 2 binding which helps overcome the activation energy barrier of MB's dissociation. However, the instability of the inter-gate 4J junction led to a 62% reduction in the population of signal propagating units completing the cascade, as shown in Figure 22A (right panel).

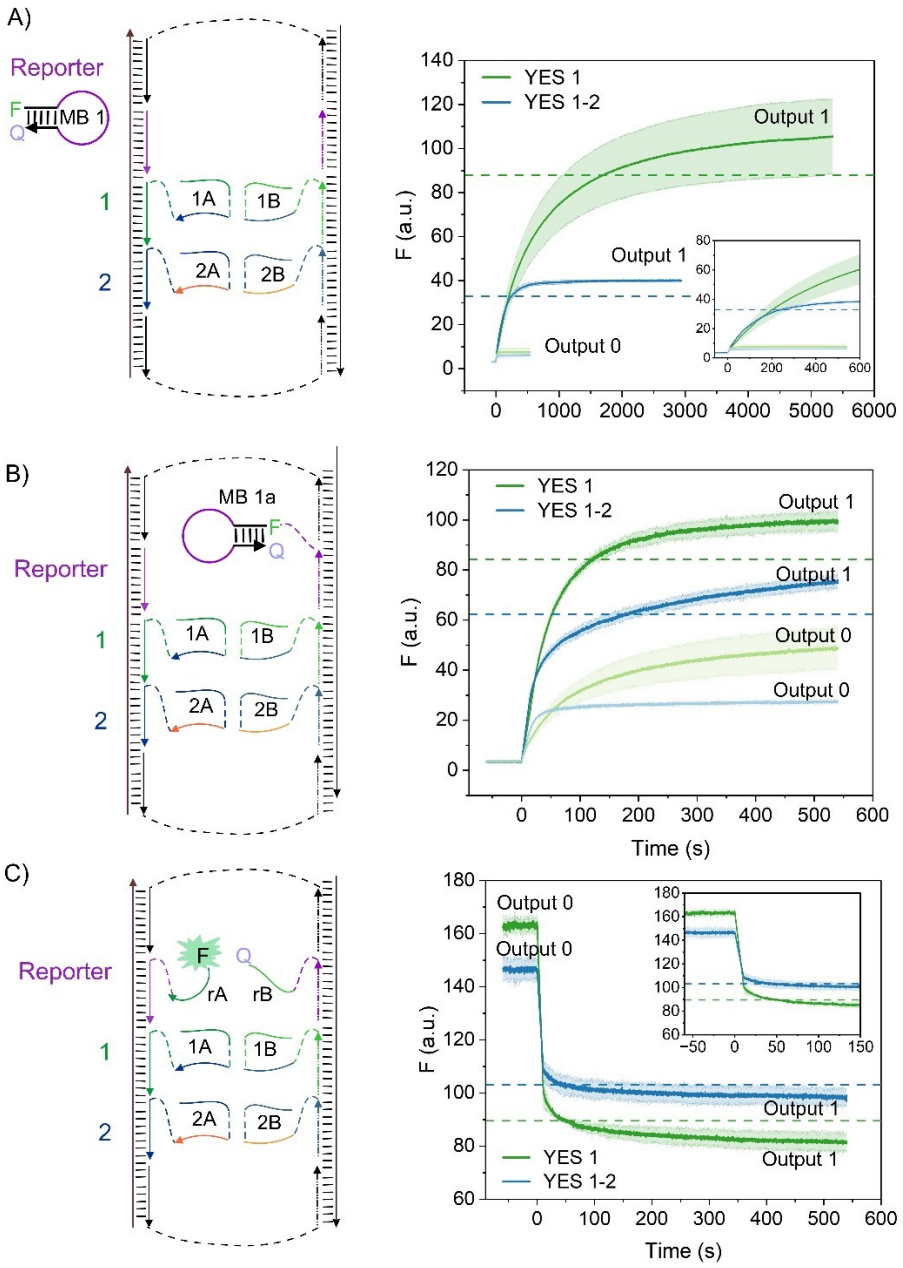

Figure 22. DNA IC module 1.2's readout using different molecular probes. DNA IC module 1.2 cascades two 4J gates, where the output sequence released by YES 1 is translated into a fluorescence readout by A) MB1 probe in free diffusion, B) MB1b probe that is attached to the DNA board, and C) DNA board-attached binary probe where rA is tagged with a fluorophore and rB tagged with a quencher. For MB1 and MB1b, binding to the output sequence triggers an increase in fluorescence (right graphs). For the rA + rB reporter, binding to the output sequence leads to a decrease in fluorescence due to the colocalization of the fluorophore near the quencher. read collected. The average kinetic profile of three independent samples using each probe is shown to the right of each panel. YES 1 outputs are represented by a green-colored line and the cascaded YES 1 -YES 2 outputs are represented by a blue-colored line. The standard deviations are indicated

by the light-colored area around each line. Colored-dashed lines indicate the 90% fluorescence change achieved after input addition.

The attachment of the MB1 probe to the DNA board (MB1a) improved t_{90} by 14-fold for YES 1 and by 1.4-fold the two 4J cascade (Table 8). This result shows that the localization of the molecular probe within the DNA IC can provide a faster readout of the molecular computing processes. Furthermore, we observed an increase in the population of signal-propagating units completing the cascade when using MB1a (Figure 22B right panel). However, an increase in the population of signal-leaking units was observed due to the increased local concentration of the probe close to YES 1. Differently from the MB 1 system, t_{90} of two cascaded 4J gates was higher than t_{90} YES 1. We considered that by colocalizing the reporter and the 4J computing units, we can observe the inter-gate binding time.

Table 8. Computation processing times using different molecular probes for readout.

Reporter	Max # of 4J YES gates	t_{90}, s
MB 1	1	1697 ± 10
	2	244 ± 1
MB 1a	1	119 ± 2
	2	177 ± 8
rA + rB	1	50 ± 4
	2	46 ± 10

Lastly, by using a two-labeled ssDNA as a reporter (rA + rB), t_{90} for YES 1 improved by 34-fold in comparison to using MB1 which corresponds to a reduction of the computation time readout from 28 min to <1 min (Table 8). Due to the lack of any secondary structure in rA and rB, the activation energy barrier for the binding of both strands to their output sequence complement is significantly reduced (Figure 22). Interestingly, cascading the two 4J YES gates achieved a similar t_{90} than only one 4J YES gate on the DNA board. Therefore, this reporter system shows that the localization of the A and B YES computing components and the inter-gate binding time between the two 4J YES gates occur in a scale of seconds. Although, we observed an increase in signal-leaking units (Figure 22C right panel) when cascading the two 4J units, the population of signal propagation units outnumbered them by 1.5-fold.

4.3.2 Kinetics of a DNA IC cascading 4J YES gates

From the different molecular probes/reporters assessed, we decided to continue with the rA + rB reporter system to measure the kinetic profile of larger 4J YES gate cascades since this system showed minimal additive effect on the computation readout times. From the results in Figure 23, we observed that for YES 1 i) the initial fluorescence at $t \leq 0$ s was lowered and ii) ΔF and S/B was higher than on module 1.2. In cascading two 4J YES gates on module 1.4, we also observed that S/B increased from 1.5 (module 1.2) to 3.2. This fluctuation is S/B and ΔF when increasing the size of the DNA board was observed before in Chapter Three.

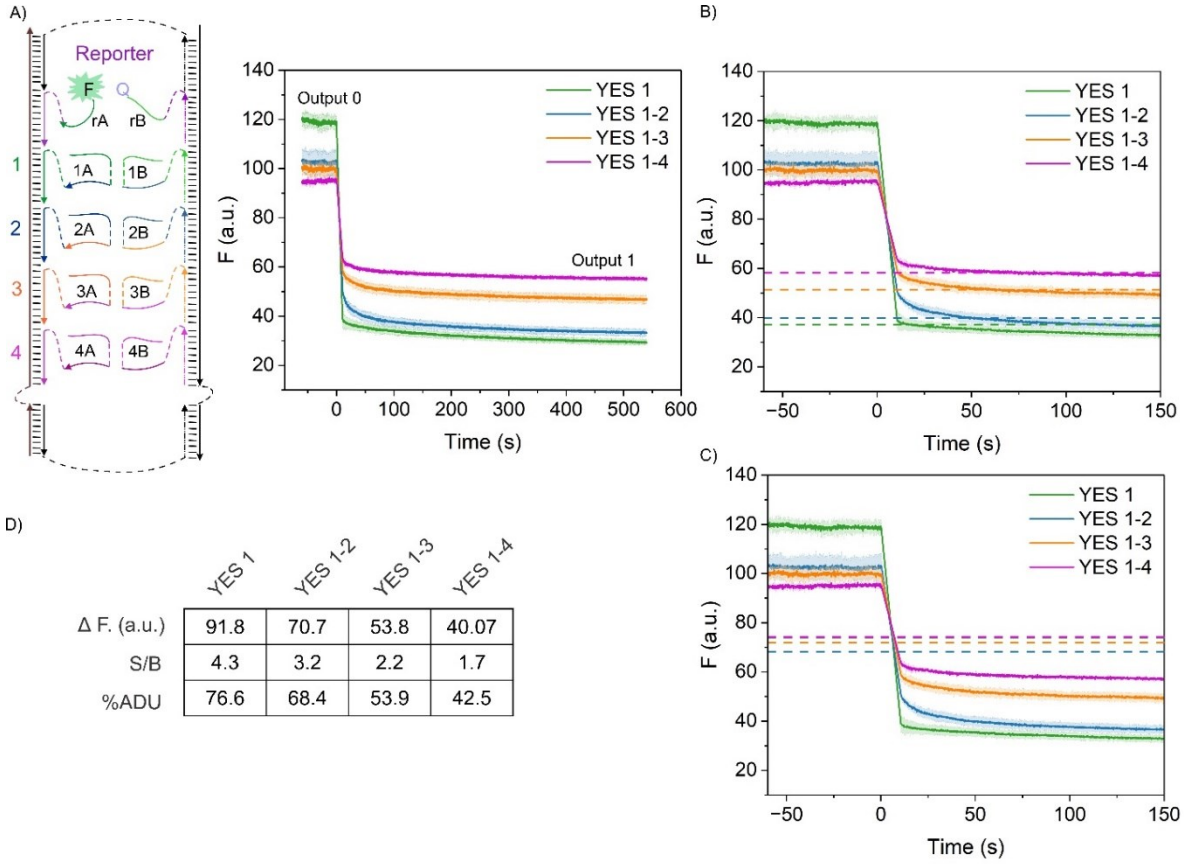

	YES 1	YES 1-2	YES 1-3	YES 1-4
Δ F. (a.u.)	91.8	70.7	53.8	40.07
S/B	4.3	3.2	2.2	1.7
%ADU	76.6	68.4	53.9	42.5

Figure 23. Kinetics of four cascaded 4J YES gates. A) DNA IC module 1.4 scheme using rA + rB probe (left) for fluorescence readout of the computation time after input addition (right). Zoom in of the kinetic profile at the first 150 s is shown in B) and C). The colored-dashed lines in B) indicate the 90% fluorescence change and C) indicate the 50% fluorescence change achieved after input addition. D) The different thermodynamic parameters observed from cascading up to four 4J YES gates using the rA + rB probe are shown in the table.

We also observed a difference in the performance of the DNA IC cascading 4J YES gates when using an MB vs rA + rB reporter. When close to equilibrium, we observed that overall ΔF, S/B, and ADU values slightly decreased when using the rA +rB. This reduction can be attributed to the lack of the fixed localization that the output sequence (1A and 1B green fragments) has when bound to an MB probe. Since rA and rB are two independent components and their readout results from the proximity and strength of the stacking interactions holding 1A and 1B green fragments

together, the population of signal-propagating units minimizes. In terms of the computation times, we also observed fluctuation in the performance of YES 1 and YES1-2 between DNA IC module 1.2 and module 1.4. YES 1 t_{90} was lower on module 1.4, achieving 90% fluorescence change in less than 30 s (Table 8 and Table 9). In this DNA IC module, t_{90} increased proportionally with the number of cascaded 4J units. From Table 9, we can estimate the computation time of each inter-gate binding event. For example, assuming that the diffusion and nucleation reaction rates of each input are the same, the inter-gate binding time between YES 1 and YES 2 occurred in 34 s (YES 1-2 t_{90} – YES 1 t_{90}).

Table 9. Computation times for four cascading 4J YES gates on DNA IC Module 1.4

Max # of 4J YES gates	t_{90}, s	Inter-gate binding	t_{90}, s
1	17 ± 2	NA	NA
2	51 ± 4	YES 1-2	34 ± 2
3	60 ± 11	YES 2-3	9 ± 7
4	81 ± 30	YES 3-4	21 ± 19

Although the median t_{90} for each cascading 4J gate shows a non-predictable t_{90} for the inter-gate binding time across the gates, the inter-gate communication time between YES 2 and 3, and YES 3 and 4 correspond to exactly 2 s if we compared the difference from their minima t_{90}. These results suggest that 4J YES gate holds the potential to cascade binding events at a higher speed than other gate motif reported in the literature.[45,47,48,94] The colored dashed lines in Figure 23C

show that the t_{50} after cascading up to four 4J YES gates occurred within t = 0 and <10 s, a window that is blind during data collection due to the pausing of the instrument for input mixing. This suggests that the computation times might be even lower than what is reported in Table 9. For this reason, we performed the same experiment on a stopped-flow instrument (Figure 36, Appendix C) automated to inject and mix both DNA IC and input solution mechanically.

The results on stopped-flow showed that all t_{90} were achieved in <0.5 s and t_{50} < 0.1 s (Figure 36, Appendix C); however, these times did not show the same trends as seen on Table 9. Furthermore, due to the difference in instrumental components (detectors, wavelength selectors, etc.) ΔF, S/B, and ADU differed from the observed values on Figure 23. From the best fit of each graph (Figure 37, Appendix C), we determined the kinetic rate constants observed from both instruments (Figure 38, Appendix C). The kinetic rate constants observed from stopped-flow are three orders of magnitude higher than the observed from a regular fluorometer (Figure 38 and Figure 40). However, there was no trend associated with the number of cascading 4J units, which could be due to artifacts during the data collection, thus further experimentation is needed.

4.3.3 DNA board influence in the kinetic response of 4J DNA IC

From the differences in the kinetic and thermodynamic results of 4J YES gates switching their anchoring to DNA boards of different sizes, we decided to investigate the influence of the DNA board on gate performance. Due to the flexibility of the polyethylene glycol linker on the staple strands, the rail strands in the DNA board can come closer together and go back apart of each other. We hypothesize that this oscillatory feature on the DNA board changes with its size. Since 4J logic gates process their input and output by localizing the A and B ssDNA components

in proximity, these changes in rails oscillation can be reflected in their gate and circuit performance. To mitigate the dynamic mobility of the DNA board rails, we introduced a dsDNA bridge in the inner region of the DNA board by adding a ssDNA bridge that binds to complementary tails coming from A and B ssDNA components of a 4J YES gate (Figure 24A-B).

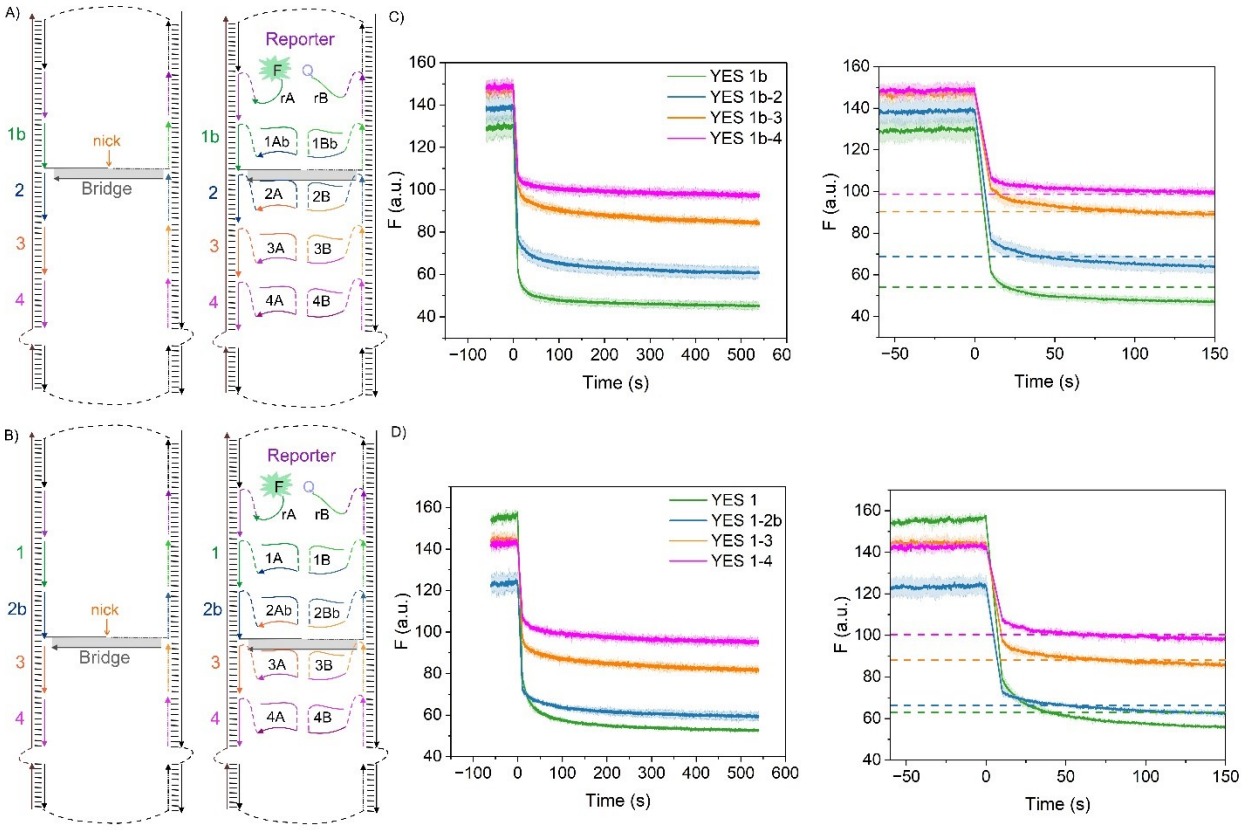

E)

	YES 1b	YES 1b-2	YES 1b-3	YES 1b-4
Δ F. (a.u.)	82.7	76.1	61.9	55.0
S/B	2.8	2.2	1.7	1.6
%ADU	64.4	55.4	42.4	37.1

F)

	YES 1	YES 1-2b	YES 1-3	YES 1-4
Δ F. (a.u.)	100.9	63.0	61.2	46.0
S/B	2.9	2.1	1.7	1.5
%ADU	65.6	51.2	42.7	32.4

Figure 24. Kinetics of four cascaded 4J YES gates with rigidity added to DNA board by placing a dsDNA bridge either at YES 1 (YES 1b) A) or at YES 2 (YES 2b) B) position. The dsDNA bridge is formed from the association of a ssDNA bridge with complementary binding tails extending out of the A and B strands. C) and D) show the kinetic profile of each DNA IC of the total time of collection (left) and zoom in at the first 150 s (right), the colored-dashed lines indicate the 90%

fluorescence change after input addition. E) Thermodynamic parameters observed on the DNA board where rigidity is localized at YES 1b and D) at YES 2b.

In Figure 24, we observed that the kinetic profiles of the four cascading 4J YES gates differ with the location of the dsDNA bridge. Although ΔF, S/B, and ADU values are similar between the two explored dsDNA bridge locations (Figure 24E-F), the initial fluorescence of each cascading 4J YES gate before input addition differs in both DNA IC modules (Figure 24C-D). In Figure 23, we observed that the decrease in the initial fluorescence was proportional to the number of cascaded 4J YES gates, a factor we attributed to the increase in the population of signal-leaking units. This proportionality is not observed in Figure 24C-D which could implicate that the increase in the number of signal-leaking units is affected by the dsDNA bridge and its location on the DNA board. This dependence on the dsDNA bridge position suggests that the location of the rigidity can favor or disfavor the spurious communication between 4J gates.

The dsDNA bridge location also played a role in the computation times achieved by each module (Table 10). The increase in t90 proportional to the increase in cascading 4J gates was observed, which was a similar trend from the DNA board lacking the dsDNA bridge (Table 9). In terms of inter-gate binding times, the dsDNA bridge reduced the binding time between YES1 and YES 2, showing a higher binding speed when located at YES 2b. However, we observed higher inter-gate binding times as the number of cascading 4J YES gates increased when the dsDNA bridge was located at YES 1b rather than YES 2b (Table 10). YES 3-4 inter-gate binding had a higher speed than the inter-gate binding of cascading YES 3-YES2-YES 1. This result could be attributed to random errors introduced during the mixing of the input and further experimentation is needed to confirm its reproducibility.

Table 10. Computation times for four cascading 4 YES gates on DNA IC Module 1.4 with added dsDNA bridge for DNA board rigidity.

Max # of 4J YES gates	Bridge at YES 1b t_{90}, s	Bridge at YES 2b t_{90}, s
1	20 ± 1	39 ± 3
2	41 ± 5	45 ± 11
3	104 ± 19	77 ± 14
4	307 ± 143	63 ± 20
Inter-gate binding	Bridge at YES 1b t_{90}, s	Bridge at YES 2b t_{90}, s
YES 1-2	21 ± 4	8 ± 6
YES 2-3	63 ± 14	32 ± 3
YES 3-4	203 ± 162	-14 ±6

The kinetic rate constants calculated from the best-fit of each graph on Figure 24C-D are shown in Figure 43 and Figure 45. From the comparison of the rate constants k1 and k2 obtained, we observed that the DNA IC module with dsDNA bridge at YES 1b had a proportional decrease of both k1 and k2, as the number of cascading 4J YES gates increased. For the DNA IC without the dsDNA bridge or with the dsDNA bridge at YES 2b, both k1, and k2 did not show a clear trend related to the increase in cascading 4J YES gates. Furthermore, these results suggest that the location of the dsDNA bridge on the output-releasing gate may provide additional support to keep the localization of rA + rB in proximity since the highest YES 1's rate constants k1 and k2 were observed for this DNA IC module.

4.4 Conclusions

In conclusion, we report that the computation times observed from a DNA IC can be influenced by the type of reporter (molecular readout probe) used and dynamic structural changes of the DNA board. Our results indicate that in translating the nucleic acid output to a readout signal, the localization and lack of secondary structures from the molecular readout reporter are necessary to minimize its additive contribution to the observed computation times. Furthermore, our results demonstrate that the dynamic mobility and rigidity provided to the DNA board can influence the computation times of the cascading 4J YES gates and further investigation is needed. Overall, the computation time (t_{90}) achieved by a cascade of four 4J YES gates was < 3 min and with t_{50} < 1 s which are the shortest computation times reported. These suggest that 90% of the DNA ICs had released their output in < 3 min, accounting for a signal propagation rate of 4.5 nm/min. Thus, using 4J YES gates as computation units can overcome the limitations of slower computation speeds when building DNA molecular computers with higher-density DNA ICs.

.

CHAPTER FIVE: EXPLORING A CHEMICAL LIGATION FOR THE COVALENT CROSSLINKING OF DNA IC COMPONENTS

5.1 Introduction

Protein enzymes facilitate chemical reactions by using multiple functional groups brought in proximity to specific substrates. Up to 10^{14}-fold enhancement of the reaction rates is possible due to the simultaneous use of several catalytic strategies including proximity and orientation effect, preferential binding to the transition state, general acid/base, electrophilic and nucleophilic catalysis.[150] The proximity and orientation effect lowers the entropic barrier to form the transition state. This simple strategy has been explored in nucleic acid-templated reactions, in which two reactive groups are conjugated to the opposite ends of two oligonucleotides and then brought together by hybridization. Nucleic acid-templated reactions have been used for the discovery of new chemical reactions,[151] DNA-triggered drug releases,[152] DNA templated ligation,[153] and nucleic acids analysis[154] among other applications.[155] The approaches use B-DNA helix formation to bring in proximity the 3'-end of one to the 5'-end of another oligonucleotide in two major topological arrangements shown in Figure 25A.

DNA nanotechnology has introduced non-natural 2D and 3D DNA nanostructures, such as an immobile four-way junction,[156] paranemic crossover,[157] tensegrity triangle,[158] to name a few.[159] These blocks may allow building complex 3D arrangements of functional groups attached to the ends of DNA strands. To illustrate the feasibility for DNA nanostructures to be used as catalysts,

we explored the 5'-5' chemical ligation of two oligonucleotides.[160] Even though a 5'-5' phosphodiester bond is known in nature (e. g. found in mRNA cap structure), no known catalyst is capable of the 5'-5' ligation of two DNA strands of arbitrary sequences.

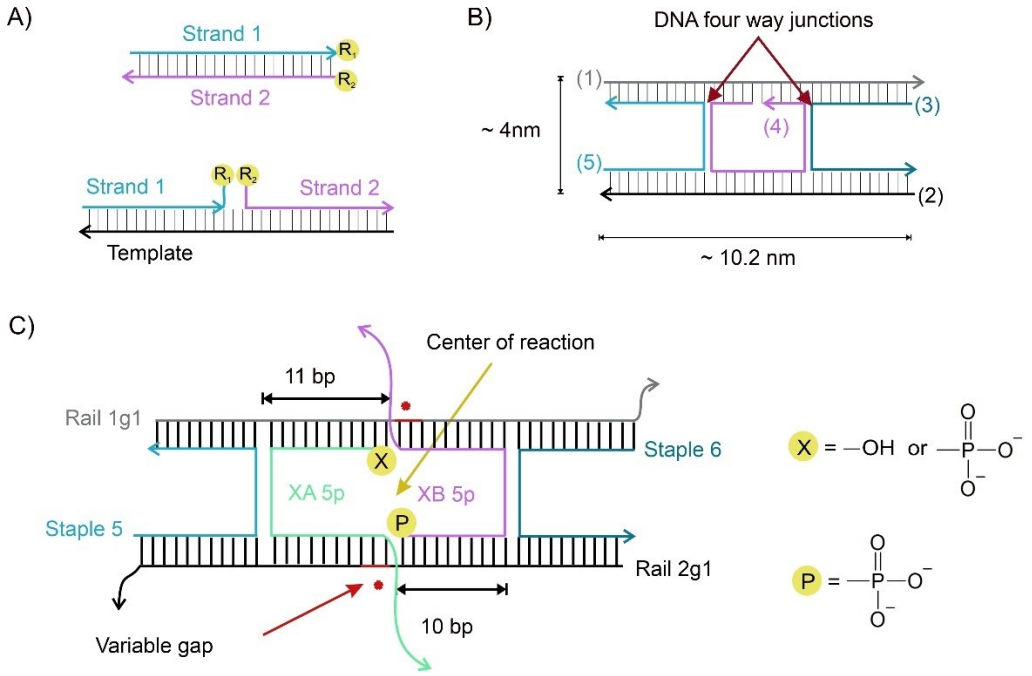

Figure 25. The topology of DNA template-assisted and DX tile-assisted reactions. A) Conventional template-assisted reaction: strands 1 and 2 hybridize with each other or to a DNA template to bring the two reactive groups R1 and R2 in proximity, thus facilitating the reaction.[151–155] B) Scheme of a DX tile developed by Fu and Seeman, reproduced with permission from ref 160. C) Scheme of a DX tile designed in this study to catalyze the ligation of oligonucleotides at their 5'-phosphorylated termini.

To achieve the 5'-5' DNA ligation, we turned our attention to a DNA nanostructure called double-crossover antiparallel even (DAE) tile (also known as a DX tile) introduced by Fu and Seeman in 1993.[161] DX tile consists of five DNA strands (Figure 25B), which form two DNA helixes bound to each other via two DNA 4J crossovers. Figure 25C shows how a DX tile-like

nanostructure can be used as a template for bringing the 5'-ends of two nucleic acid strands (XA 5p and XB 5p) in proximity. This approach may become a step toward exploring DNA nanostructures for rational design of enzyme-like catalytic centers for drug discovery, energy storage, and consolidation of sequence-independent higher-ordered DNA nanostructures as one molecular device.

In DNA molecular computing, the ability to isolate and store DNA logic circuits is necessary for later usage.[50] Due to the multi-component nature of the developed 4J DNA ICs, they can be prone to disassemble their components during harsh or non-equilibrium conditions (e.g. temperature, pH, chaotropic agents, electric polarization). To consolidate a 4J DNA IC into one molecular unit, the covalent crosslinking between each component is necessary. The use of click chemistry such as azide-alkene ligation[66] and photoinduced crosslinking[162,163] have been previously reported. However, in these approaches i) the modification of each oligonucleotide is necessary to tag the reactive groups, increasing their commercial price or synthesis steps, or ii) the crosslinking occurs only at specific nucleotides, limiting the sequence directory of the DNA IC.

Here, we explored the used of the 1-cyanoimidazole (1-CNI) condensation system developed by Kanaya and Yanagawa,[164] which was shown to be effective for the 5'-3' templated ligation of oligoadenylates in aqueous solutions.[164] Mn^{2+}, Zn^{2+}, Cu^{2+}, Cd^{2+}, Co^{2+}, Ni^{2+}, Mg^{2+} has been coupled with 1-CNI due to their influence in the ligation yield, with Mn^{2+} and Zn^{2+} most commonly used.[165–167] The reaction involves the activation of the terminal phosphate with 1-CNI to facilitate its attack by a nucleophile. The reaction mechanism for phosphate activation[164,165] and divalent cation assisting the nucleophilic attack has been proposed and characterized.[164,165,168]

In our, DNA IC module cascading five 4J YES gates, we consider the chemical ligation of a terminal reactive group from one strand with an internal reactive group from another strand, such as a terminal phosphate and a 2'hydroxyl group from a ribonucleotide (Figure 26). A similar chemical ligation system was explored by Weizenmann and coworkers, where the chemical ligation of the staple strands from a DNA origami was achieved using *N*-(3-dimethylaminopropyl)-*N*′-ethylcarbodiimide as a condensation agent to form a phosphate-amine covalent bond.[169] Here, by using phosphate and hydroxyl as reactive groups, we aimed to conserve the integrity of the DNA canonical backbone and avoid a covalent modification that could compromise assembly and overall circuit performance.

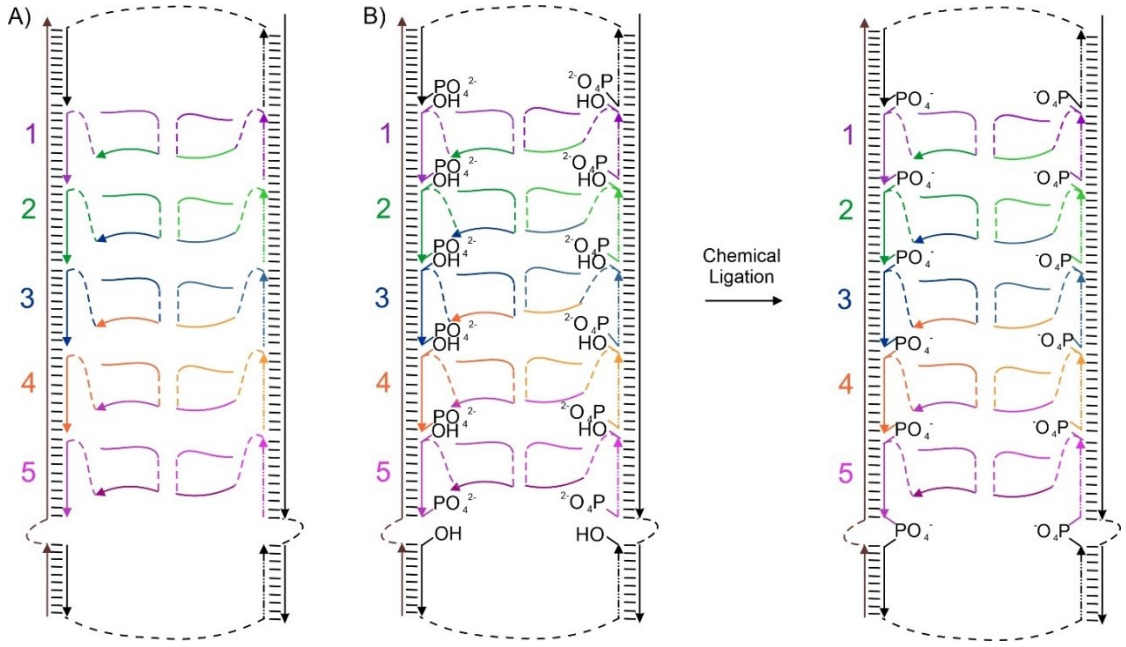

Figure 26. DNA IC module 1 cascading five 4J YES gates where A) shows the original nanostructure while B) indicates the positions of phosphorylated ends and 2' hydroxyl groups on each component of the DNA IC module. After chemical ligation, these reactive groups condensate into a phosphodiester bond.

Figure 27 shows a closer look on the chemical ligation between a staple 3' phosphorylated end and the 2' hydroxyl from 1A's ribonucleotide to form a phosphodiester bond. Figure 27C shows the reaction mechanism followed by these two DNA IC components based on the previously proposed mechanisms of Kanaya and Yanagawa reaction.[164–166]

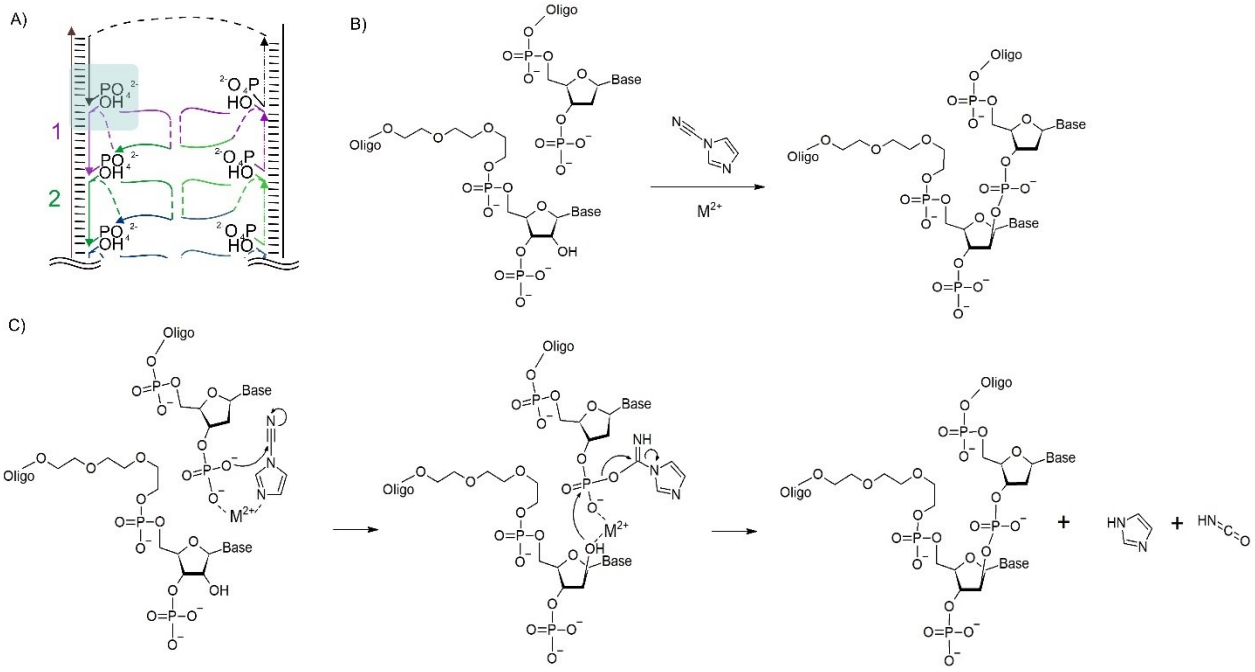

Figure 27. Reaction mechanism for using 1-CNI and a divalent metal cation (M^{2+}) as condensing agents. A) DNA IC fragment showing the localization of phosphorylated ends and 2' hydroxyl groups to serve as nucleophiles for the chemical ligation between two DNA IC components; a closer look of the strands highlighted by the blue box is shown in B) to indicate the reaction product after the chemical ligation. C) Reaction mechanism of the chemical ligation induced by 1-CNI and M^{2+} resulting in the formation of a phosphodiester bond.

Due to the coordination of a divalent metal cation with the 3' phosphate and 1-CNI, speeds the nucleophilic attack of the phosphate group to directly bind to 1-CNI , forming an imidate intermediate that leads to the activation of the phosphorus for the nucleophilic attack of the 2'

hydroxyl group from another strand as shown in Figure 27C. In this process, the two DNA fragments are ligated by a phosphodiester bond and the release of imidazole and carbylamine. The reaction mechanism in Figure 27C can apply if other nucleophilic groups are used instead of a 2' hydroxyl group.

5.2 Materials and Methods

5.2.1 Materials and Methods

DNase/protease-free water was purchased from Fisher Scientific Inc. (Pittsburg, PA) and used for all buffers and the stock solutions of oligonucleotides. $MgCl_2$ (1 M solution) was purchased from Teknova (Hollister,CA), 1-cyanoimidazole was purchased from Toronto Research Chemicals Inc. (Toronto, Canada), imidazole, $ZnCl_2$, $MnCl_2$, and HCl were from ThermoFisher Scientific (Waltham, MA). All oligonucleotides were custom-made by Integrated DNA Technologies, Inc. (Coraville, IA), and their stock solutions were prepared by resuspension in water and stored at – 20°C until use. The concentrations of the oligonucleotides' stock solutions were determined from the Beer-Lambert equation, for which absorbance at 260 nm was measured with a Thermo Scientific Nanodrop One UV-Vis Spectrophotometer, while the corresponding extinction coefficients were determined using OligoAnalyzer 3.1 software (Integrated DNA Technologies, Inc.). Gel electrophoresis experiments were performed using BioRad electrophoresis equipment (Hercules, CA), and visualized using BioRad Gel Doc XR+. Exonucleases Exo VIII truncated and Exo III were purchased from New England Biolabs, Inc (NEB).

5.2.2 DX-Tile assembly and chemical ligation reactions

For the DX tile assembly, all DNA oligonucleotides comprising the DX-tile complex were mixed at 20 μM in equimolar ratios in a buffer containing 200 mM imidazole-HCl buffer at pH 6.5, and 75 mM $MgCl_2$. The DX-tile samples were annealed by denaturing at 95°C for 2 min and cooling to 22°C within 8 h. For the crosslinking reaction, 1-cyanoimidazole and $MnCl_2$ were added to the annealed samples to a final concentration of 30 mM and 100 mM, respectively, and the reaction mixtures were incubated at 37°C for 16 h (or 1-24 h for the kinetics experiment).

5.2.3 Gel electrophoresis assays

Denaturing gels were prepared to contain 8 M urea and 12% acrylamide (19:1 acrylamide: bisacrylamide). TBE buffer (89 mM Tris Base, 89 mM boric acid, and 2 mM EDTA) was used as the running buffer. Electrophoretic samples were prepared using a 2× denaturing loading buffer (85% Formamide, TBE, and traces of Bromophenol blue and Xylene Cyanol). Gels were run at constant voltage (95 V) for up to 110 min.

Native gels were prepared at 8-10% acrylamide (19:1 acrylamide:bisacrylamide) and contained 70 mM $MgCl_2$. Gels were run at constant voltage (100 V) for up to 80 min. Samples were prepared using a 6 × Cyan/Yellow loading dye (TrackIt™, Thermofisher). Gel-Red was used as a staining dye for the visualization of DNA bands.

Quantification of product yield: Image analysis was performed using the Image Lab™ software supplied by Bio-Rad Laboratories Inc. Lanes and bands were automatically identified by the software and manual resizing was done to ensure equal band area selection in all lanes. The band of Rail 2g0/1 or 2 was chosen as reference to obtain the relative intensities of each band and to normalize the relative intensities of the XA and XB bands. The product yield was determined

by the equation (6), where $[Ri]_{initial}$ and $[Ri]_{final}$ is the normalized relative intensity before reaction and after reaction, respectively.

(6) $$\text{Product Yield } \% = \frac{[Ri]_{initial} - [Ri]_{final}}{[Ri]_{initial}} x100$$

5.2.4 Exonuclease treatment

Reaction mixtures were precipitated by adding 2% $LiClO_4$/acetone followed by centrifugation at 10,000 RPM for 5 min; the supernatant was discarded, and the steps were repeated one more time using pure acetone to wash the pellets. The pellets were let to dry completely and then resuspended in DNA-grade water.

For 5'-5 crosslinked product: Oligonucleotide strands complementary to the DX-tile components were added at the equimolar concentration to allow the formed duplexes to serve as substrates for the exonuclease Exo VIII truncated. The samples were prepared by following the NEB recommended protocol with Exo VIII truncated and the supplied NEB buffer™ 4.

For 3'-3 crosslinked product: Addition of complementary strands was unnecessary. Samples were prepared according to the NEB recommended protocol with Exo III and the supplied NEB buffer™.

Isolation from exonucleases: After the completion of exonuclease digestion, 1x volume of phenol:chloroform:isoamyl alcohol (25:4:1) was added, and the mixtures were centrifuged at 10,000 RPM for 5 min. The aqueous phase was saved, and DNA was precipitated by overnight incubation at -20℃ with 0.3 M sodium acetate (pH 5.6) and 70% ethanol and separated by

centrifugation at 4℃ for 25 min at 10,000 RPM. DNA was resuspended in DNA-grade water or a buffer containing 50 mM Tris-HCl (pH 7.4) and 2 mM $MgCl_2$.

5.2.5 Gel extraction of ligated DNA IC components.

3 nmol of the ligated DNA IC was loaded into a 12% dPAGE -8M urea gel. For gel extraction, gels were run at constant voltage (165 V) and 65 ℃ for 1 h 40 min. The target band was identified and cut with a scalpel blade, followed by thinly crushed, soaked in 1 mL DNA grade water, and incubated under shake (120 rpm) at 37℃ for up to 24 h. Supernatant was filtered using a X-Spin Coastar filter. From the collected supernatant, DNA was precipitated by adding a 2-fold volume 2 % LiClO4 – acetone solution and separated from the supernatant by centrifugation at 10,000 RPM for 3 min (step repeated with pure acetone). DNA pellet was dried under vacuum for 30-60 min and then resuspended with DNA-grade water.

5.2.6 Assembly of ligated DNA IC components for fluorescence assay

All DNA oligonucleotides intended for assembly into the target DNA logic circuit were mixed at 200 nM in equimolar ratios in a buffer mix containing 100 mM Tris-HCl at pH 7.4, 100 mM MgCl2, 0.06 % Triton X100; followed by vortex and centrifuged to make sure all the solution was dragged down. The samples were annealed by placing them in a water bath at 95 ℃ for 2 min and slowly cooling down to 22 ℃ within 8 h. After assembly, a master mix solution was prepared containing molecular beacon (MB) probe solution and the DNA assembly. From this master mix, aliquots were dispensed in individual microcentrifuge tubes for the addition of the different inputs, followed by incubation at room temperature (22-25 ℃) for 20 min. The fluorescence emission was read from those samples, containing 100 nM DNA logic gate assembly, 50 nM MB probe (12.5

nM for YES 1 and IMPLY), 100-200 nM input, 50 mM Tris-HCl at pH 7.4, 50 mM MgCl2, 0.03 % Triton X100.

Average and standard deviations were calculated from three independent samples. To normalize the fluorescence response of each output signal, we subtracted the average fluorescence response of a MB only solution. Each graph plots the average fluorescence difference *(ΔF): fluorescence output signal – fluorescence MB signal*; Error bars represent the standard deviation from three independent samples.

5.2.7 AFM imaging

AFM sample preparation: wXA 5p- wXB 5p ligation product was associated with AFM complement strands (Table 11) in an assembly buffer (10mM Tris-HCl pH 7.4 and 2mM MgCl2) followed by gel isolation and resuspended in an assembly buffer. Samples were stored at 4 ℃ before deposition on modified mica. Mica substrates are modified with 1-(3-aminopropyl)silatrane (APS) to create a positively charged surface for deposition of DNA and RNA-DNA hybrid structures via electrostatic attraction between negatively charged DNA backbone and positively charged APS-mica28. 5μL of each sample was deposited on APS-modified mica and waited for 2 min before rinsing excess DNA with di-water. Optimal sample concentration ranges from 10 – 100 nM to avoid overlapping of DNA structures. Mica samples were dried under a flow of ultra-high purity argon gas and incubated overnight under vacuum before imaging. AFM imaging: Images were obtained using a Multimode AFM Nanoscope IV system (Bruker Instruments, Santa Barbara,CA) operating in tapping mode in air with a RTESPA-300 AFM probe.

Table 11. List of Oligonucleotides used in Chapter five studies

Name	comments	Sequence
DX-tile		
Rail 1g2	2 nt gap	TG TCT CCC TC C CAT TGT ATC G TT GT GCG TTG CTT CCT CTA TG TTT TTT TTT T
Rail 1g1	1 nt gap	TG TCT CCC TC C CAT TGT ATC G T GT GCG TTG CTT CCT CTA TG TTT TTT TTT T
Rail 1g0	no gap	TG TCT CCC TC C CAT TGT ATC G AA GT GCG TTG CTT CCT CTA TG TTT TTT TTT T
Rail 2g2	2 nt gap	CTGAC TGAAT AAT ATG CTA G TT GTG TGT TA GT TCA TCTCTC TTT TTT
Rail 2g1	1 nt gap	CTGAC TGAAT AAT ATG CTA G T GTG TGT TA GT TCA TCTCTC TTT TTT
Rail 2g0	no gap	CTG ACT GAA T AA TAT GCT AG AA GT GTG TTA GTT CAT CTC TCT TT
Staple 5		GAG AGA TGA ACG AGG GAG ACA
Staple 6		CATAG AGG AAG ATTCA GTCAG
dsDNA-tile		
ds-Rail a		TGTCT CCCTC CTT CCT CTATG C CAT TGT ATC G AT GT GCG TTG GAGAGA TGAACATTCA GTCAG TTT TTT TTT T
ds-Rail b		CTGAC TGAAT GTTCA TCTCTC AAT ATG CTA G AA GTG TGT TA GT TCA TCTCTC CATAG AGGAAG GAGGG AGACA TTT TTT

Name	comments	Sequence
Reactive strands		
XA		CGA TAC AAT GG **TAA CAC ACT** T TTT TT
XA 5p		/5Phos/CGA TAC AAT GG **TAA CAC ACT** T TTT TT
XA/isp9/5p	Phosphate group bound via a linker	/5Phos//iSp9/CGA TAC AAT GG **TAA CAC ACT** T TTT TT
XB 5p		/5Phos/C TAG CAT ATT CAA CGC AC TT TTT TTT TTTTT
XB/isp9/5p	Phosphate group bound via a linker	/5Phos//iSp9/C TAG CAT ATT CAA CGC AC TT TTT TTT TTTTT
XA 3p		T TTT TT CGA TAC AAT GG TAA CAC ACT /3Phos/
XB 3p		TT TTT TTT TTTTT C TAG CAT ATT CAA CGC AC /3Phos/
wXA 5p		/5Phos/ CGA TAT AAT GG TAA CAC ACT TTA ACT AT CTTA C TT TCATTTTAATT GCG GGC GTC GCA TGT TTA TGT TAG
wXB 5p		/5Phos/C TA G CAT ATT CAA CGC ACT TTT TTT CTT GTA GAT TT AT CCT T TC A TAA CAACC TTT CAT TTA TTT TAA TGT C GAC GCC CGC ATA CTT CGC TCT TTG
Complements of DX-tile strands		
Cpl Rail 1g2	Also complement of rail 1g1 or 1g0	AAAAAAAAAAAAACATAGAGGAAG CAACGCAC AA CGATACAATGG GAGGGAGACA

Name	comments	Sequence
Cpl Rail 2g2	Also complement of rail 2g1 or 2g0	AAAAAAAA GAGAGATGAAC TAACACAC AA CTAGCATATT ATTCAGTCAG
Cpl Staple 5		TGTCT CCCTC GTTC ATCTCTC
Cpl Staple 6		CTGAC TGAAT CTT CCT CTATG
Cpl XA 5p		AAAAAAAGTGTGTTACCATTGTATCG
Cpl XB 5p		AAAAAAAAAAAAAGTGCGTTGAATATGCTAG
AFM Complements of DX-tile strands		
W1-Tri-A-2		AAT TAA AAT GAA AGT AAG ATA GTT AAA GTG TGT TAC CAT TAT A
W1-Tri-B		ATT AAA ATA AAT GAA AGG TTG TTA TGA AAG GAT AAA TCT ACA AGA AAA AAA GTG CGT TGA ATA TGC
DNA IC reacting strands		
Rail 1A		CAC TCT AGT TTA CAG/iSp9/ G ATC GTA TCA CCT ATC GTG TT TTG TCG CTGA CAC CAC CT GAC CCA TC GTA TCG CTT CCT CTATG
Rail 1B		CTGAC TGAAT GAG CT CTA CA GA CGA CTA CAG C TGC AGT ACC AC CGT TAG TCA ACT CACT CTG /iSp9/ GT ACTT TCT ACT AAC

Name	comments	Sequence
Rail 1AT		CCT ATC GTG TT TTG TCG CTGA CCA TC GTA TCG CTT CGT CTATG
Rail 1BT		CTGAG TGAAT GAG CT CTA CT C TGC AGT ACC AC CGT TAG TCA
Staple 1pp		/5Phos/ATTCA CTCAG /iSp18//iSp18/ CATAG ACG AAG/3Phos/
Staple 2pp		/5Phos/AA CAC GAT AGG/iSp18//iSp18/ TGA CTA ACG GT/3Phos/
1A		TCACCTGG /iSp9/ CATGCAAG /iSp9/ rC GATAC GATGG /3Phos/
1B		/5Phos/AGTAG AGCT rC /iSp9/ GCCTAACA /iSp9/ ACGTACGA
1ANH2		TCACCTGG /iSp9/ CATGCAAG /iSp9/ /iUniAmM/ C GATAC GATGG /3Phos/
1BNH2		/5Phos/AGTAG AGCTC /iUniAmM//iSp9/ GCCTAACA /iSp9/ ACGTACGA
2A		CTTGCATG /iSp9/ TCTCCATG /iSp9/ rG TCAG GTGGTG/3Phos/
2B		/5Phos/ CTGTA GTCGT rC /iSp9/ TACCCACT /iSp9/ TGTTAGGC
MB1		/FAM/CCT CGT ACG TCC AGG TGA GG/BHQ1/

Name	comments	Sequence
I 1		CTTGCATG TGTTAGGC

Sequences of the same color in different strands are complementary to each other, the color code correspond to that shown in Schemes 1, S1 and 2. The nucleotides introduced to form a gap are in red; iSp9, internal spacer 9 (IDT); /5Phos/, 5' terminal phosphate group; /3Phos/, 3' terminal phosphate group. Each sequence is entered as 5'→ 3'; iSp9 and iSp18 are oligoethylene glycol spacers 9 and 18 from Integrated DNA Technologies (IDT); FAM and BHQ1 correspond to 6-carboxyfluorescein and 3'Black Hole Quencher-1 respectively; r indicates ribonucleotide, and iUniAmM indicates a free primary amine attached to the 5'-end of an oligo via a six carbon aliphatic spacer arm.

5.3 Results and Discussion

5.3.1 5'-5' and 3'-3' chemical ligation catalyzed by DX tile

First, we designed a 5'-5' DNA ligation system by forming a DX tile containing strands Rail 1, Rail 2 and four crossover strands –XA 5p, XB 5p, staples 5 and 6 (Figure 25C). The sequence of the XA 5p and XB 5p oligonucleotides to be ligated were arbitrarily chosen with ~ 50% G/C content and absence of stable intramolecular secondary structures (Table 11). Both XA 5p and XB 5p were elongated with 3'-terminal oligo T tails to be 26 and 31 nucleotides (nt), respectively, to have different electrophoretic mobilities and enable analysis of the tile formation and ligation reaction using gel electrophoresis. The sequences of the Rail 1 and Rail 2 strands included a 10-nt fragment complementary to both XA 5p and XB 5p. Similarly, they contained oligo T tails of different lengths to be distinguished in polyacrylamide gel electrophoresis (PAGE). Staples 5 and 6 were designed to bind Rail 1 and 2 strands at a distance of two DNA helical turns (21 nt) apart from each other to accommodate XA 5p and XB 5p in the middle of the tile (Figure 25C). In the resulting 6-stranded complex, the 5'ends of XA 5p and XB 5p were positioned on the inner sides of the DNA helixes ("inside" the tile) in proximity to each other, as shown in Figure

28B. Therefore, their chemical ligation could take place right in the center of the nanostructure. The correct association of the 6 strands into the expected complex was confirmed by native PAGE analysis prior to crosslinking (Figure 46).

For the chemical ligation, we used the 1-cyanoimidazole (1-CNI) condensation system developed by Kanaya and Yanagawa.[164] We ran a series of optimization experiments to increase the yield of the DX tile-assisted 5'-5' ligation. The 5'-end of one strand was either phosphorylated (XA 5p) or lacked the phosphate group (XA), while the 5' end of another strand was always phosphorylated (XB 5p). To study the effect of the gap between the strands to be ligated, we left 1- or 2-nt single-stranded gaps, as shown in Figure 25C.

The best 5'-5' ligation yields were obtained when (i) both strands were 5'-end phosphorylated (XA 5p + XB 5p, Figure 48A); (ii) Mn^{2+} rather than Zn^{2+} was used as a metal cofactor (Figure 48B), which aligns with previous reports;[164,166] (iii) at 37°C rather than at 22°C (Figure 49); (iv) at the optimal Mn^{2+} concentration of 100 mM (Figure 49); and (v) the strands bound to both Rails 1 and 2 were separated by a 1-nt gap (Figure 50). Under the optimized conditions, the reaction reached a plateau within 16 h with a yield of ~ 65% producing no ligation side products (Figure 28D-E and Figure 51). Furthermore, to increase the flexibility of the two reacting phosphate groups, we attached them to strands XA 5p and XB 5p via a flexible triethylene glycol spacer (iSp9). However, this did not improve the reaction yield (Figure 52).

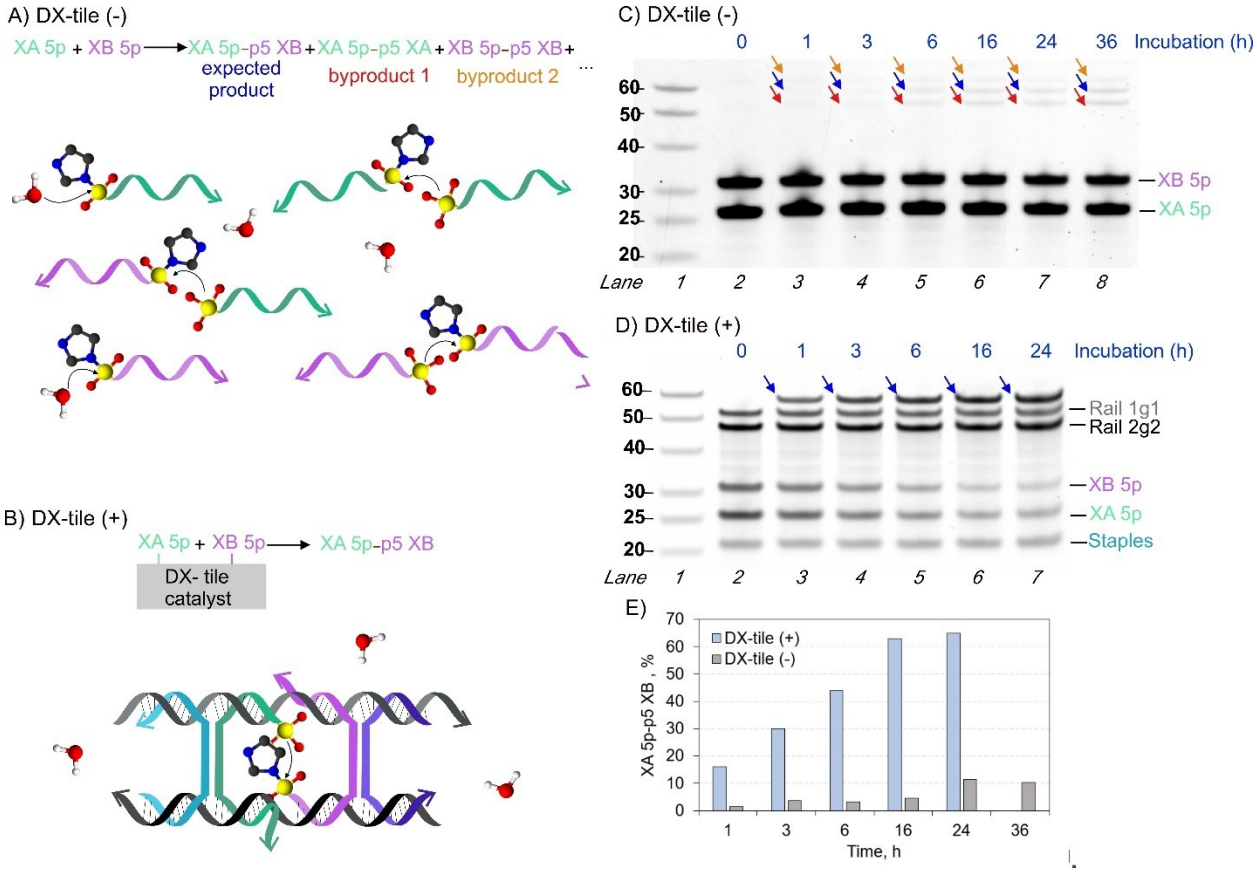

Figure 28. Comparison of DX-tile (-) 'uncatalyzed' vs catalyzed DX-tile catalyzed chemical ligation of XA 5p and XB 5p.A) Scheme of uncatalyzed chemical ligation and B) Schemes of DX-tile catalyzed chemical ligation C) and D) PAGE analysis of the ligation products for uncatalyzed and DX-tile catalyzed reactions. Lane 1: ssDNA ladder; lane 2: prior crosslinking of 5' ends; lane 3-7 or 8: samples after ligation terminated at different incubation times (as indicated). Blue arrows indicate the ligated product XAp-pXB with the expected length of 57 nt, orange and red arrows indicate byproducts of the reaction. E) Comparison of the yields of the ligation reaction on DX tile (blue bars) and in solution (grey bars). The yield quantification was done as described in Methods.

In contrast, the uncatalyzed (DX tile-free) ligation under similar conditions produced less than 5% of the expected product after 16h incubation. We observed a 2- fold yield increase after 24h, however, after 36h the DX-tile free ligation seemed to plateau (Figure 28C-E). The reaction rates for DX-tile and DX-tile free ligation were calculated to be 0.40 ± 0.096 μmol $L^{-} h^{-}$ and 0.07 ± 0.019 μmol $L^{-} h^{-}$, respectively, indicating that DX-tile can also enhance the reaction rate. In

addition, two side products: 52-nt XA-XA and 62-nt XB-XB – were formed in noticeable amounts in the absence of DX-tile (Figure 28A and C indicated by red and orange arrows, respectively). We, therefore, concluded that, as a catalyst, the DX tile-like association increases the ligation yield by ~12-fold, the reaction rate by ~5.7-fold, and improves the reaction specificity.

We also tested the possibility of bringing the ends of the two DNA strands together using a simpler arrangement than the DX tile, where Rail 1 and 2 strands were bound to each other directly (without staple strands) and formed a 'bubble' with the sequences complementary to the strands to be cross-linked (Figure 54). However, such a system produced only ~7 % of the ligation product, thus confirming the advantage of the DX tile as a template for chemical ligation.

The identified optimal conditions were also applied for the ligation of XA 3p and XB 3p strands to achieve the 3'-3' ligation of two DNA strands (Figure 53). Under these conditions, the reaction reached a plateau within 16 h with a yield of 52 % for the 3'-3' ligation products (Figure 29B, Lane 3). This ligation yield was lower than for the 5'-5' ligation product, most likely due to the lower reactivity of the secondary phosphate group and unassembled reacting strands (Figure 46B). However, we do not exclude that further optimization may improve the yield of the 3'-3' ligation.

5.3.2 Isolation of the ligation products

After the ligation reaction, the DNA strand with switched polarity remained in the mixture with other DX tile-forming DNA strands. To isolate the ligation product, we added oligonucleotides that were fully complementary to the strands Rail 1g1 and 2g1, Staple 5 and 6. This mixture was digested with Exo VIII, an exonuclease that degrades double-stranded DNA

(dsDNA) in the 5’ to 3’ direction. We hypothesized that since the XA 5p-p5 XB ligation product did not have free 5’ ends, it would remain resistant to the Exo VIII treatment.

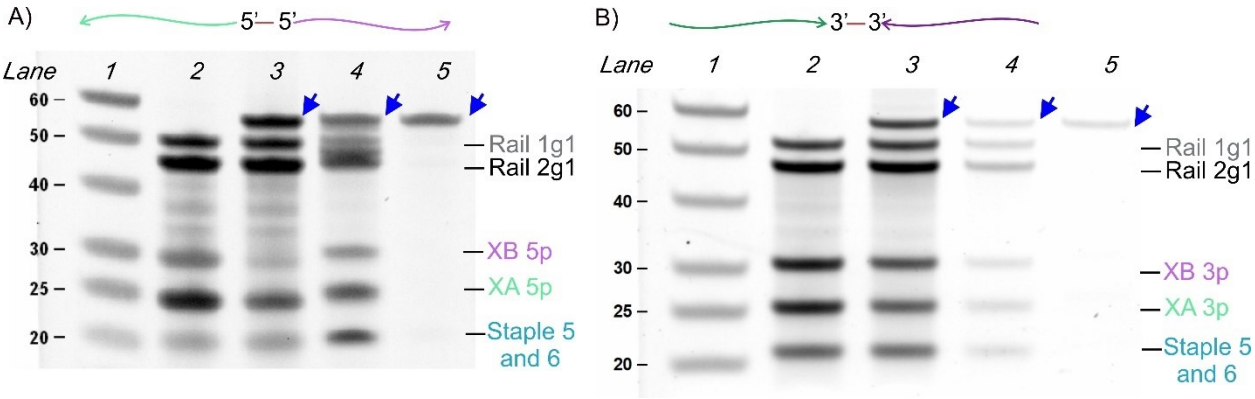

Figure 29. 12% dPAGE analysis of the synthesis and isolation steps for the A) 5’-5’ ligation products or B) 3’-3’ ligation product. Lane 1: ssDNA ladder (the sizes of the ladder bands are indicated to the left of the lane); lane 2: DX-tile prior to crosslinking; lane 3: DX-tile after the reaction (the 5’-5’ and 3’-3’ ligation yield is ~70% and 52%, respectively); lane 4: Ligation reaction mixture prior to the digestion of the tile components by the exonuclease treatment; lane 5: same as lane 4 after the exonuclease treatment. Blue arrows indicate the crosslinking product XAp-pXB with the expected length of 57 nt.

Indeed, after treatment, we obtained a single DNA strand (Figure 29A, *Lane 5*), which could be further purified from Exo VIII by routine phenol extraction and ethanol precipitation. The size of the 5’-5’ ligation product corresponds to the expected length (indicated by blue arrows in Figure 29A, *Lanes 3-5*). Similarly, we achieved isolation of the pure XA 3p-p3 XB product upon treatment with Exo III, which degrades both dsDNA and ssDNA in the 3’ to 5’ direction. In this case, there was no need to add DNA strands complementary to Rail 1g1 and 2g1 or the staple strands. Similar to the 5’-5’ ligation product, the length of the 3’-3’ product did not change during the enzymatic treatment, which indicates the absence of the free 3’-ends and confirms the structure

of the ligation product (Figure 29B, *Lane 5*). Therefore, the switched polarity feature of the ligation products makes them suitable for an easy isolation procedure affordable by even low-resource laboratories. Furthermore, both the purified and unpurified 5'-5' ligation products are stable at room temperature over 30 days (Figure 55).

5.3.3 Synthesis and characterization of 'the impossible wheel'.

DNA strands with switched polarity have been used for ligation of plasmid DNA via triplex formation,[170] as probes for nucleic acid analysis,[171,172] for the DNA-peptide library display system,[167] and to improve hemin-dependent peroxidase activity of G-quandruplexes.[173] However, to the best of our knowledge, such strands have not been explored by DNA nanotechnology, possibly due to a limited accessibility of this material. To illustrate the potential of DNA strands with switched polarity in DNA nanotechnology, we designed and synthesized a circular DNA nanostructure that we named an 'impossible DNA wheel' (Figure 30A). This structure is impossible to create by plain intramolecular self-hybridization of a regular DNA oligonucleotide because of the parallel orientation of the DNA fragments in the double-stranded region (Figure 30A, left). However, it is possible to form the 'impossible wheel' from a DNA strand with switched polarity (Figure 30A, right).

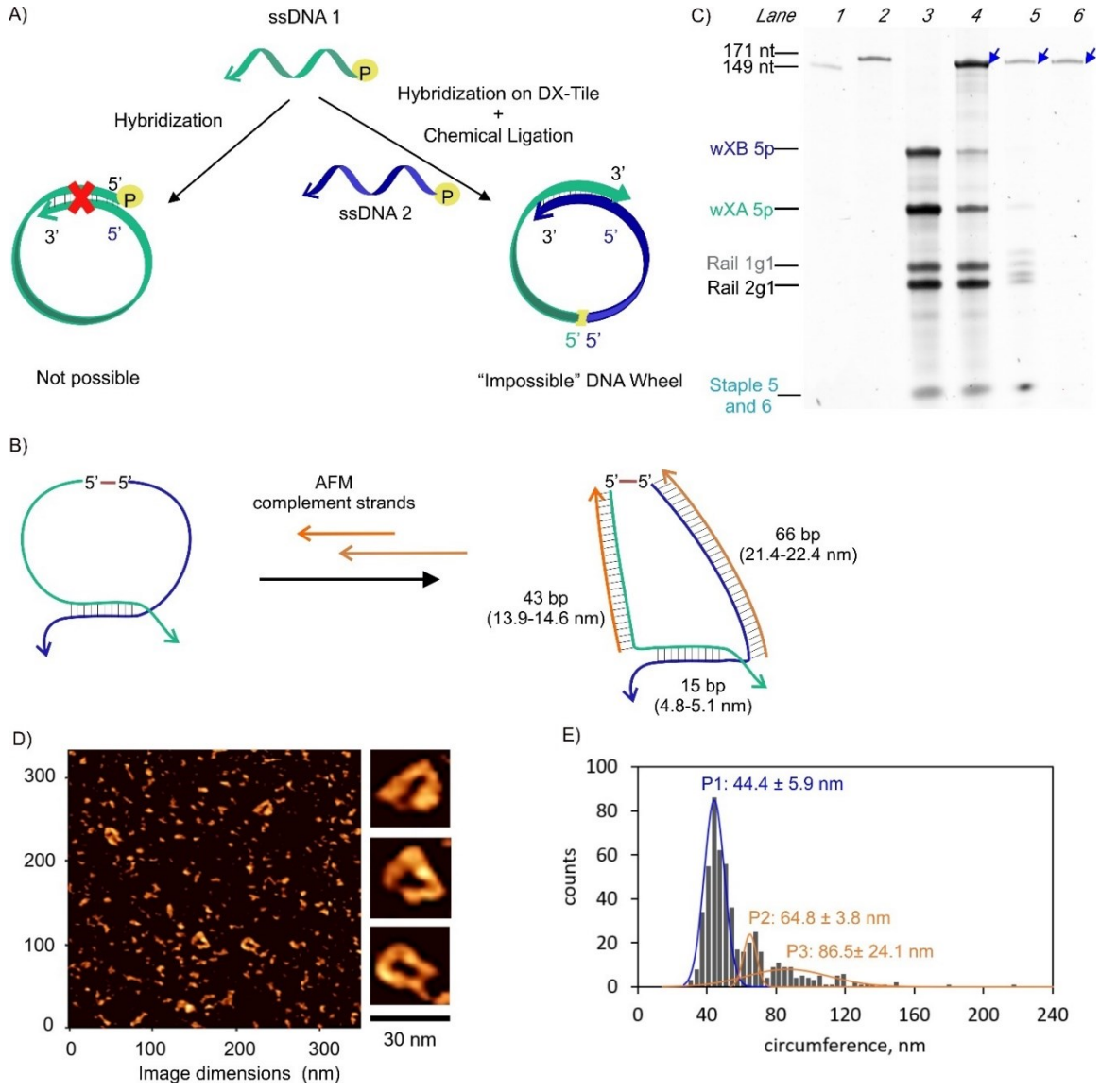

Figure 30. A) Scheme comparing the structural requirements for 'the impossible DNA wheel' structure, B) enforcement of the wXA 5p-p5 wXB assembly with the complementary strands to form a triangle-shaped-impossible DNA wheel for AFM imaging, C) 8% dPAGE ran at 60°C; *lane 1*: 149 nt DNA marker; *lane 2*: 171 nt DNA marker; *lane 3*: impossible DNA wheel sample before the ligation reaction; *lane 4*: same as lane 3 after the reaction, yield 69 ± 4 %; *lane 5*: ligation product before Exo VIII treatment; *lane 6*: ligation product after Exo VIII digestion. D) Representative AFM image of the triangle-shaped-impossible DNA wheel. E) Gaussian distribution of the contour measurements, N: 521

In this work, we designed a DNA wheel to be 166 nt and formed by the 5'-5' ligation of a 70-nt long wXA 5p and 96-nt long wXB 5p complementary to each other by 15 bp (60% GC). As a scaffold, we used the same DX-tile system to hold the reacting strands wXA 5p and wXB 5p as was used in our prior experiments. Thus, synthesis of DNA wheels shorter or longer than 166 nt can be attempted by using the same DX-tile system if the DX-tile binding site of both reacting strands is conserved. The reaction yield was 68 ± 4 %, (Figure 30C, *Lane 4*), and isolation of the pure product was achieved by Exo VIII treatment (Figure 30C, *Lane 6*), as explained above.

To detect the 'impossible DNA wheel' by atomic force microscopy (AFM), this structure was re-shaped into a dsDNA triangle (Figure 30B) by adding two oligonucleotide strands – W1-Tri-A and W1-Tri-B (Table 11), which were complementary to the ssDNA region of the ligation product. This was needed to increase the rigidity and visibility of the structure in the AFM image.[174] The triangle shape was visualized by AFM imaging (Figure 30D). Based on the pitch of ds B-DNA (0.32-0.34 nm/bp), our impossible DNA wheel was estimated to have a circumference of 40 - 42 nm in its triangular shape. To confirm the presence of the expected DNA wheel, contour measurements were performed on a population of 521 ring structures observed during AFM imaging (Figure 56). From the Gauss distribution of the observed formations, 3 distinct populations were observed, with 385 of the structures falling under population P1 (44.4 ± 5.9 nm), which is closer to the expected circumference of 42 nm. We hypothesize that the observed broad range of sizes (P2 and P3) can be explained by the polymerization of the DNA wheel due to its self-complementarity (Figure 30B).

5.3.4 Chemical Ligation of DNA IC cascading 4J YES gates

From the understanding of the chemical ligation that 1-CNI with Mn^{2+} induces on DNA oligonucleotides and optimal conditions achieved in section 5.3.1, we investigated this chemical ligation for the covalent crosslinking of the DNA ICs components. We decided to explore the chemical ligation of Staple 1 with 1A and 1B (Figure 31A) and additionally with 2A and 2B (Figure 31B). To maintain a DNA canonical backbone, we attempted to ligate each phosphorylated end with a 2' hydroxyl group from a ribonucleotide positioned at the beginning of the rail binding fragments. Figure 31C, *lanes 1* and *2* show the results from before and after the reaction of the DNA IC in Figure 31A, while *lanes 3* and *4* show the results from before and after the reaction of the DNA IC in Figure 31B. The ligation product from DNA IC Figure 31A was expected to be 74 nt long; however, we only observed the appearance of a new band at around 52 nt (*lane 2* yellow arrow, Figure 31C). This new band could correspond to the ligation of staple 1 with either 1A or 1B since their ligation product would be 48-49 nt long. Although the rail strands ran around the 75 nt marker, we did not observe an increase of intensity from their bands to indicate a product formed was matching their gel mobility. On the other hand, the ligation product from DNA IC B was expected to be 128 nt long. In Figure 31C, *lane 4*, we observed traces of migrating oligonucleotides near 100 nt mark, however, their yield was poor for later assays to confirm their identity. We also observed the appearance of a new band at around 80 nt (blue arrow). This band could correspond to the ligation of staple 1 along with two 4J YES components (e.g. staple 1-1B-2B, staple 1-1A-1B, etc) since their ligation product would correspond to 76 nt. Moreover, the same product at the 52 nt mark appeared with a higher intensity than in *lane 2* yellow arrows. In both ligation reactions, we also observed the appearance of lower than 20 nt long, which we hypothesized it could be the result of a cyclization product.

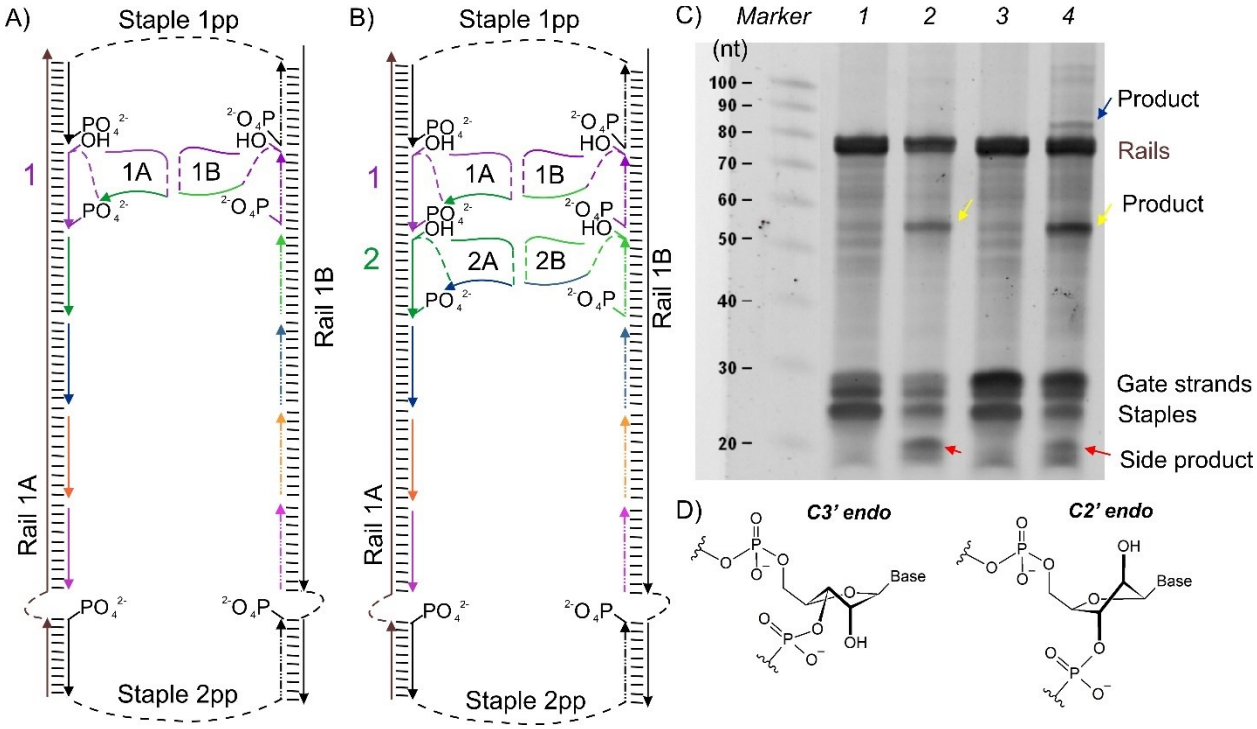

Figure 31. Covalent crosslinking of DNA IC module 1. A) Rails were assembly with staple 1 and 2 with phosphorylated termini and 1A and 1B with one ribonucleotide at the beginning and a phosphate at the end of the fragment binding its respective rail. The addition of YES 2 components with the same characteristics is shown in B). C) 12% dPAGE – 8 M urea for the analysis of the chemical ligation. Lane Marker: ssDNA ladder (the nt sizes of the ladder bands are indicated to the left of the lane); lane 1: DNA IC with YES 1 prior to crosslinking; lane 2: DNA IC with YES 1 after the reaction; lane 3 DNA IC with YES 1 and YES 2 prior to the reaction, and lane 4: DNA IC with YES 1 and YES 2 after the reaction. D) ribose C3' and C2' endo conformations.

Due to the C3' endo conformation that RNA's ribose adopts (Figure 31D), we hypothesized that the positioning of the 2' hydroxyl group hinders its nucleophilic attack. This position would specifically affect the crosslinking between 2A with 1A and 1A with staple 1, where the 3' phosphate must be reached preferentially by a C2' endo hydroxyl group. On the other hand, the C3' endo conformation would favor the crosslinking of staple 1 with 1B and 1B with 2B since the 5' phosphate can be reached by the axial 2'hydroxyl group.

To overcome the limitations inherent in the ribose conformation and weak nucleophilic strength from the oxygen in the 2' hydroxyl, we explored the use of a primary amine linked to the phosphate backbone of DNA through an aliphatic chain (Figure 32). This amino linker is a commercially available modification that could be integrated internally into the DNA backbone; thus, facilitating its position at either an A or B 4J YES component (Figure 32A) for their chemical ligation with a 5' or 3' terminal phosphate group. In Figure 32B, we show the chemical structure of the modified DNA IC components highlighted with a blue box (Figure 32A) and product after the chemical ligation using 1-CNI and M^{2+} (e.g. Mn^{2+}).

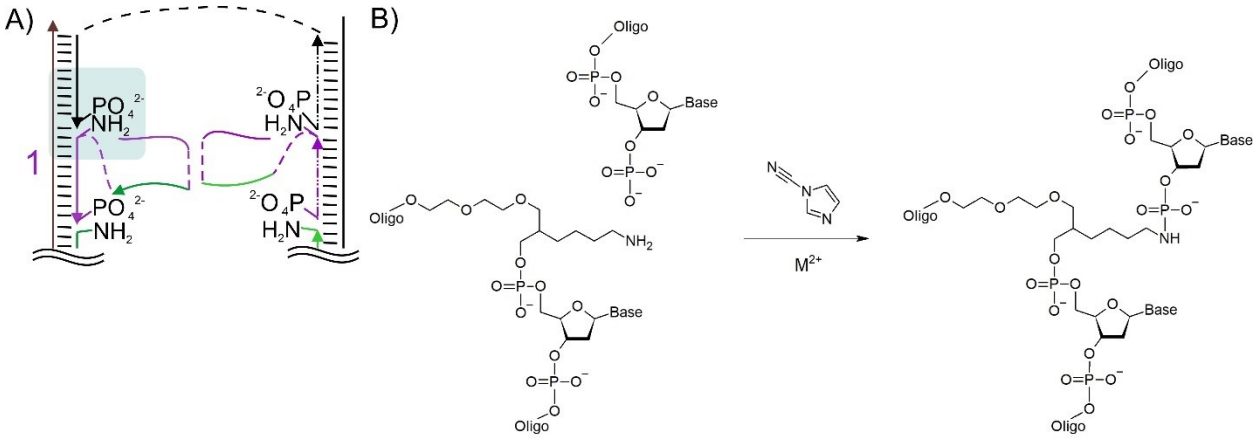

Figure 32.Replacement of 2' hydroxyl for a primary amine as anucleophile for the ligation of two DNA fragments. A) A fragment of the DNA IC shows the position of the primary amino linkers for their close localization to the phosphorylated ends of the DNA IC components. B) the chemical reaction for the ligation of the two DNA fragments (highlighted blue on A) by a phosphoramidate bond using 1-CNI and M^{2+} (e.g. Mn^{2+}) as condensing agents.

We performed the chemical ligation of the DNA IC structure shown in Figure 33A by using the same condensing agents and conditions established in section 5.3.1. We opted to reduce the length of the DNA board rails to avoid the possible overlapping migration of these strands with

the target product. Lanes 1 and 2 of Figure 33B show the before and after chemical ligation, where the appearance of two highly intense bands occurred with a PAGE mobility at 59 nt (yellow arrow) and 90 nt (blue arrow) based on the ssDNA marker bands. The expected size of the ligation product of structure A was 74 nt; however, due to the weight contribution of the polyethylene glycol linkers (dashed lines) and aliphatic chain attaching the primary amine its PAGE mobility can slow down. Thus, we hypothesize that the 90 nt band could be our target product. To isolate this product from the reaction mixture, we performed a gel extraction of this specific band and confirmed its successful gel elution on lane 3, Figure 33B.

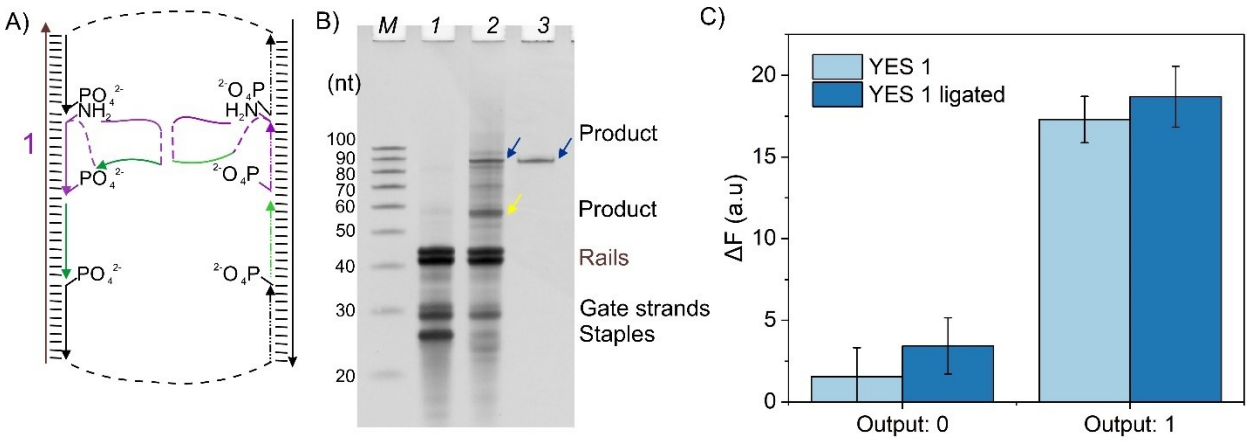

Figure 33. Chemical ligation of DNA IC YES 1 gate by phosphoramidate linkage. A) DNA IC structure showing the location of primary amino groups at YES 1 (1A and 1B) and the localization of all phosphorylated DNA termini. B) 12% dPAGE- 8M urea. M: ssDNA ladder (the nt sizes of the ladder bands are indicated to the left of the lane); lane 1: DNA IC with YES 1 before crosslinking; lane 2: DNA IC with YES 1 after the reaction; lane 3: ligation product after gel extraction step. C)Fluorescence readout at 515 nm λ emission after excitation at 485 nm using MB1 as a reporter of the YES 1 after ligation and a YES 1 without any strand modifications both 4J YES gates were anchored on DNA board module 1 of Chapter Three.

Lastly, we performed a fluorescence assay using the gel extracted ligation product alongside its unmodified and non-ligated counterpart (Figure 33C). The results indicate no

significant difference in the performance of the ligated 4J YES 1 gate in comparison to its non-ligated and unmodified version. These results suggest that this reaction could be used to scale the number of covalently crosslinked 4J computing units and that their computation performance can remain intact after their ligation and isolation.

5.4 Conclusions

DNA nanotechnology has introduced several sophisticated structures, many of which are being applied in biotechnology, gene therapy, and molecular computation.[159] For example, the DX tile (Figure 25B), a more rigid building block than dsDNA, has been used for assembling two-dimensional DNA crystals,[175] algorithmic self-assembly of DNA Sierpinski triangles,[176] barcode-patterned lattices,[177] DNA scissors,[178] hexagonal RNA nanotubes,[179] among other applications.[159] Here, we used the DX tile in yet another role: as a catalyst of a chemical reaction. We hypothesized that the 2D structure of the DX tile can broaden the capabilities of the DNA-templated reactions explored earlier.[151–155] To illustrate the feasibility of using the DX tile as a catalyst, we synthesized 5'-5' and 3'-3' linked oligonucleotides of random sequences because of the practical significance of the reaction products, as well as the absence of catalysts of these reactions. Such oligonucleotides can be prepared by the automated chemical nucleic acid synthesis using both conventional 3'-phosphoramidites and non-conventional and expensive 5'-phosphonamidites.[167,171,172] In practice, however, synthesis of such strands requires a laboratory equipped with a DNA synthesizer, which makes such synthetic products unaffordable by an overwhelming majority of potential users. A DNA templated synthesis of 5'-5' and 3'-3' linked oligonucleotides was reported by Chen et al.,[167] who took advantage of the parallel duplex

formation between poly A and poly T sequences. This method, however, puts a limitation on the choice of the sequences of oligonucleotides to be ligated: at least one DNA strand must be poly T or poly A oligonucleotide.

The DX tile-assisted ligation uses only the proximity and orientation effect to achieve >12-fold yield enhancement, >5-fold reaction rate, and unlike the corresponding uncatalyzed reaction, results in no byproducts. Both yield enhancement and high reaction specificity are attributes of enzymatic catalysis. In this work, we did not explore multiple catalytic turnovers under the conditions when reactants are used in excess over the DX tile structure. Such reactions have been studied in the context of DNA and RNA templated synthesis and were reported to achieve up to 92 turnovers when optimized.[180] We also did not attempt to achieve the highest possible reaction yields of 1-CNI chemistry, since this was performed earlier using 3'-5' templated oligonucleotide ligation.[164,165,168]

While developing this technique, we noticed that the ligation yield was significantly improved when both reacting strands had phosphorylated ends, in comparison with the earlier used systems having only one strand phosphorylated. This higher reactivity can be explained both by a greater probability for the reactants to be activated by 1-cyanoimidazole, as well as greater nucleophilicity of the phosphate group in comparison with hydroxyl group under the chosen conditions. The ligation products in this case contained a phosphoanhydride instead of a regular phosphodiester linkage, which raised a question regarding its chemical stability in aqueous solutions. However, we did not observe degradation of the ligation product over 30 days at 22°C at pH 7.4. (Figure 55).

For downstream applications, oligonucleotides with switched polarity obtained via the DX tile-assisted ligation may need to be isolated from the mixture of the DX tile-forming strands, which would traditionally require HPLC or gel electrophoresis. To avoid a tedious purification procedure, we took advantage of the absence of free 5'-ends in the 5'-5' ligation product or free 3'-ends in the 3'-3' ligation products and treated the reaction mixtures with either 5'- or 3'-exonuclease that would degrade all DNA present except the ligation products and treated the reaction mixtures with either 5'- or 3'-exonuclease that would degrade all DNA present except the ligation products. This experiment highlights the improved nuclease resistance of the 5'-5' and 3'-3' oligonucleotides and inspires follow-up investigations. Furthermore, we demonstrated that the ligation approach is applicable to form oligonucleotides with switched polarity of different lengths. Indeed, we used the DX tile-assisted ligation to synthesize a 166-nt long 'impossible DNA wheel' structure. We hope that the high ligation yield, applicability to any nucleic acid sequences, and simple purification procedure will make the reported synthetic scheme useful in laboratory practice.

It is worth noting that the DX-like structure can accommodate up to four functional groups in the middle if both 3' and 5' of XA and XB strands are functionalized. Some of the functional groups can act as catalysts, while others as reagents. This would create a more sophisticated arrangement of functional groups, which may enable exploration of several catalytic strategies to mimic natural enzymes. Other structures that allow bringing together more than 4 groups, such as 5-, 8- and 12-way DNA junctions,[181,182] can be explored for building even more sophisticated catalytic sites. We demonstrated that a DNA nanostructure can be used to facilitate reactions not achievable by any known enzyme. DNA strands of arbitrary sequences can be joined together by their 3'-3' or 5'-5' ends with a rate and yield enhancement of more than 5 and 12-fold, respectively,

and greater specificity than for the uncatalyzed reaction. This was achieved due to the proximity and orientation catalytic strategy provided by the DX tile-like scaffold. Building catalytic centers by attaching functional groups to specific positions of DNA nanostructures can become a new strategy for the rational design of artificial catalysts.

Lastly, from the understanding and expertise of using 1-CNI and Mn2+ as condensing agents for the chemical ligation of DNA oligonucleotides, we applied this chemical reaction to the crosslinking of the DNA components in our DNA IC computation module from Chapter Three. We successfully achieved the chemical ligation of a full YES 1 (1A + 1B) with its neighboring staple 1pp. Their covalent crosslink occurred through the linkage of an internal amino group at 1A and 1B with the terminal phosphates from Staple 1pp forming a phosphoramidate bond. After their chemical ligation, YES 1 shows a similar computation performance as its non-modified and non-ligated version, which demonstrates the suitability of this type of linkage for the consolidation of a DNA IC into one molecular computation unit without compromising its function.

CHAPTER SIX: CONCLUSIONS

The pathway to personalized medicine is sought to consider all genetic heterogeneity driving a genetic disease. Thus, there is a need for diagnostics and therapeutic tools with multiplex and smart components to compute all the molecular drivers. DNA molecular computers are sought to fill this need due to their sequence programmability, multiplex and parallel processing ability, and biocompatibility.

In this work, we provided fundamental principles and practical approaches to develop DNA molecular computers built from the integration of DNA computing units into DNA boards which results in DNA ICs. This dissertation investigated four research questions oriented to the rational construction of high-complexity DNA circuitry. Chapter One provided an outlook on the advantages of spatial localization of DNA computing units on DNA boards and the need for better design strategies and architectures to advance the technology. To allow the scalable and versatile fabrication of DNA ICs, we developed modular 4J DNA logic gate units, a novel DNA board, and a new molecular readout system to improve DNA IC computing speed determination.

From Chapter Two, we demonstrated for the first time that DNA 4J gates with YES and NOT Boolean functions can be connected to make IMPLY, while two NOT gates can make NAND functionally complete logic functions by following non-Boolean connectivity pathways. This approach opens a route to building computational circuits of arbitrary complexity from simple YES and NOT 4J DNA logic gates. This modular connectivity could ease the burden of developing new architectures when realizing new Boolean circuitries and demonstrated that DNA molecular computing systems may offer opportunities unrealized in electronics.

The results in Chapter Three demonstrated that our DNA board nanostructure provides spatial localization support for inter-gate communication of DNA computation units. This DNA board provided: i) adjustable size based on circuit density, ii) a reduced number of constituents to minimize misassembling, iii) connectivity with one or more DNA board modules, and iv) rational spatial orientation of the computing units. None of these features have been attributed to previously proposed DNA board systems. Furthermore, we reported a CGP of 3.4 nm corresponding to the shortest spatial distancing among DNA logic gates anchored on a DNA board. From a DNA IC module cascading up to ten 4J YES gates as a signal transmission wired, we observed that after the seventh cascaded gate signal propagation and signal dissipation reached a plateau, and adding more cascading units did not affect this borderline.

In Chapter Four, we reported that DNA IC computation times can be influenced by the type of molecular readout reporter used and dynamic structural changes of the DNA board. Therefore, a new reporter was developed to be localized in the DNA board and lack secondary structures, minizing its additive contribution to the observed computation times. Using this reported we observed a computation time (t_{90}) < 3 min achieved by a cascade of four 4J YES gates and its t_{50} < 1 s which are the shortest computation times reported. These suggest that 90% of the DNA ICs had released their output in < 3 min, accounting for a signal propagation rate of 4.5 nm/min. Thus, using 4J YES gates as computation units can overcome the limitations of slower computation speeds when building DNA molecular computers with higher-density DNA ICs.

Lastly in Chapter Five, we demonstrated that using 1-CNI and Mn^{2+} as condensing agents for the chemical ligation of DNA IC components through a phosphoramidate linkage was possible without compromising the computation performance of the ligated computing unit. The results

suggest that this bioconjugation route could be implemented to consolidate a full DNA IC into one molecular unit. Furthermore, we reported that a DNA nanostructure can be used to facilitate reactions not achievable by any known enzyme. DNA strands of arbitrary sequences can be joined together by their 3'-3' or 5'-5' ends with a rate and yield enhancement of more than 5 and 12-fold, respectively, and greater specificity than for the uncatalyzed reaction. This was achieved due to the proximity and orientation catalytic strategy provided by the developed DX tile-like scaffold. Thus, building catalytic centers by attaching functional groups to specific positions of DNA nanostructures can become a new strategy for the rational design of artificial catalysts.

In summary, the outcomes from the investigation of each research question covered in this dissertation aim to provide designing and fabrication pathways to advance DNA molecular computing technologies. The scalability and customization of these DNA molecular devices can lead to their use as biotechnological and biomedical tools, as well as for general-purpose computations.

APPENDIX A: COPYRIGHT PERMISSIONS

Bardales, A.C.; Smirnov, V.; Taylor, K.; Kolpashchikov, D.M. DNA Logic Gates Integrated on DNA Substrates in Molecular Computing. *ChemBioChem* **2024**, *25*, e202400080. DOI:10.1002/cbic.202400080. Copyright 2024 John Wiley & Sons, Inc

JOHN WILEY AND SONS LICENSE

TERMS AND CONDITIONS

Sep 01, 2024

This Agreement between Andrea C. Bardales ("You") and John Wiley and Sons ("John Wiley and Sons") consists of your license details and the terms and conditions provided by John Wiley and Sons and Copyright Clearance Center.

License Number 5860441143407

License date Sep 01, 2024

Licensed Content Publisher John Wiley and Sons

Licensed Content Publication ChemBioChem

Licensed Content Title DNA Logic Gates Integrated on DNA Substrates in Molecular Computing

Licensed Content Author Dmitry M. Kolpashchikov, Katherine Taylor, Viktor Smirnov, et al

Licensed Content Date Mar 8, 2024

Licensed Content Volume 25

Licensed Content Issue 8

Licensed Content Pages 10

Type of use Dissertation/Thesis

Requestor type Author of this Wiley article

RightsLink Printable License

https://s100.copyright.com/App/PrintableLicenseFrame.jsp?publisherI...

1 of 6 9/1/2024, 6:49 PM

Format Print and electronic

Portion Full article

Will you be translating? No

Title of new work Developing integrated DNA molecular circuits

Institution name University of Central Florida

Expected presentation date Dec 2024

Order reference number 10

The Requesting Person / Organization to

Appear on the License Andrea C. Bardales

Requestor Location

University of Central Florida

4111 Libra Dr #255

ORLANDO, FL 32816

United States

Attn: University of Central Florida

Publisher Tax ID EU826007151

Total 0.00 USD

Terms and Conditions

TERMS AND CONDITIONS

This copyrighted material is owned by or exclusively licensed to John Wiley & Sons, Inc. or one of its group companies (each a"Wiley Company") or handled on behalf of a society with which a Wiley Company has exclusive publishing rights in relation to a particular work (collectively "WILEY"). By clicking "accept" in connection with completing this licensing transaction, you agree that the following terms and conditions apply to this transaction (along with the billing and payment terms and conditions established by the

publisher. You shall also duplicate the copyright notice that appears in the Wiley publication in your use of the Wiley Material. Permission is also granted on the understanding that nowhere in the text is a previously published source acknowledged for all or part of this Wiley Material. Any third party content is expressly excluded from this permission.

• With respect to the Wiley Materials, all rights are reserved. Except as expressly granted by the terms of the license, no part of the Wiley Materials may be copied, modified, adapted (except for minor reformatting required by the new Publication), translated, reproduced, transferred or distributed, in any form or by any means, and no derivative works may be made based on the Wiley Materials without the prior permission of the respective copyright owner.For STM Signatory Publishers clearing permission under the terms of the STM Permissions Guidelines only, the terms of the license are extended to include subsequent editions and for editions in other languages, provided such editions are for the work as a whole in situ and does not involve the separate exploitation of the permitted figures or extracts, You may not alter, remove or suppress in any manner any copyright, trademark or other notices displayed by the Wiley Materials. You may not license, rent, sell, loan, lease, pledge, offer as security, transfer or assign the Wiley Materials

on a stand-alone basis, or any of the rights granted to you hereunder to any other person.

• The Wiley Materials and all of the intellectual property rights therein shall at all times remain the exclusive property of John Wiley & Sons Inc, the Wiley Companies, or their respective licensors, and your interest therein is only that of having possession of and the right to reproduce the Wiley Materials pursuant to Section 2 herein during the continuance of this Agreement. You agree that you own no right, title or interest in or to the Wiley Materials or any of the intellectual property rights therein. You shall have no rights hereunder other than the license as provided for above in Section 2. No right, license or interest to any trademark, trade

name, service mark or other branding ("Marks") of WILEY or its licensors is granted hereunder, and you agree that you shall not assert any such right, license or interest with respect thereto

• NEITHER WILEY NOR ITS LICENSORS MAKES ANY WARRANTY OR REPRESENTATION OF ANY KIND TO YOU OR ANY THIRD PARTY,

EXPRESS, IMPLIED OR STATUTORY, WITH RESPECT TO THE MATERIALS OR THE ACCURACY OF ANY INFORMATION CONTAINED IN THE MATERIALS, INCLUDING, WITHOUT LIMITATION, ANY IMPLIED WARRANTY OF MERCHANTABILITY, ACCURACY, SATISFACTORY QUALITY, FITNESS FOR A PARTICULAR PURPOSE, USABILITY, INTEGRATION OR NON-INFRINGEMENT AND ALL SUCH WARRANTIES ARE HEREBY EXCLUDED BY WILEY AND ITS LICENSORS AND WAIVED BY YOU.

• WILEY shall have the right to terminate this Agreement immediately upon breach of this Agreement by you.

• You shall indemnify, defend and hold harmless WILEY, its Licensors and their respective directors, officers, agents and employees, from and against any actual or threatened claims, demands, causes of action or proceedings arising from any breach of this Agreement by you.

• IN NO EVENT SHALL WILEY OR ITS LICENSORS BE LIABLE TO YOU OR ANY OTHER PARTY OR ANY OTHER PERSON OR ENTITY FOR ANY SPECIAL, CONSEQUENTIAL, INCIDENTAL, INDIRECT, EXEMPLARY OR PUNITIVE DAMAGES, HOWEVER CAUSED, ARISING OUT OF OR IN

CONNECTION WITH THE DOWNLOADING, PROVISIONING, VIEWING OR USE OF THE MATERIALS REGARDLESS OF THE FORM OF ACTION, WHETHER FOR BREACH OF CONTRACT, BREACH OF WARRANTY, TORT, NEGLIGENCE, INFRINGEMENT OR OTHERWISE (INCLUDING, WITHOUT LIMITATION, DAMAGES BASED ON LOSS OF PROFITS, DATA, FILES, USE, BUSINESS OPPORTUNITY OR CLAIMS OF THIRD PARTIES), AND WHETHER OR NOT THE PARTY HAS BEEN ADVISED OF THE POSSIBILITY OF SUCH DAMAGES. THIS LIMITATION SHALL APPLY NOTWITHSTANDING ANY FAILURE OF ESSENTIAL PURPOSE OF ANY LIMITED REMEDY PROVIDED HEREIN.

• Should any provision of this Agreement be held by a court of competent jurisdiction to be illegal, invalid, or unenforceable, that provision shall be deemed amended to achieve as nearly as possible the same economic effect as the original provision, and the legality, validity and enforceability of the remaining provisions of this Agreement shall not be affected or impaired thereby.

• The failure of either party to enforce any term or condition of this Agreement shall not constitute a waiver of either party's right to enforce each and every term and condition of this Agreement. No breach under this agreement shall be deemed

waived or excused by either party unless such waiver or consent is in writing signed by the party granting such waiver or consent. The waiver by or consent of a party to a breach of any provision of this Agreement shall not operate or be construed as a waiver of or consent to any other or subsequent breach by such other party.

• This Agreement may not be assigned (including by operation of law or otherwise) by you without WILEY's prior written consent.

• Any fee required for this permission shall be non-refundable after thirty (30) days from receipt by the CCC.

• These terms and conditions together with CCC's Billing and Payment terms and conditions (which are incorporated herein) form the entire agreement between you and WILEY concerning this licensing transaction and (in the absence of fraud) supersedes all prior agreements and representations of the parties, oral or written. This Agreement may not be amended except in writing signed by both parties. This Agreement shall be binding upon and inure to the benefit of the parties' successors, legal representatives, and authorized assigns.

• In the event of any conflict between your obligations established by these terms and conditions and those established by CCC's Billing and Payment terms and conditions, these terms and conditions shall prevail.

• WILEY expressly reserves all rights not specifically granted in the combination of (i) the license details provided by you and accepted in the course of this licensing transaction, (ii) these terms and conditions and (iii) CCC's Billing and Payment terms and conditions.

• This Agreement will be void if the Type of Use, Format, Circulation, or Requestor Type was misrepresented during the licensing process.

• This Agreement shall be governed by and construed in accordance with the laws of the State of New York, USA, without regards to such state's conflict of law rules. Any legal action, suit or proceeding arising out of or relating to these Terms and Conditions or the breach thereof shall be instituted in a court of competent jurisdiction in New York County in the State of New York in the United States of America and each party hereby consents and submits to the personal jurisdiction of such court, waives any objection to venue in such court and consents to service of process by registered or certified mail, return receipt requested, at the last known address of such party.

WILEY OPEN ACCESS TERMS AND CONDITIONS

Wiley Publishes Open Access Articles in fully Open Access Journals and in Subscription journals offering Online Open. Although most of the fully Open Access journals publish open access articles under the terms of the Creative Commons Attribution (CC BY) License only, the subscription journals and a few of the Open Access Journals offer a choice of Creative Commons Licenses. The license type is clearly identified on the article.

The Creative Commons Attribution License

The Creative Commons Attribution License (CC-BY) allows users to copy, distribute and transmit an article, adapt the article and make commercial use of the article. The CC-BY license permits commercial and nonRightsLink Printable License https://s100.copyright.com/App/PrintableLicenseFrame.jsp?publisherI...

5 of 6 9/1/2024, 6:49 PM

Creative Commons Attribution Non-Commercial License

The Creative Commons Attribution Non-Commercial (CC-BY-NC)License permits use, distribution and reproduction in any medium, provided the original work is properly cited and is not used for commercial purposes.(see below)

Creative Commons Attribution-Non-Commercial-NoDerivs License

Bardales, A.C.; Vo, Q.; Kolpashchikov, D.M. A Laboratory Class: Constructing DNA Molecular Circuits for Cancer Diagnosis. *J. Chem. Educ.* **2024**, *101,* 10, 4360-4369. DOI: 10.1021/acs.jchemed.4c00675. Copyright 2024 American Chemical Society and Division of Chemical Education, Inc.

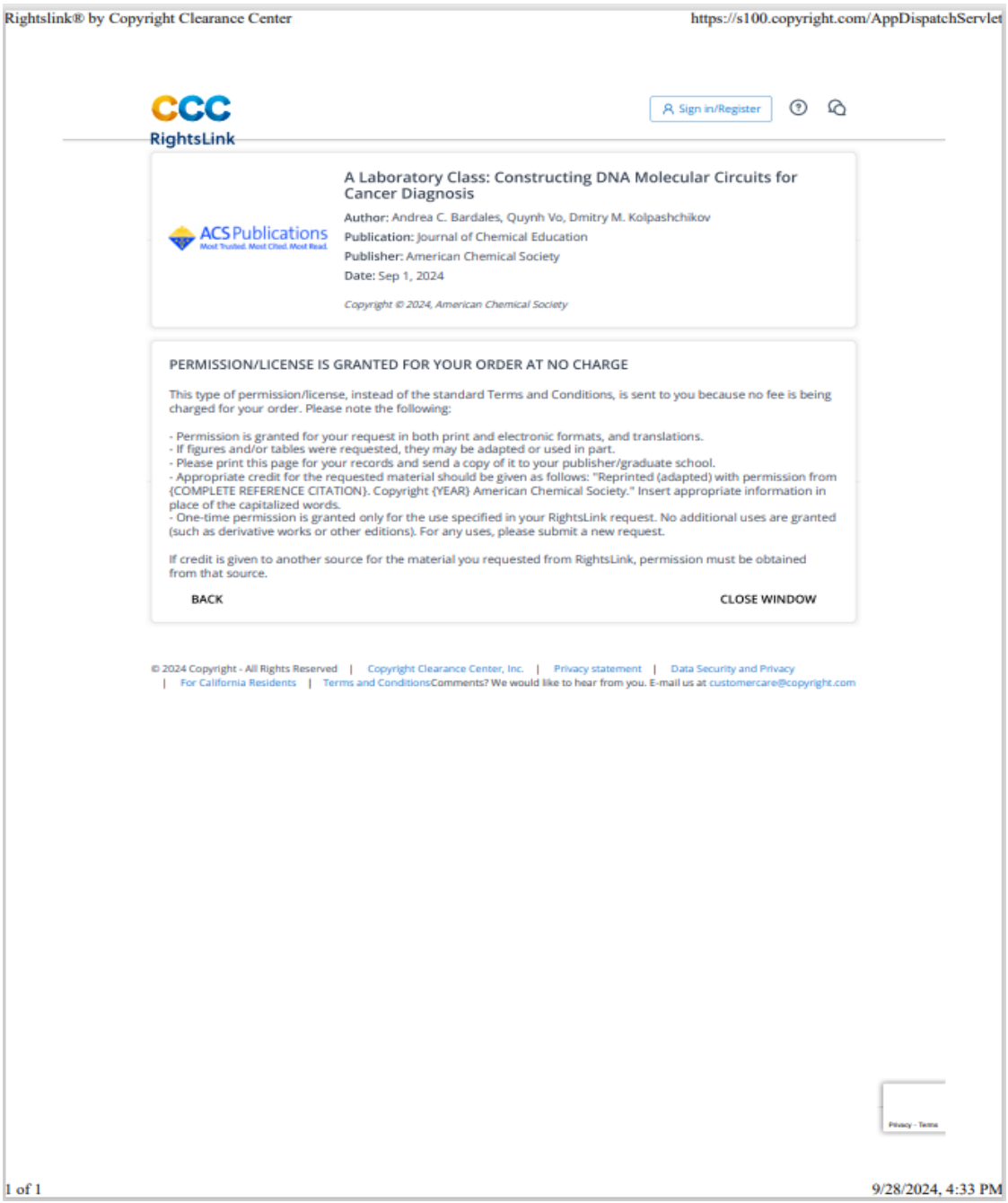

Bardales, A.C.; Vo, Q.; Kolpashchikov, D.M. Singleton {NOT} and Doubleton {YES; NOT} Gates Act as Functionally Complete Sets in DNA-Integrated Computational Circuits. *Nanomaterials* **2024,** *14*, 600. DOI: 10.3390/nano14070600. Open Access-Creative Commons CC by 4.0

Singleton {NOT} and Doubleton {YES; NOT} Gates Act as Functionally Complete Sets in DNA-Integrated Computational Circuits

Bardales, Andrea C.;Vo, Quynh;Kolpashchikov, Dmitry M.

Nanomaterials, 01 Apr 2024, Vol. 14, Issue 7, pages 600 - ...

ISSN: 20794991

DOI: 10.3390/nano14070600

PMID: 38607134

PMCID: PMC11013093

Publisher: MDPI AG

Language: English

Country: Switzerland

URL: https://www.mdpi.com/2079-4991/14/7/600

Less Details >

Abstract:

A functionally complete Boolean operator is sufficient for computational circuits of arbitrary complexity. We connected YES (buffer) with NOT (inverter) and two NOT four-way junction (4J) DNA gates to obtain IMPLY and NAND Boolean functions, respectively, each of which represents a functionally complete gate. The results show a technological path towards creating a DNA computational circuit of arbitrary complexity based on singleton NOT or a combination of NOT and YES gates, which is not possible in electronic computers. We, therefore, concluded that DNA-based circuits and molecular computation may offer opportunities unforeseen in electronics.

everyone is free to re-use the published material if proper accreditation/citation of the original publication is given;

open access publication is supported by the authors' institutes or research funding agencies by payment of a comparatively low Article Processing Charge (APC) for accepted articles.

Permissions

No special permission is required to reuse all or part of article published by MDPI, including figures and tables. For articles published under an open access Creative Common CC BY license, any part of the article may be reused without permission provided that the original article is clearly cited. Reuse of an article does not imply endorsement by the authors or MDPI. Furthermore, no special permission is required for authors to submit their work to external repositories. This policy extends to all versions of a paper: submitted, accepted, and published.

Bardales, A.C.; Mills, J.R.; Kolpashchikov, D.M. DNA Nanostructures as Catalysts: Double Crossover Tile-Assisted 5' to 5' and 3' to 3' Chemical Ligation of Oligonucleotides. *Bioconjugate Chem.* **2024**, *35*,1, 28-33. Copyright 2023 American Chemical Society.

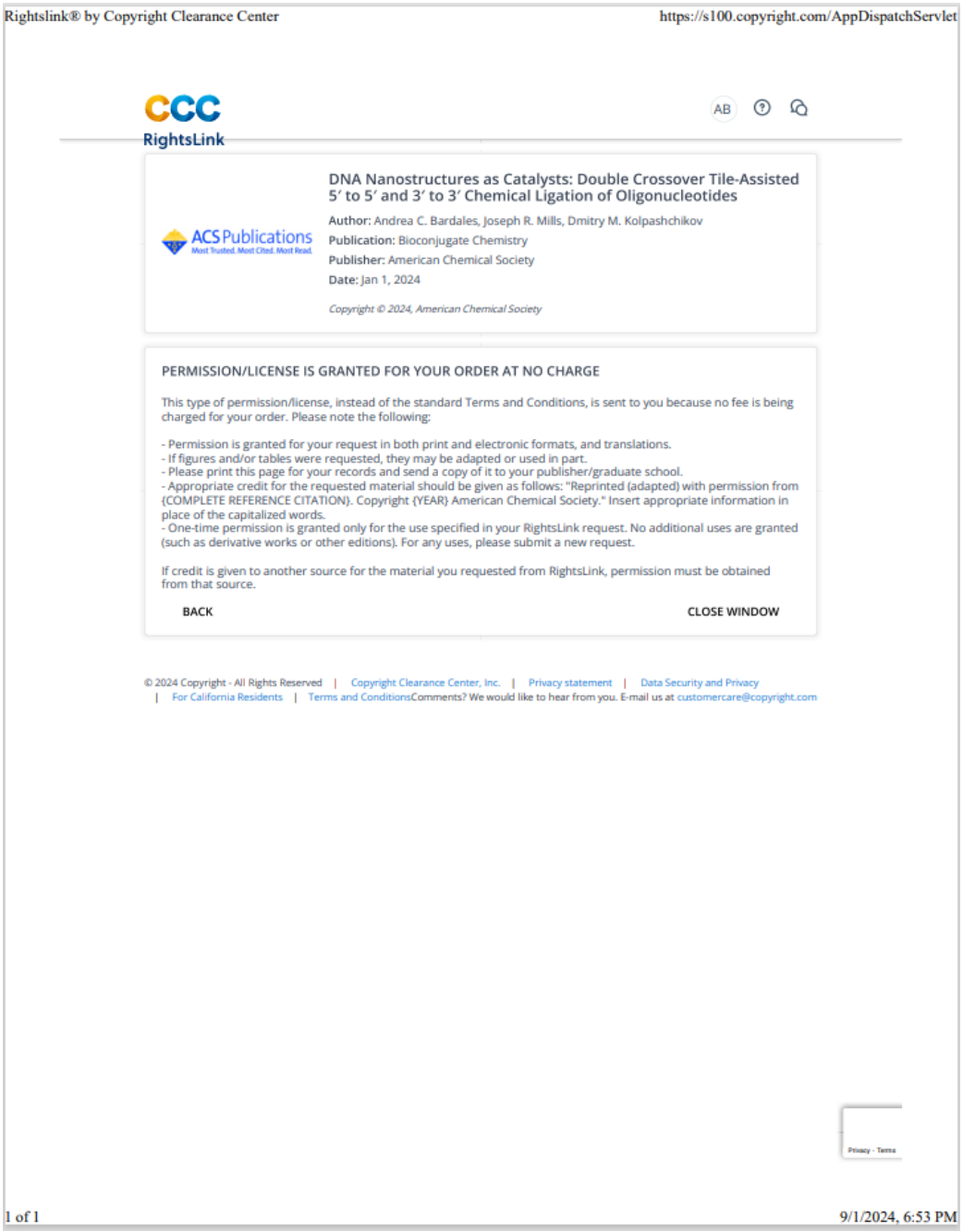

APPENDIX B: CHAPTER THREE SUPPORTING INFORMATION

Table 12. List 2 of Oligonucleotides used in Chapter Three studies

Name	Sequences
DNA Board Module 2	
4J Rail 3	TGTCT CCCTC ACT ATG CTA G TC C TGT ATG TC A TGC CGT TGT GCT TGA GCA CC CTC AGT CCT TC /iSp9/ GAG AGA GAA TAC ACA
4J Rail 4	CAA CTA AAG ACA TAG /iSp9/ C TAC TTC GGG GC AAC TAC GGA CAC GTA CTG T AT CGT ATC GGA CGC TACC TCG GT TCA TCTCTC
4J Staple 3	CTA TGT CTT TAG TTG /iSp18//iSp18/ TGT GTA TTC TCT CTC
4J Staple 4	GAG GGA GAC A/iSp18//iSp18/GA GAG ATG AAC
Blck 8-9A	ACG GCA TGA CAT ACA
Blck 8-9	G ATA CGA TGC AGT AC
Long DNA Board Control	
4J Rail 5	TGTCT CCCTC ACTATGCTAG TCCTGTATGTC ATGCCGTTGT GCTTGAGCACC CTCAGTCCTTC GATC GTA TCA CCT ATC GTG TT TTG TCG CTGA CAC CAC CT GAC CCA TC GTA TCG CTT CCT CTATG
4J Rail 6	CTGAC TGAAT GAG CT CT ACA GA CGA CTA CAG CTGC AGT ACC ACC GTTAG TCA ACT CACT CTG CTACTTCGGG GCAACTACGGA CACGTACTGT ATCGTATCGGA CGCTACCTCG GTTCA TCTCTC
4J Connector 1	TGT GTA TTC TCT CTC CTG TAA ACT AGA CTG
4J Connector 2	GTT AGT ACA AAGT AC CTA TGT CTT TAG TTG

Name	Sequences
YES 6	
6A	CACTGACA /iSp9/ CAATAGATC /iSp9/ GAAGG ACTGAG
6B	CCGA AGTAG /iSp9/ GTTAACATA /iSp9/ CAACACAAG
YES 7	
7A	GAT CTA TTG /iSp9/ A TGG ACAC /iSp9/ GG TGC TCA GGC
7B	TCC GTA GTT GC/iSp9/ TGAAGCAT /iSp9/ TAT GTT AAC
YES 8	
8A	GTGT CCA T /iSp9/ GC GCT AGA /iSp9/ ACA ACG GCA T
8B	G CAG TAC GTG /iSp9/ GA ACT CTC /iSp9/ ATGCTTCA
YES 9	
9A	TCT AGC GC /iSp9/ GAA GA CTC/iSp9/ GA CAT ACA G GA
9Bvi	TCC GAT ACG AT /iSp9/ CT CAA GCC /iSp9/ GAG AG
YES 10	
10Avi	GTC TTC /iSp9/ TCA CCA CAC/iSp9/ CTA GCA TAG T
10Bvi	CGA GGTA GCG /iSp9/GAC AGA CGT /iSp9/ GGC TTG
MB probes	
MB 6	/FAM/CGCTC TTG TGT TG T GTC AGT GAGCG/BHQ1/
Inputs	
I 6	GATCTATTGTATGTTAAC
I 7	GTGT CCA T ATGCTTCA
I 8	TCT AGC GC GAG AGT TC

Name	Sequences
I 9	GAG TC TTC GGC TTG AG
I 10	GTG TGG TGA ACG TCT GT

Each sequence is entered as 5'→ 3'; iSp9 and iSp18 are oligoethylene glycol spacers 9 and 18 from Integrated DNA Technologies (IDT); FAM and BHQ1 correspond to 6-carboxyfluorescein and 3'Black Hole Quencher-1 respectively; /5'-phos/ represents a 5' terminal phosphate group and r indicates ribonucleotide. Extinction coefficients were obtained from OligoAnalizer online calculator OligoAnalyzer from IDT website.

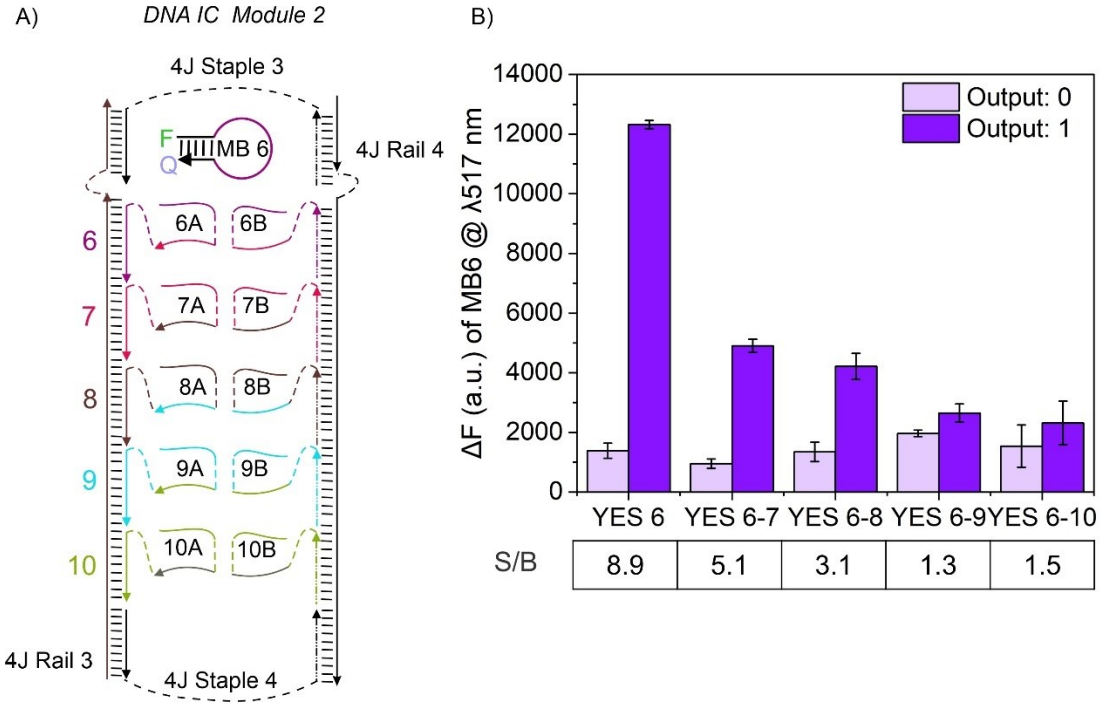

Figure 34. DNA IC Module 2 cascading up to five 4J YES gates (YES 6 to YES 10) A). The DNA board for this module is composed of 4J Rail 3, 4J Rail 4, 4J Staple 3 and 4J Staple 4. B) Fluorescence readout of DNA IC Module 2, where output sequence of YES 6 is translated to fluorescence by MB 6. Each set of bars correspond to the gradual addition of 4J YES gate into the DNA board. Error bars indicate the standard deviation of two independent trials. Data was collected on an RF6000 Shimadzu Fluorescence Spectrometer with a xenon lamp.

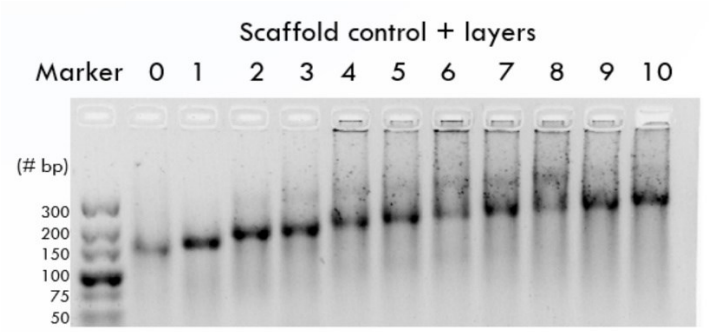

Figure 35. Assembly of ten 4J YES gates on a long DNA board. Samples were loaded on a 4% agarose gel with 20 mM $MgCl_2$ and run with 1xTBE at 70V for 110 min.

APPENDIX C: CHAPTER FOUR SUPPORTING INFORMATION

Fluorescence kinetic measurements on Stopped-Flow

Stopped-flow fluorescence measurements were performed using a SX20 Stopped-flow spectrometer (Applied Photophysics, Ltd.) incorporated with a Xenon Lamp and a photodiode array (PDA) detector. Samples were irradiated at 490 nm within an optical path length of 1.0 mm. Fluorescent emission was detected in volts by setting a long pass filter with a cutoff λ = 515 nm at the entrance slit of the PDA detector and setting the photomultiplier at 365 V.

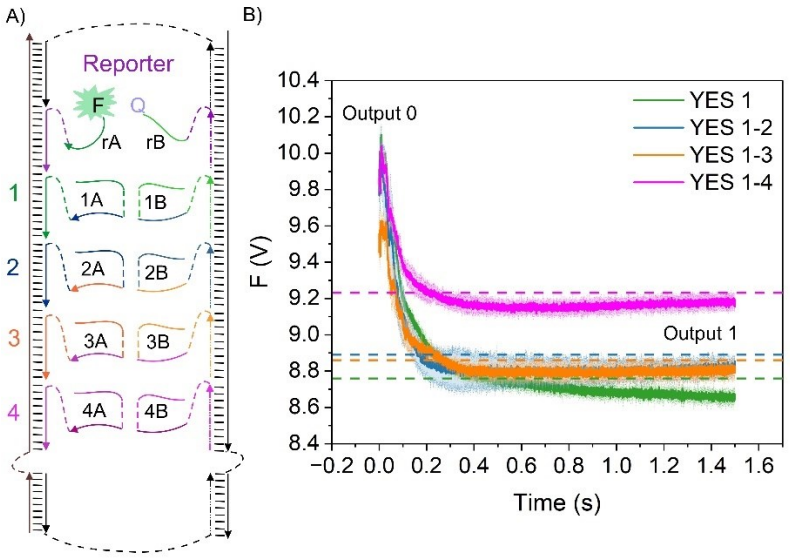

C)

	YES 1	YES 1-2	YES 1-3	YES 1-4
Δ F. (V)	1.17	0.97	0.66	0.66
S/B	1.14	1.1	1.07	1.07
%ADU	12	9	7	7
t_{90}, s	0.474 ± 0.108	0.171 ± 0.01	0.261 ± 0.03	0.212 ± 0.04
t_{50}, s	0.095 ± 0.03	0.074 ± 0.03	0.089 ± 0.07	0.08 ± 0.01

Figure 36. Kinetics of four cascaded 4J Yes gates measured on Stopped-flow fluorescence spectrometer. A) DNA IC module 1.4 scheme. B) kinetic profile of each cascaded 4J YES gate added to the DNA IC; The colored area around each line represents the standard deviation and colored-dashed lines correspond to the 90% fluorescence change achieved after the mixing of the

DNA IC and its corresponding input. C) Thermodynamic parameters and computation times calculated from B).

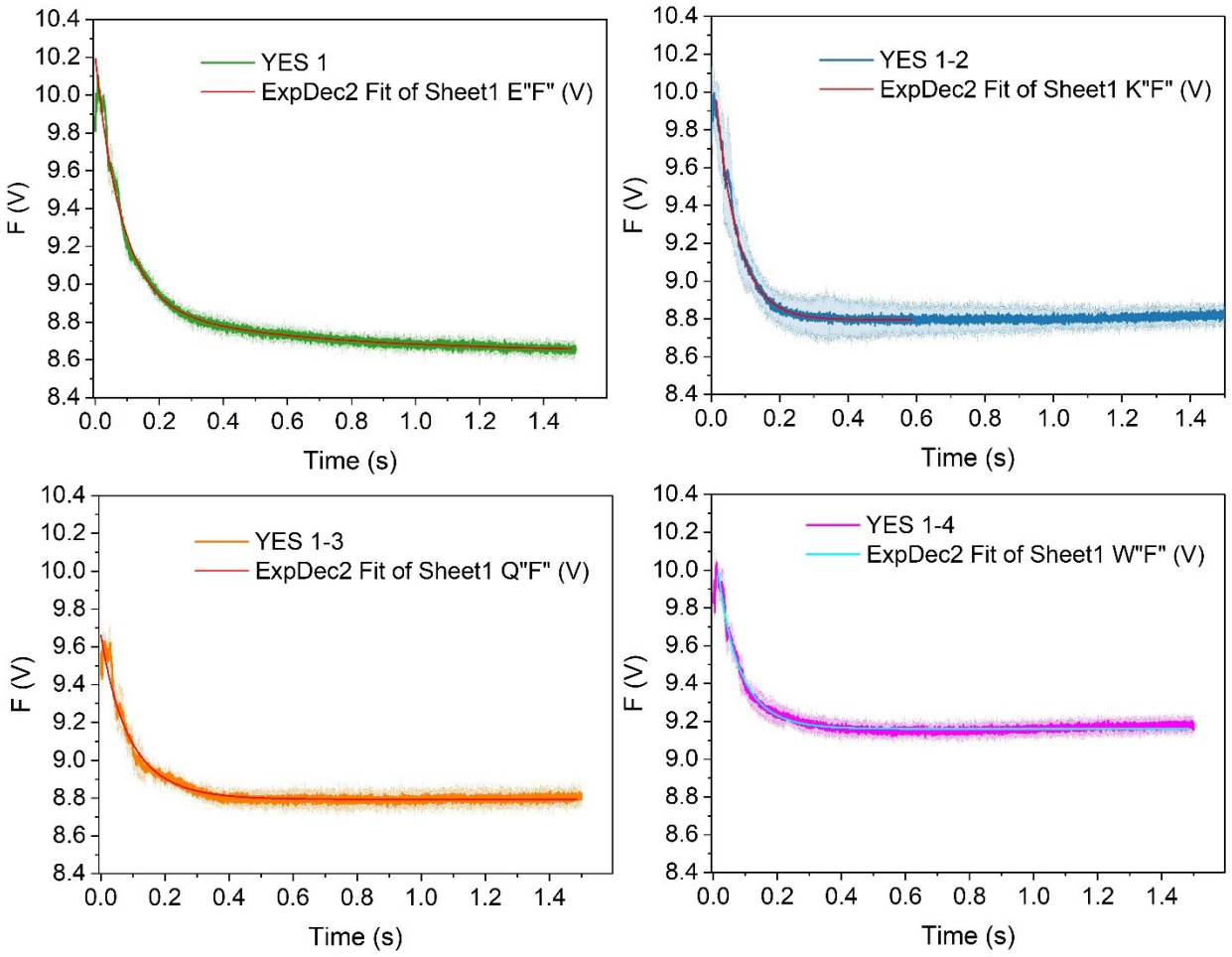

Figure 37. Fitted curves from Figure 36B kinetic profiles. The best fit achieved for each kinetic profile is highlighted by ExpDec2 line in each panel. This best fit corresponds to the biphasic exponential decay equation and the solution of each of the function parameters is shown in Figure 38.

		Value	Standard Error	t-Value	Prob>|t|	Dependenc
YES 1	y0	8.64159	0.00128	6761.1928	0	0.98347
	A1	1.2989	0.00364	357.31792	0	0.8262
	t1	0.08291	3.81818E-4	217.15714	0	0.93493
	A2	0.26467	0.0028	94.38887	0	0.97901
	t2	0.5409	0.012	45.0741	0	0.99085
	k1	12.06062	0.05554			
	k2	1.84878	0.04102			
	thalf1	0.05747	2.64656E-4			
	thalf2	0.37492	0.00832			
YES 1-2	y0	8.79524	3.32563E-4	26446.869	0	0.61526
	A1	0.67481	--	--	--	1
	t1	0.06425	3.76485	0.01707	0.98638	1
	A2	0.79079	--	--	--	1
	t2	0.06425	3.21288	0.02	0.98405	1
	k1	15.56319	911.89378			
	k2	15.56451	778.33231			
	thalf1	0.04454	2.60959			
	thalf2	0.04453	2.227			
YES 1-3	y0	8.7933	2.40488E-4	36564.473	0	0.58083
	A1	0.2641	0.04345	6.07877	1.25578E-9	0.99797
	t1	0.05402	0.00488	11.07774	2.360E-28	0.9898
	A2	0.60963	0.04477	13.61633	7.620E-42	0.99933
	t2	0.1137	0.00276	41.144	0	0.99591
	k1	18.51119	1.67103			
	k2	8.79473	0.21375			
	thalf1	0.03744	0.00338			
	thalf2	0.07881	0.00192			
YES 1-4	y0	9.16015	1.69904E-4	53913.707	0	0.28188
	A1	0.667	0.07084	9.41504	5.797E-21	0.99944
	t1	0.08794	0.00283	31.09429	1.58E-202	0.99404
	A2	0.38479	0.06553	5.8721	4.443E-9	0.99767
	t2	0.04232	0.00437	9.67928	4.635E-22	0.99489
	k1	11.37148	0.36571			
	k2	23.62756	2.44105			
	thalf1	0.06095	0.00196			
	thalf2	0.02934	0.00303			

Figure 38. Biphasic exponential decay parameters calculated from Figure 37 fitted curves which correspond to the stopped flow kinetic measurements of the four cascaded 4J YES gates on DNA IC module 1.4

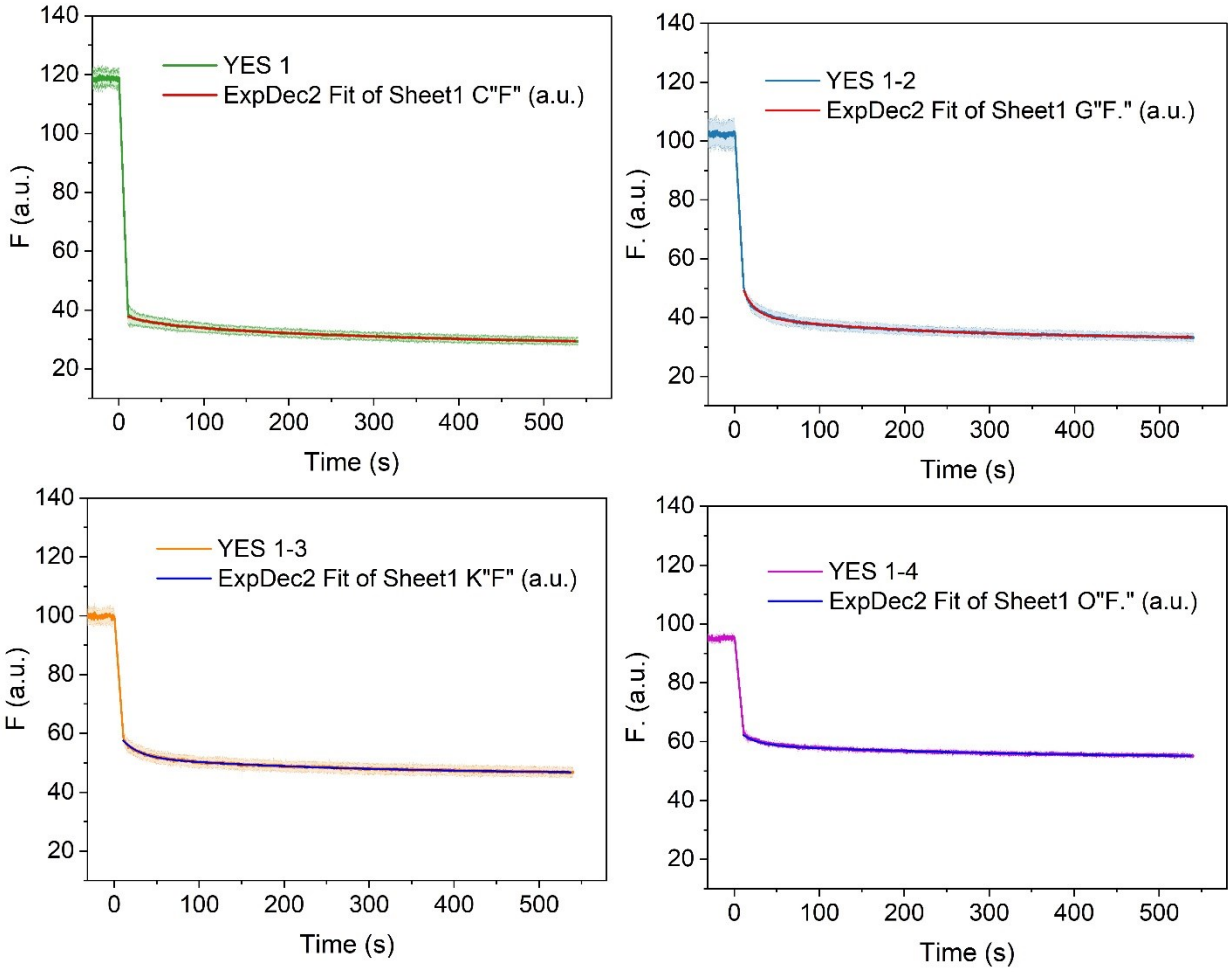

Figure 39. Fitted curves from Figure 23A kinetic profiles. The best fit achieved for each kinetic profile is highlighted by ExpDec2 line in each panel. This best fit corresponds to the biphasic exponential decay equation and the solution of each of the function parameters is shown in Figure 40.

		Value	Standard Er	t-Value	Prob>|t|	Dependenc
YES 1	y0	27.99041	0.04187	668.51809	0	0.9976
	A1	2.98919	0.05494	54.4077	0	0.77719
	t1	33.78622	1.19163	28.35285	1.08E-164	0.95428
	A2	7.84071	0.01913	409.7883	0	0.94531
	t2	315.67926	4.89097	64.54335	0	0.99735
	k1	0.0296	0.00104			
	k2	0.00317	4.90798E-5			
	thalf1	23.41882	0.82598			
	thalf2	218.81219	3.39016			
YES 1-2	y0	32.75969	0.01628	2012.0905	0	0.97311
	A1	18.98916	0.14066	134.99768	0	0.89573
	t1	13.94936	0.11971	116.52218	0	0.94221
	A2	8.05775	0.01963	410.44385	0	0.86929
	t2	208.01183	1.56841	132.6261	0	0.97789
	k1	0.07169	6.15229E-4			
	k2	0.00481	3.62479E-5			
	thalf1	9.66896	0.08298			
	thalf2	144.18281	1.08714			
YES 1-3	y0	46.04115	0.02914	1579.7712	0	0.99084
	A1	9.65588	0.09545	101.16488	0	0.82696
	t1	19.98448	0.27343	73.08757	0	0.93362
	A2	6.11526	0.01874	326.27635	0	0.89087
	t2	261.31483	3.82485	68.32024	0	0.99008
	k1	0.05004	6.84642E-4			
	k2	0.00383	5.60127E-5			
	thalf1	13.85219	0.18953			
	thalf2	181.12964	2.65119			
YES 1-4	y0	54.25546	0.05051	1074.2583	0	0.99761
	A1	5.80395	0.19999	29.02133	6.61E-172	0.93529
	t1	19.45684	0.624	31.1809	5.16E-196	0.97751
	A2	4.77593	0.02845	167.88839	0	0.98034
	t2	325.35135	8.30876	39.15764	1.45E-294	0.99492
	k1	0.0514	0.00165			
	k2	0.00307	7.8493E-5			
	thalf1	13.48645	0.43252			
	thalf2	225.51637	5.75919			

Figure 40. Biphasic exponential decay parameters calculated from Figure 39 fitted curves which correspond to Figure 23 kinetic measurements of the four cascaded 4J YES gates on DNA IC module 1.4.

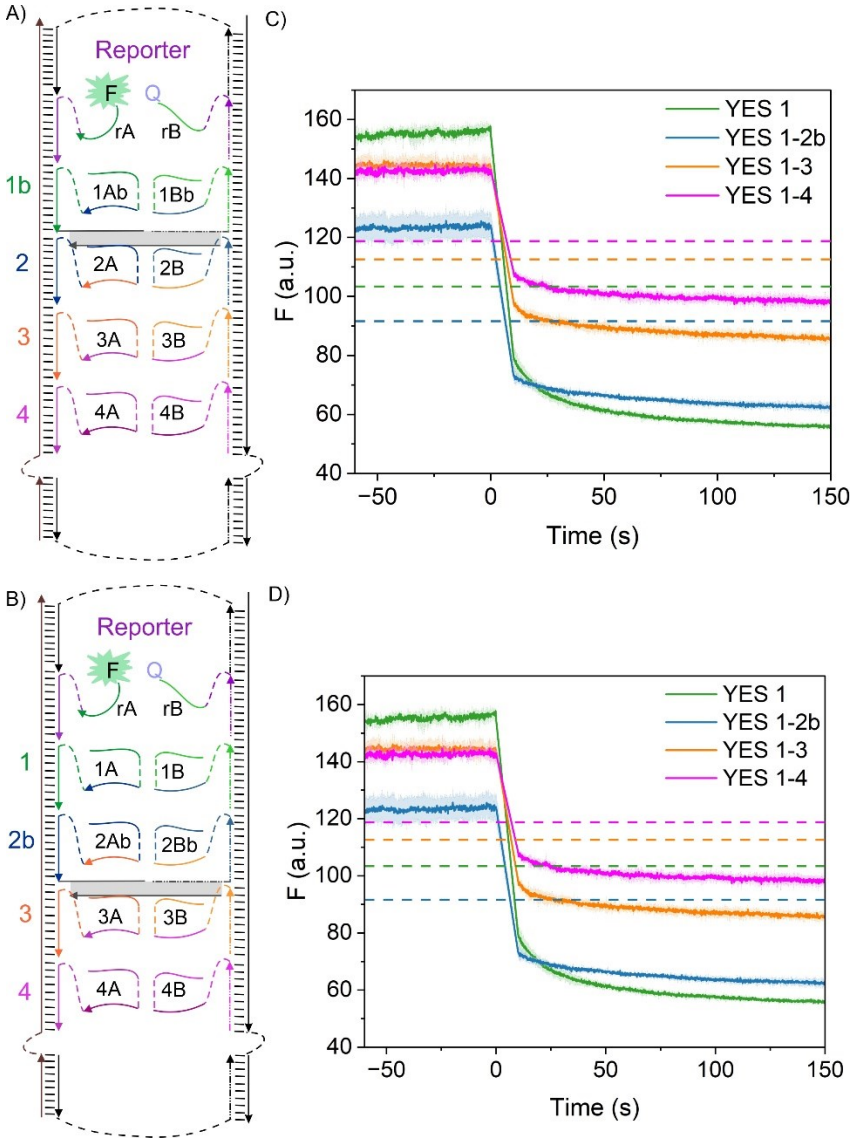

Figure 41. t_{50} of four cascaded 4J YES gates with rigidity added to the DNA board by placing a dsDNA bridge at YES 1 (YES 1b) A) or at YES 2 (YES 2b) B) position. C) kinetic profiles correspond to the DNA IC module shown in A), and the kinetic profiles in D) correspond to the DNA IC module shown in B). The colored-dashed lines here indicate the 50% fluorescence change achieved after input addition.

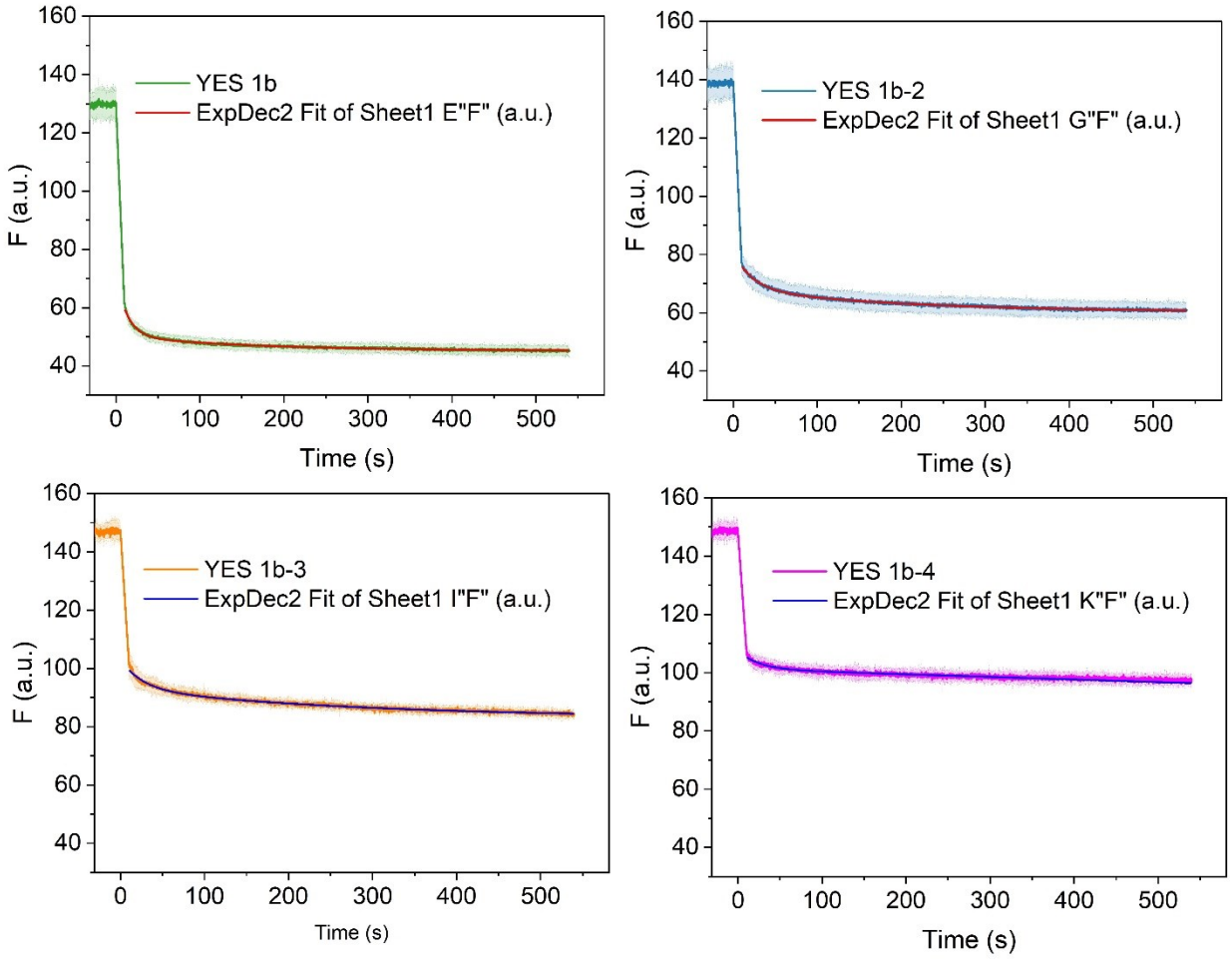

Figure 42. Fitted curves from Figure 24C kinetic profiles. The best fit achieved for each kinetic profile is highlighted by ExpDec2 line in each panel. This best fit corresponds to the biphasic exponential decay equation and the solution of each of the function parameters is shown in Figure 43.

		Value	Standard Er	t-Value	Prob>|t|	Dependenc
YES 1b	y0	45.12452	0.01455	3101.5672	0	0.94904
	A1	20.96944	0.21104	99.36357	0	0.88828
	t1	13.3916	0.13392	99.99775	0	0.94344
	A2	5.15703	0.02834	181.98839	0	0.90242
	t2	168.58239	2.11878	79.56573	0	0.96703
	k1	0.07467	7.46753E-4			
	k2	0.00593	7.45524E-5			
	thalf1	9.28235	0.09283			
	thalf2	116.85241	1.46863			
YES 1b-2	y0	60.23526	0.02616	2302.3130	0	0.97827
	A1	12.81906	0.11512	111.35108	0	0.80869
	t1	22.34385	0.33164	67.37375	0	0.94484
	A2	8.01716	0.04636	172.9155	0	0.95181
	t2	200.87471	2.8024	71.67946	0	0.98622
	k1	0.04476	6.6428E-4			
	k2	0.00498	6.94512E-5			
	thalf1	15.48758	0.22988			
	thalf2	139.23574	1.94248			
YES 1b-3	y0	83.07161	0.06599	1258.9415	0	0.99374
	A1	9.96174	0.27115	36.73907	2.52E-263	0.79174
	t1	25.04019	0.85108	29.42179	2.56E-176	0.92391
	A2	10.12195	0.04445	227.73569	0	0.91411
	t2	276.91091	5.68941	48.67131	0	0.99413
	k1	0.03994	0.00136			
	k2	0.00361	7.41971E-5			
	thalf1	17.35654	0.58992			
	thalf2	191.94002	3.9436			
YES 1b-4	y0	1109717.9	165695.58	6.69733	2.343E-11	1
	A1	6.34065	0.20347	31.1622	7.67E-196	0.763
	t1	24.25387	0.844	28.73673	7.49E-169	0.82727
	A2	-1109617	165695.58	-6.69672	2.353E-11	1
	t2	-1.24916E8	1.86697E7	-6.69088	2.4482E-11	0.99983
	k1	0.04123	0.00143			
	k2	-8.005E-9	1.19646E-9			
	thalf1	16.8115	0.58502			
	thalf2	-8.65855E7	1.29408E7			

Figure 43. Biphasic exponential decay parameters calculated from Figure 42 fitted curves which correspond to Figure 24C kinetic measurements of the four cascaded 4J YES gates on DNA IC module 1.4 with a dsDNA bridge at YES 1b gate.

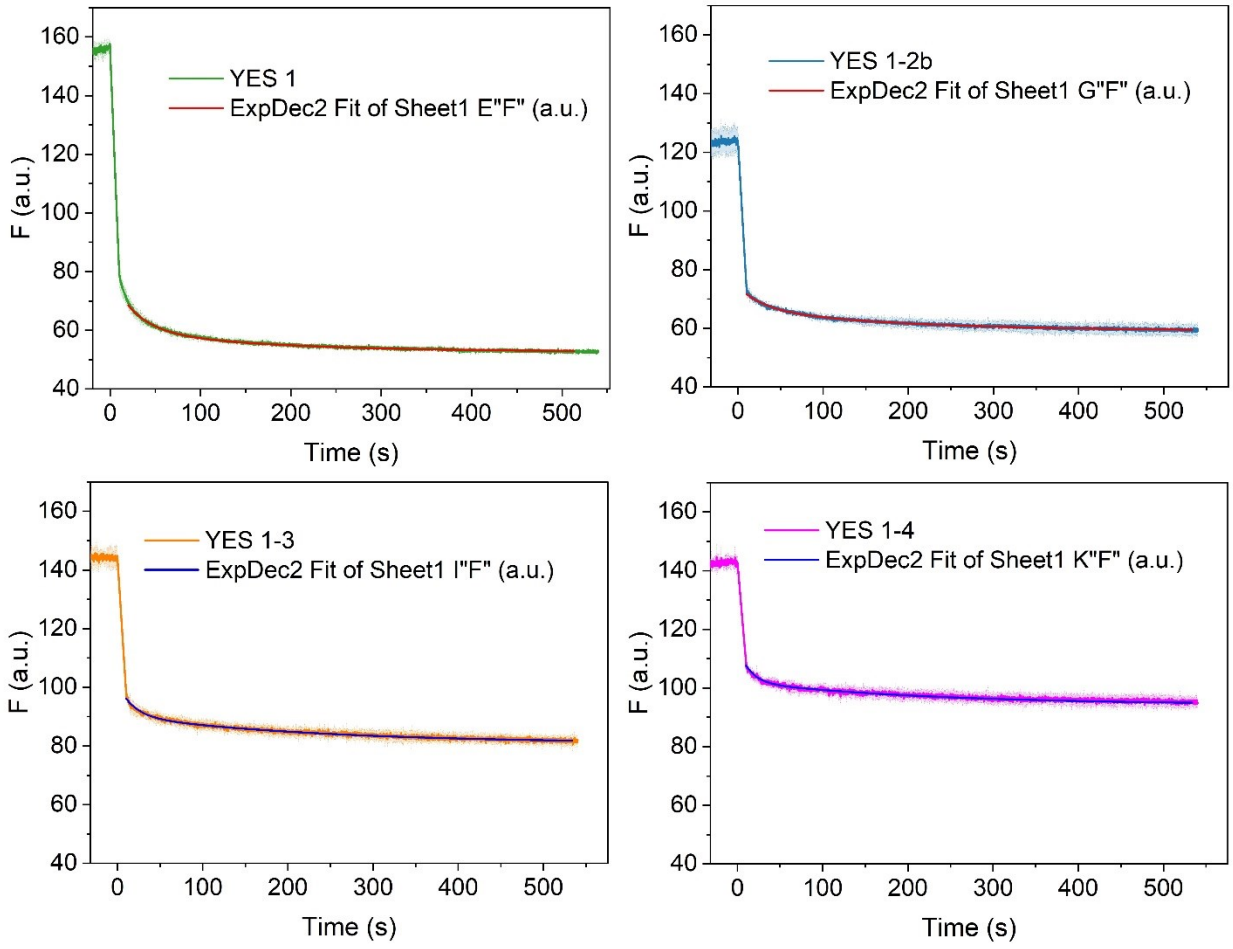

Figure 44. Fitted curves from Figure 24D kinetic profiles. The best fit achieved for each kinetic profile is highlighted by ExpDec2 line in each panel. This best fit corresponds to the biphasic exponential decay equation and the solution of each of the function parameters is shown in Figure 45.

		Value	Standard Er	t-Value	Prob>|t|	Dependenc
YES 1	y0	52.69935	0.01695	3109.4798	0	0.96491
	A1	18.56653	0.68019	27.29602	6.63E-153	0.88687
	t1	27.35958	0.86121	31.76876	1.13E-201	0.96211
	A2	7.87817	0.13699	57.50858	0	0.98424
	t2	155.98259	2.79872	55.73348	0	0.99109
	k1	0.03655	0.00115			
	k2	0.00641	1.15029E-4			
	thalf1	18.96422	0.59695			
	thalf2	108.11889	1.93993			
YES 1-2b	y0	59.13588	0.04377	1351.2004	0	0.99014
	A1	7.52365	0.09388	80.14122	0	0.92138
	t1	29.29077	0.74426	39.3554	5.83E-297	0.98798
	A2	7.64788	0.09205	83.08065	0	0.99379
	t2	181.56842	4.73382	38.3556	7.35E-284	0.99357
	k1	0.03414	8.67491E-4			
	k2	0.00551	1.43592E-4			
	thalf1	20.30281	0.51588			
	thalf2	125.85364	3.28123			
YES 1-3	y0	80.86756	0.04841	1670.6078	0	0.98628
	A1	10.87258	0.17219	63.1427	0	0.79382
	t1	18.05798	0.4407	40.97536	0	0.93349
	A2	9.57542	0.03888	246.25211	0	0.89604
	t2	231.86218	3.95957	58.55741	0	0.98653
	k1	0.05538	0.00135			
	k2	0.00431	7.36526E-5			
	thalf1	12.51684	0.30547			
	thalf2	160.71462	2.74457			
YES 1-4	y0	94.27855	0.0446	2113.8692	0	0.98402
	A1	12.32661	0.12337	99.91673	0	0.85516
	t1	13.70838	0.23686	57.87667	0	0.95691
	A2	7.91882	0.03512	225.48046	0	0.90945
	t2	222.20757	3.99105	55.67648	0	0.97997
	k1	0.07295	0.00126			
	k2	0.0045	8.08294E-5			
	thalf1	9.50193	0.16418			
	thalf2	154.02255	2.76638			

Figure 45. Biphasic exponential decay parameters calculated from Figure 44 fitted curves which correspond to Figure 24D kinetic measurements of the four cascaded 4J YES gates on DNA IC module 1.4 with a dsDNA bridge at YES 2b gate.

APPENDIX D: CHAPTER FIVE SUPPORTING INFORMATION

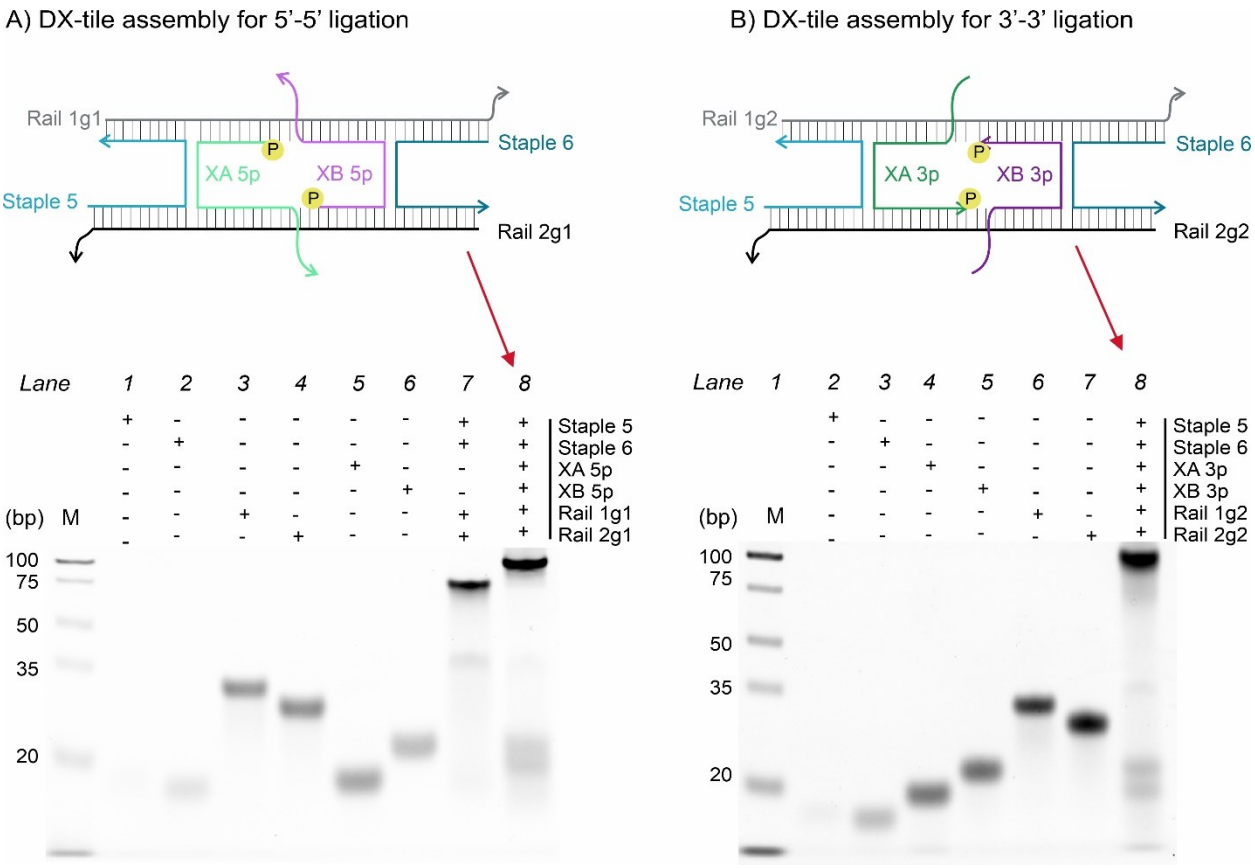

Figure 46. Assembly of DX-tile visualized by 8% Native PAGE in the presence of 70 mM MgCl2. Lane M: GeneRuler Ultra Low Range Ladder (Thermofisher); Lanes 1-6: 12 pmol of each individual strand as indicated on the right; lanes 7 and 8: 12 pmol complexes of the strands annealed as detailed in Materials and Methods. A) DX-Tile assembled with oligonucleotides XA 5p and XB 5p for the 5'-5' chemical ligation (see upper panel). B) DX-tile assembled with oligonucleotides XA 3p and XB 3p for the 3'-3' chemical ligation (see upper panel).

For the assembly of DX-tile, oligonucleotides were assembled as detailed in section 5.2.2. The oligonucleotides were not purified by PAGE prior to assembly and ligation reactions. We visualized the DX-tile assembly through native PAGE and determined that 8 to 13% of reacting strands XA 5p, XB 5p, XA 3p, and XB 3p were not associated with the DX-tile. Additionally, side

products were observed. Purification of the assembled DX prior ligation could, technically, produce 8-13% greater yield. However, work associated with purification of such nanostructures and the moderated yield (50-60%) of purification makes this procedure impractical. Moreover, DX-tile catalyzed reaction did not show any side product of ligation in observed PAGE assay, which shows that defects in DNA assembly do not impact reaction specificity.

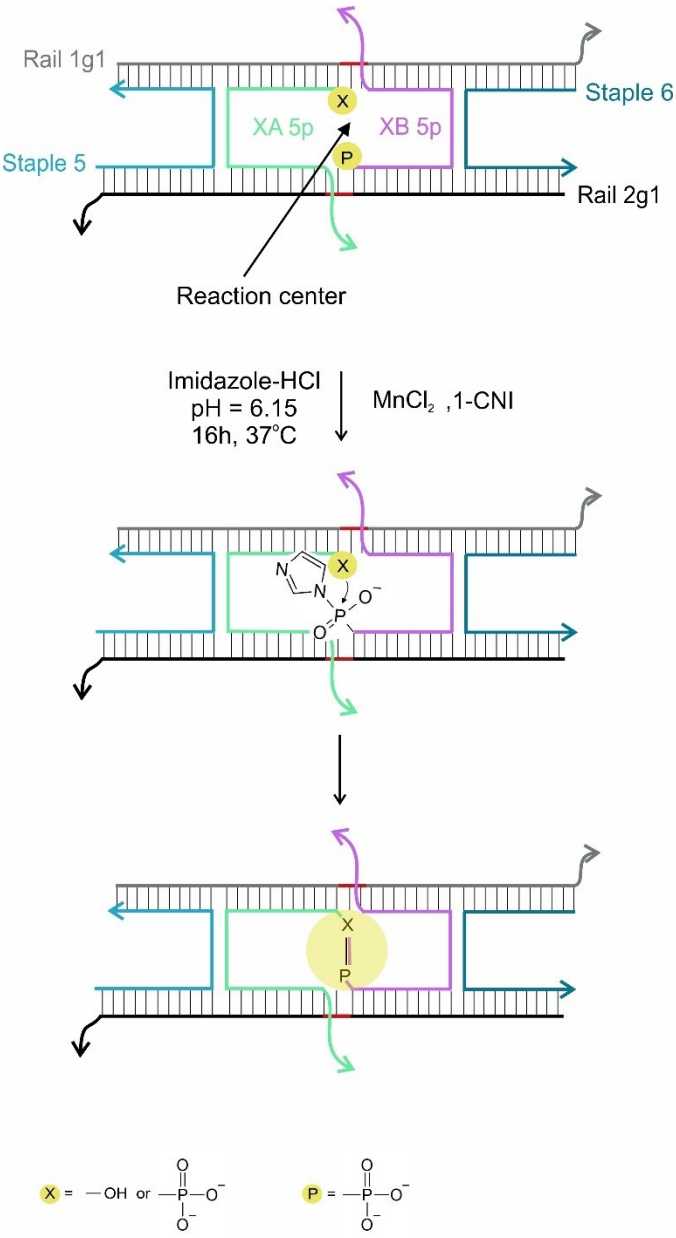

Figure 47. Chemical ligation of the oligonucleotides XA and XB. The reaction can take place in an aqueous environment with 1-cyanoimidazole in the imidazole buffer as a coupling agent and requires the presence of a divalent transition metal.1,2 In the scheme, the 5'-phosphate group is prepared for the nucleophilic attack via the formation of an intermediate phosphoimidazolide.

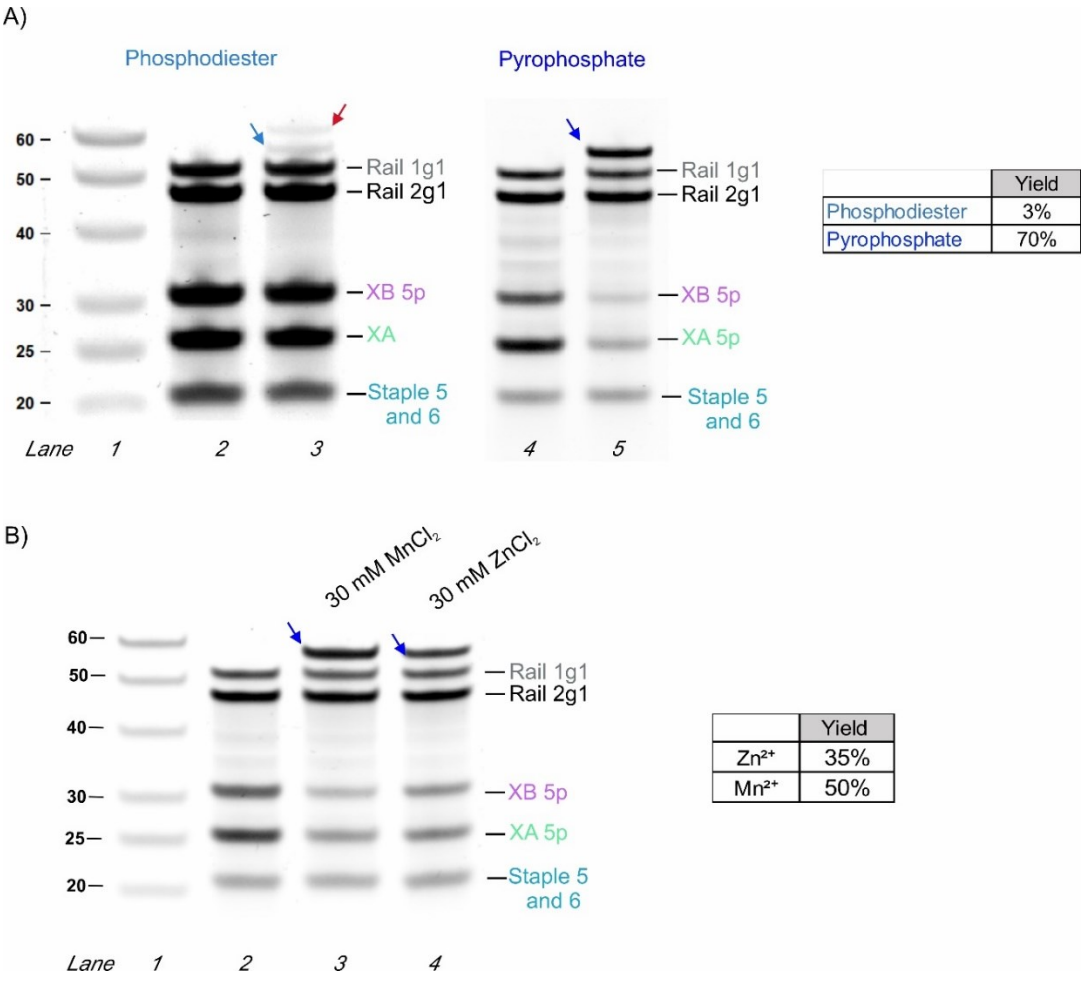

Figure 48. Chemical ligation through phosphodiester or pyrophosphate linkage and selection of crosslinking cation. A) The DX-tile-assisted chemical ligation through phosphodiester vs pyrophosphate bond formation. 12% dPAGE, Lane 1: ssDNA ladder; Lane 2 and 3: before and after the DX-tile-assisted ligation reaction assisted by via a phosphodiester linkage; Lane 4 and 5: before and after the DX-tile ligation of XA and XB via a pyrophosphate linkage; Reaction conditions: 200 mM imidazole-HCl buffer (pH 6.5), 30 mM 1-cyanoimidazole, 100 mM MnCl2, 16 h at 37℃; B) The DX-tile-assisted chemical ligation with Zn2+ vs Mn2+. 12% dPAGE, Lane 1: ssDNA ladder; Lane 2: XA 5p and XB 5p in the DX-tile prior ligation; lane 3: after the ligation of XA 5p and XB 5p in the presence of Zn2+; Lane 4: after the ligation of XA and XB in the presence of Mn2+; Reaction conditions: 200 mM imidazole-HCl buffer (pH 6.5), 30 mM 1-cyanoimidazole, 30 mM ZnCl2 or MnCl2, 16 h at 22℃. Blue or cyan arrowheads indicate the expected ligation product, red arrowhead indicates byproducts of the reaction.

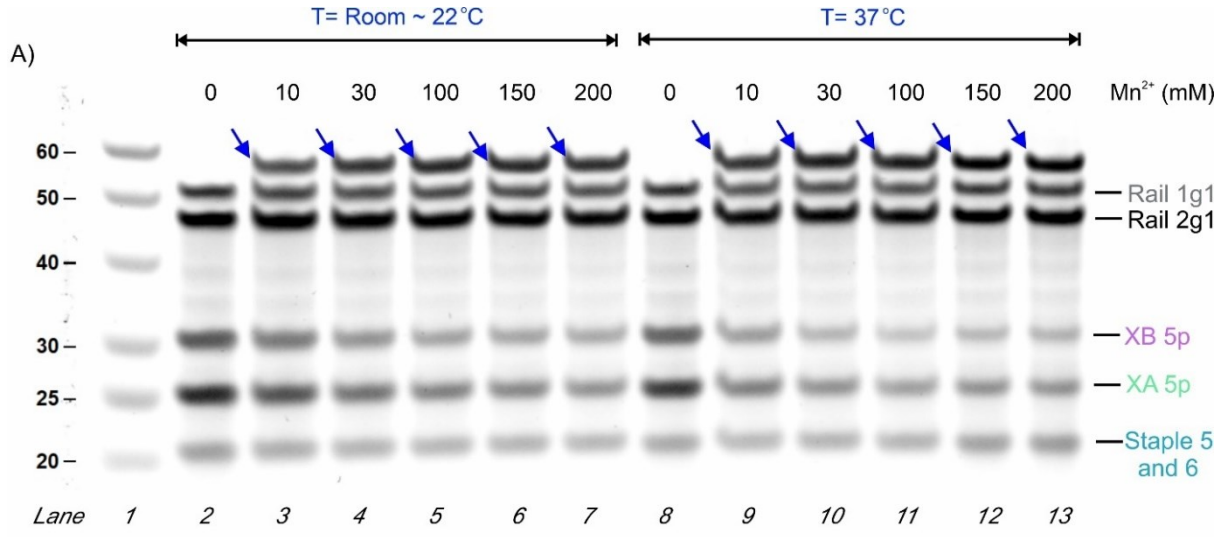

B)

	Yield %	
$MnCl_2$ (mM)	22 °C	37 °C
0	0	0
10	14	28
30	33	52
100	43	60
150	45	61
200	44	60

Figure 49. Selection of the ligation reaction conditions in the presence of Mn $^{2+}$. The highest product yield was achieved at 100 mM Mn^{2+}, after 16-h incubation at 37°C. A) Concentration of MnCl2 and temperature optimization. Reaction conditions: 200 mM imidazole-HCl buffer (pH 6.5), 30 mM 1-cyanoimidazole, 16 h incubation, temperature and MnCl2 as listed in the figure. After the reaction, the samples were analyzed by 12% dPAGE, Lane 1: ssDNA ladder; lanes 2 and 8: the DX-tile containing sample before the ligation reaction; lanes 3 – 7 and 9-13: the DX-tile containing sample after addition of 30 mM 1-cyanoimidazole, MnCl2, and incubation at a temperature as listed. B) Product percent yield determined from the gel quantification data, as described in section 5.2.3.

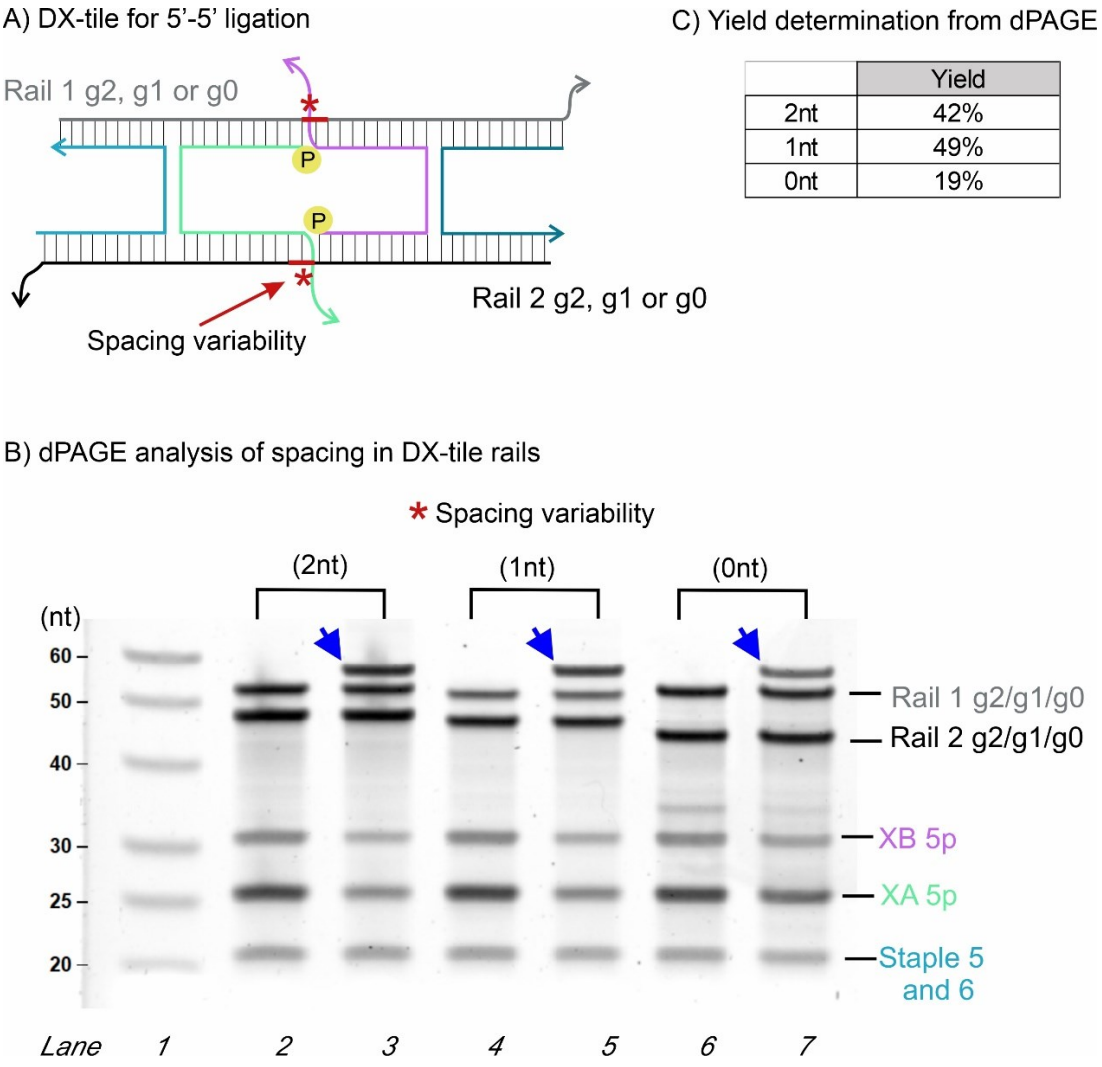

Figure 50. Effect of a single-stranded gap between the reacting strands on the ligation yield. A) Localization of the gap (red) on the DX tile-like nanostructure. B) 12% dPAGE, Lane 1: ssDNA ladder; lanes 2, 4, and 6: the DX-tile containing sample before the ligation; lanes 3,5, and 7: the DX-tile containing sample after the ligation reaction. Reaction conditions: 200 mM imidazole-HCl buffer (pH 6.5), 30 mM 1-cyanoimidazole, 100 mM MnCl2, 16 h at 37°C. C) Quantification of the reaction yield (see section 5.2.3 for the quantification details).

A)

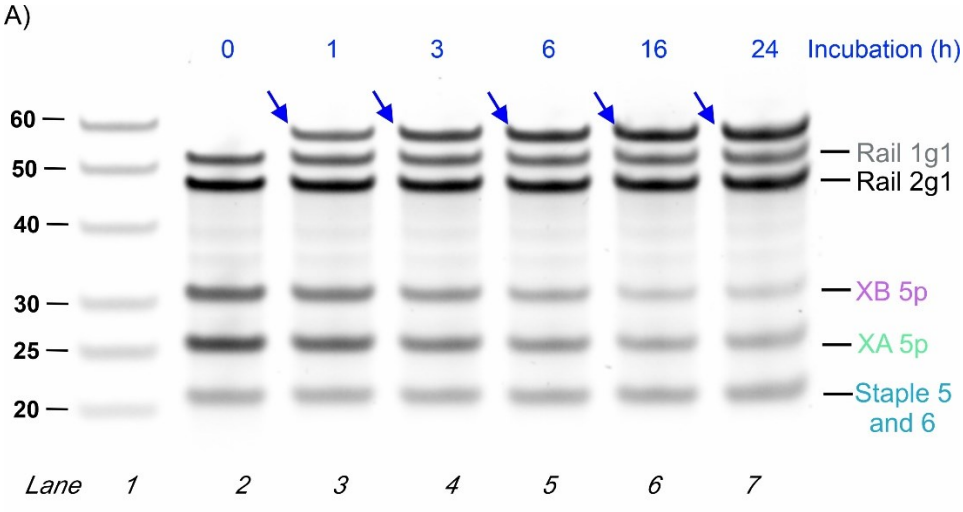

B)

Incubation (h)	Yield %
1	16
3	30
6	44
16	63
24	65

Figure 51. Kinetics of the chemical ligation. The product yield reached a plateau at 100 mM Mn2+, after 16-h incubation at 37°C. A) Optimization of MnCl2 concentration and reaction temperature. Reaction conditions: 200 mM imidazole-HCl buffer (pH 6.5), 30 mM 1-cyanoimidazole, 100 mM MnCl2 at 37°C and incubation time as listed in the figure. After the reaction, the samples were analyzed by 12% dPAGE, Lane 1: ssDNA ladder; lanes 2: the DX-tile before reaction; lanes 3 – 7: the DX-tile after addition of 30 mM 1-cyanoimidazole, 100 mM MnCl2, and incubation at 37°C at different incubation times. B) Product percent yield determined from the gel quantification data, as described in 5.2.1 Materials and Methods.

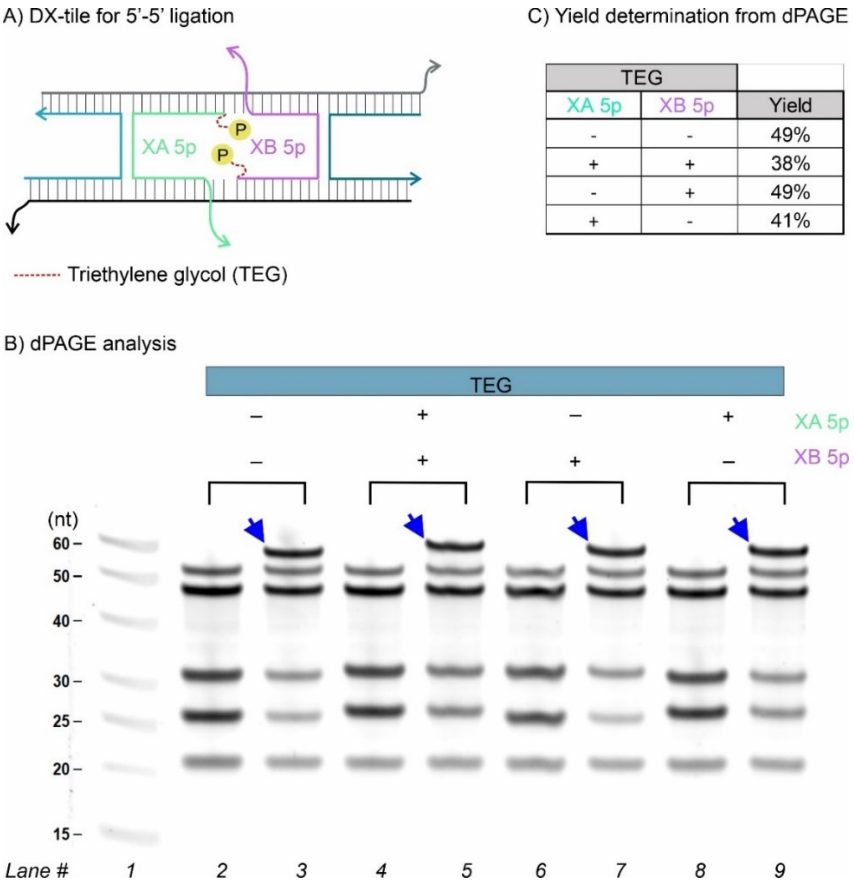

Figure 52. Effect of phosphate flexibility due to the presence of triethyleneglycol (iSp9) linkers. A) Scheme showing the point of triethylene glycol linker insertion to connect the terminal phosphates to the 5'ends of strands XA 5p and XB 5p. B) 12% dPAGE, Lane 1: ssDNA ladder; lanes 2, 4, 6, and 8: the DX-tile before ligation; lanes 3,5, 7, and 9: the DX-tile after ligation. Reaction conditions: 200 mM imidazole-HCl buffer (pH 6.5), 30 mM 1-cyanoimidazole, 100 mM MnCl2, 16 h at 37°C. C) Quantification of the reaction yield was done as described in section 1.3 of the 5.2.1 Materials and Methods.

Triethyleneglycol (iSp9) linkers covalently bind between the terminal phosphate and oligonucleotide. We hypothesized that increasing the flexibility of the reactive phosphate could potentially increase the ligation yield if the reacting phosphate have suboptimal orientation toward each other in the DNA nanostructure. However, Figure 52 above shows no significant improvement in the reaction yield when such iSp9 linkers were used. This indicates that the

orientation of the linker-free phosphate groups in the DX-tile nanostructure is near optimal since additional flexibility does not improve the reaction rate. A small reduction in the reaction rate of the TEG -linker containing strand can be explained by the increased flexibility of the reacting phosphate groups, which somewhat reduces the proximity and orientation effect.

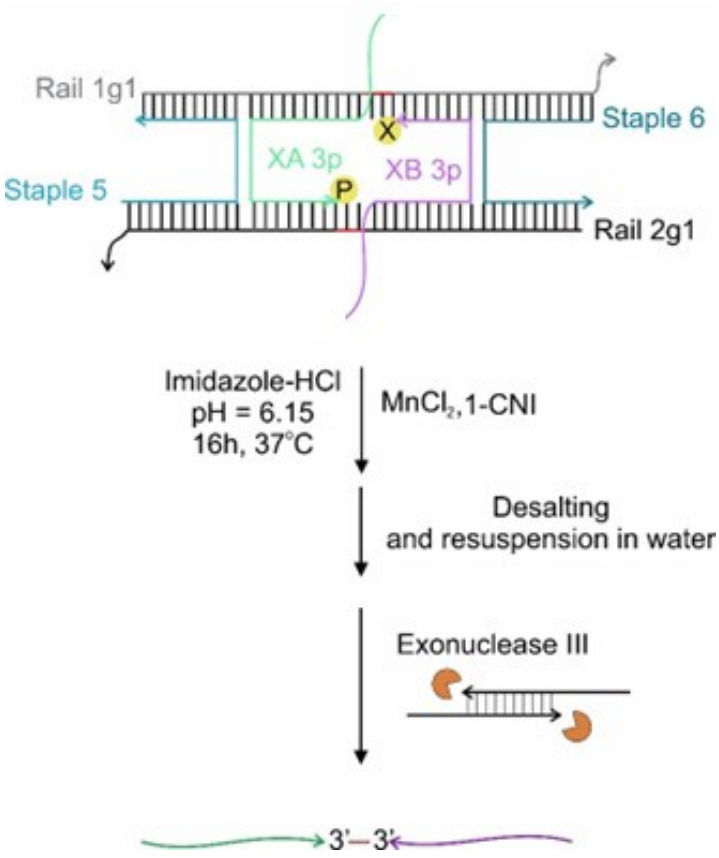

Figure 53. A route to synthesize and isolate the 3'-3' DX-tile-assisted ligated oligonucleotide. The reaction to obtain the 3'-3' linked oligonucleotides followed the same optimized conditions as for the 5'-5' ligation. The reaction product can be purified by the exonuclease III treatment, requiring a desalting step prior to the enzymatic digestion.

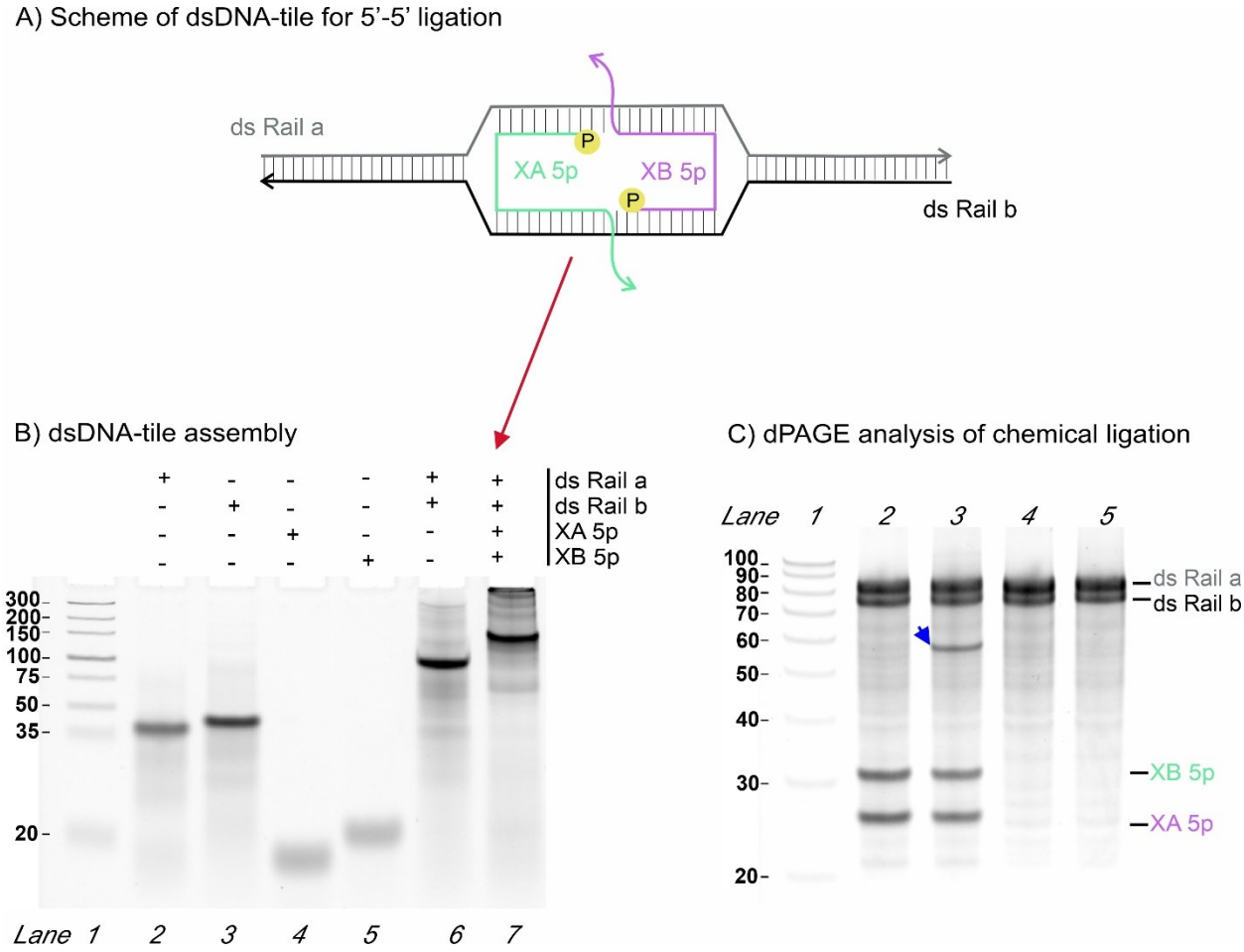

Figure 54. 5'- 5' DNA chemical ligation using a dsDNA-tile. A) Scheme of ds DNA tile localizing XA 5p and XB 5p in proximity to each other without additional staple strands. B) Analysis of the dsDNA tile assembly using 10% Native PAGE in the presence of 70 mM MgCl2. Lane 1: GeneRuler Ultra Low Range DNA Ladder (ThermoFisher Scientific); lanes 2-5: individual components of the tile, as indicated above the lanes; lane 6: association of only strands ds Rail a and ds Rail b; lane 7: full dsDNA-tile. C) Analysis of the products of dsDNA tile-assisted chemical ligation using 12% dPAGE, Lane 1: IDT DNA oligo length standard 20/100 Ladder; lane 1-3 dsDNA-tile solutions before reaction; lane 2-4: dsDNA-tile solutions after reaction with 1-cyanoimidazol/MnCl2. Reaction conditions: 200 mM imidazole-HCl buffer at pH 6.5, 30 mM 1-cyanoimidazole, 100 mM MnCl2, 16 h incubation at 37°C. In each gel (native or denaturing), 12 pmol of each DNA strand or association was loaded per lane.

dsDNA-tile shows a 9-fold lower reaction yield than the DX-tile system. We hypothesized that torsional effects within the "bubble" locating the reacting strands can reposition the reactive

phosphates far apart for their ligation. These torsional effects are absent in a system such as the DX-tile where the tension of its double-stranded rails is alleviated by the crossover staple 5 and 6 strands.

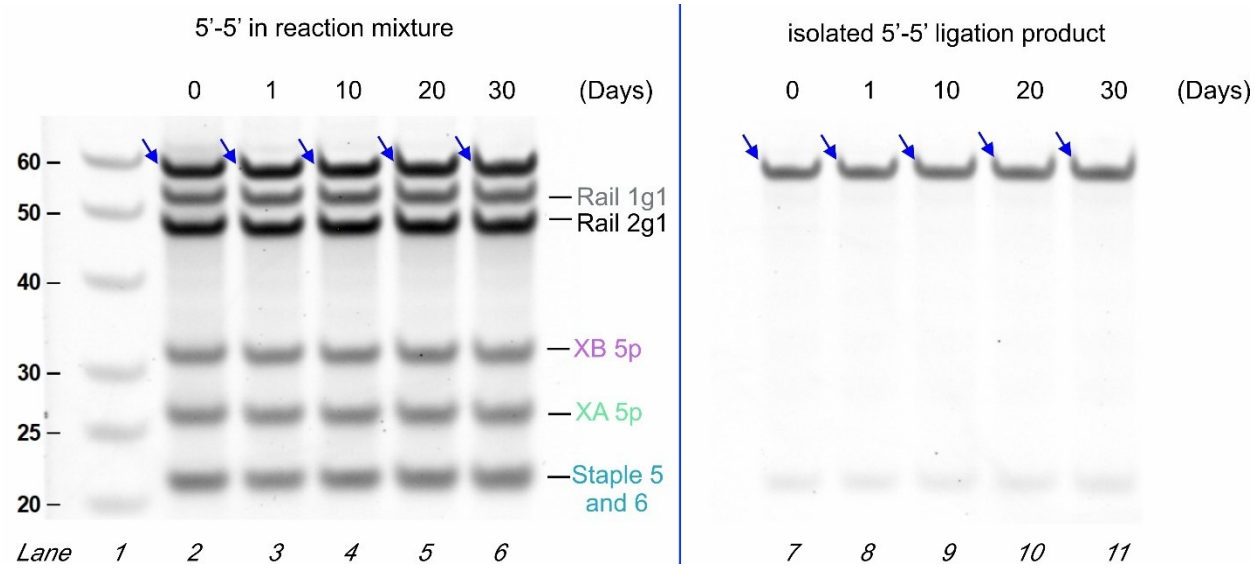

Figure 55. Chemical stability of the 5'-5' ligation product stored at room temperature (~22 °C) for up to 30 days. 12% dPAGE, Lane 1: ssDNA ladder (the marker sizes, in nts, are indicated next to the corresponding bands); lanes 2 to 6: the DX-tile containing sample after the ligation reaction stored in the reaction mixture containing 200 mM imidazole-HCl buffer (pH 6.5), 30 mM 1-cyanoimidazole, and 100 mM MnCl2 for 0-30 days as indicated; lanes 7 to 11: The 5'-5' ligated oligonucleotide isolated after exonuclease treatment was stored at room temperature in a buffer containing 10 mM Tris-HCl (pH 7.4) and 2 mM MgCl2 over a period of 30 days, as indicated. Day point aliquots were stored at –20°C in a 2xdPAGE loading buffer until analysis.

AFM Images for Contour Measurements

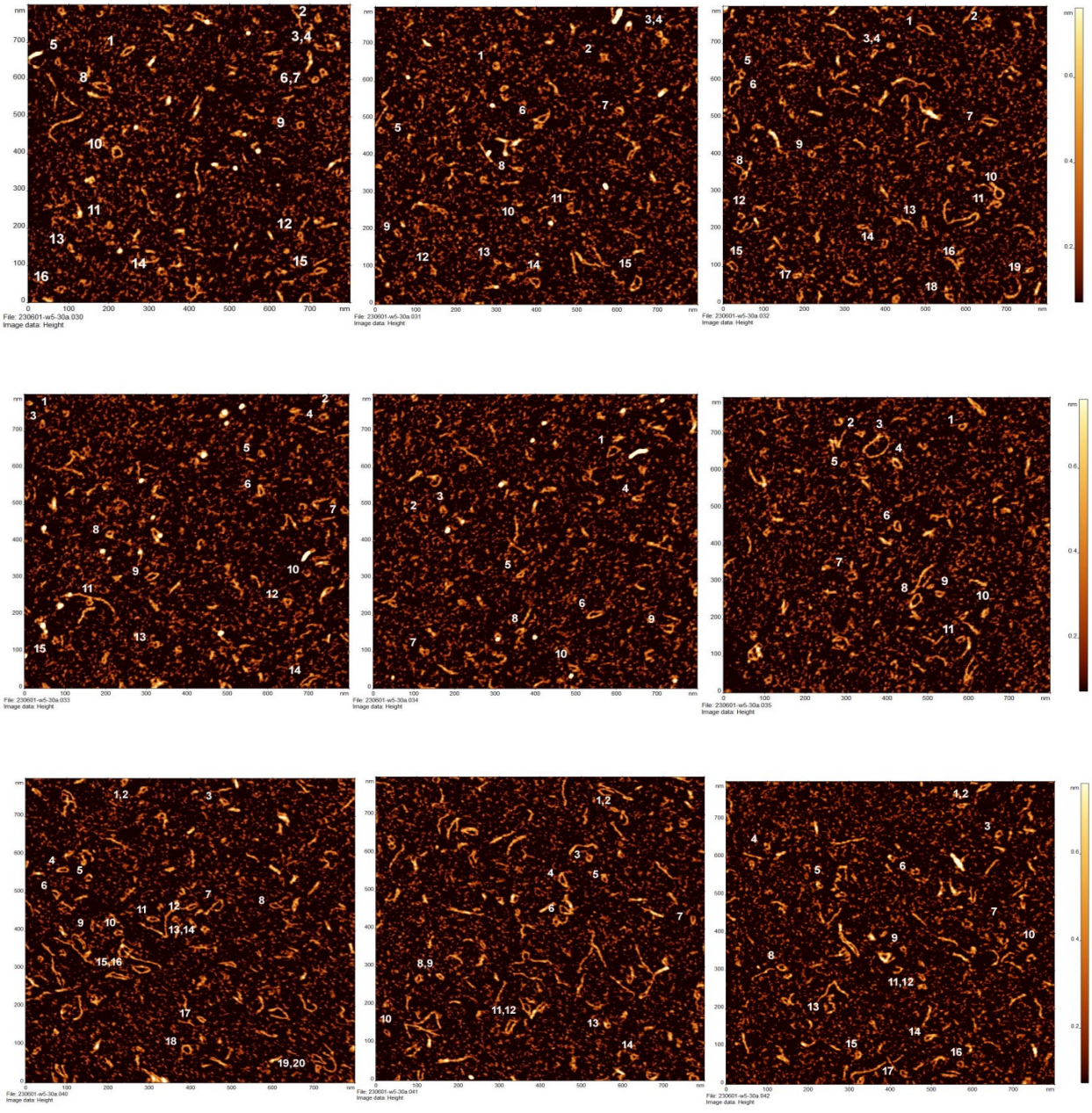

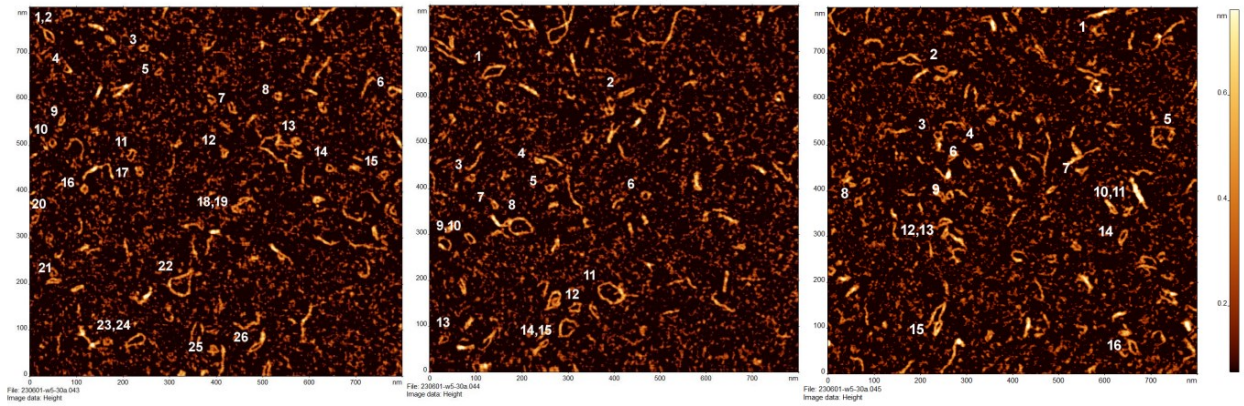
File: 230601-w5-30a.043
Image data: Height
File: 230601-w5-30a.044
Image data: Height
File: 230601-w5-30a.045
Image data: Height

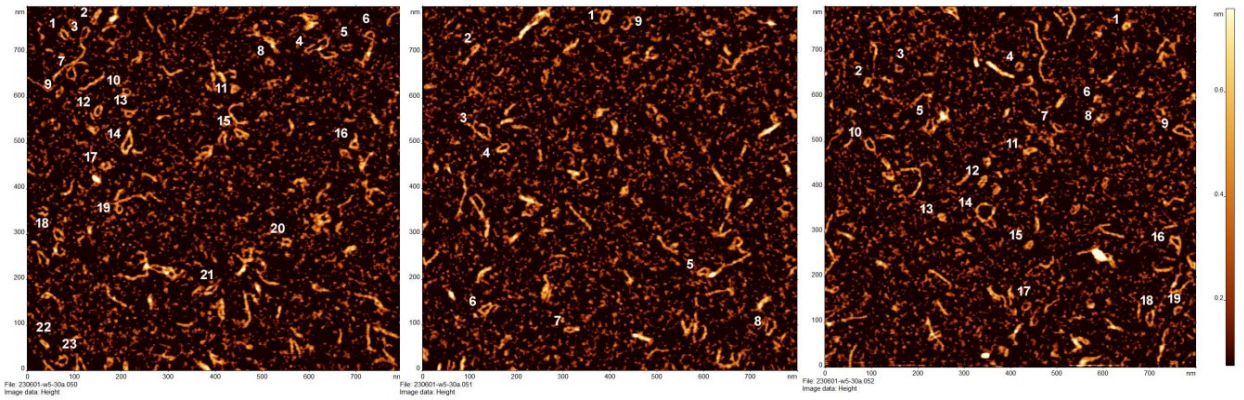
File: 230601-w5-30a.050
Image data: Height
File: 230601-w5-30a.051
Image data: Height
File: 230601-w5-30a.052
Image data: Height

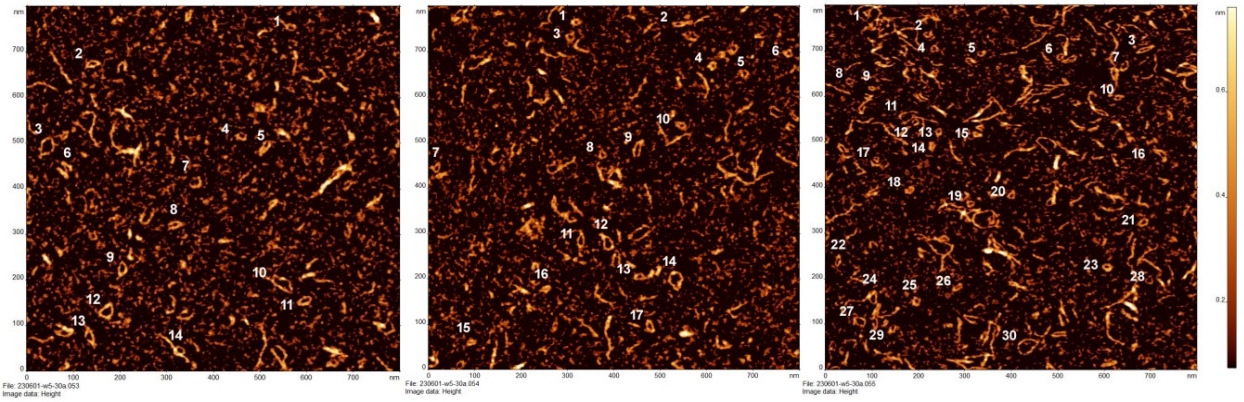
File: 230601-w5-30a.053
Image data: Height
File: 230601-w5-30a.054
Image data: Height
File: 230601-w5-30a.055
Image data: Height

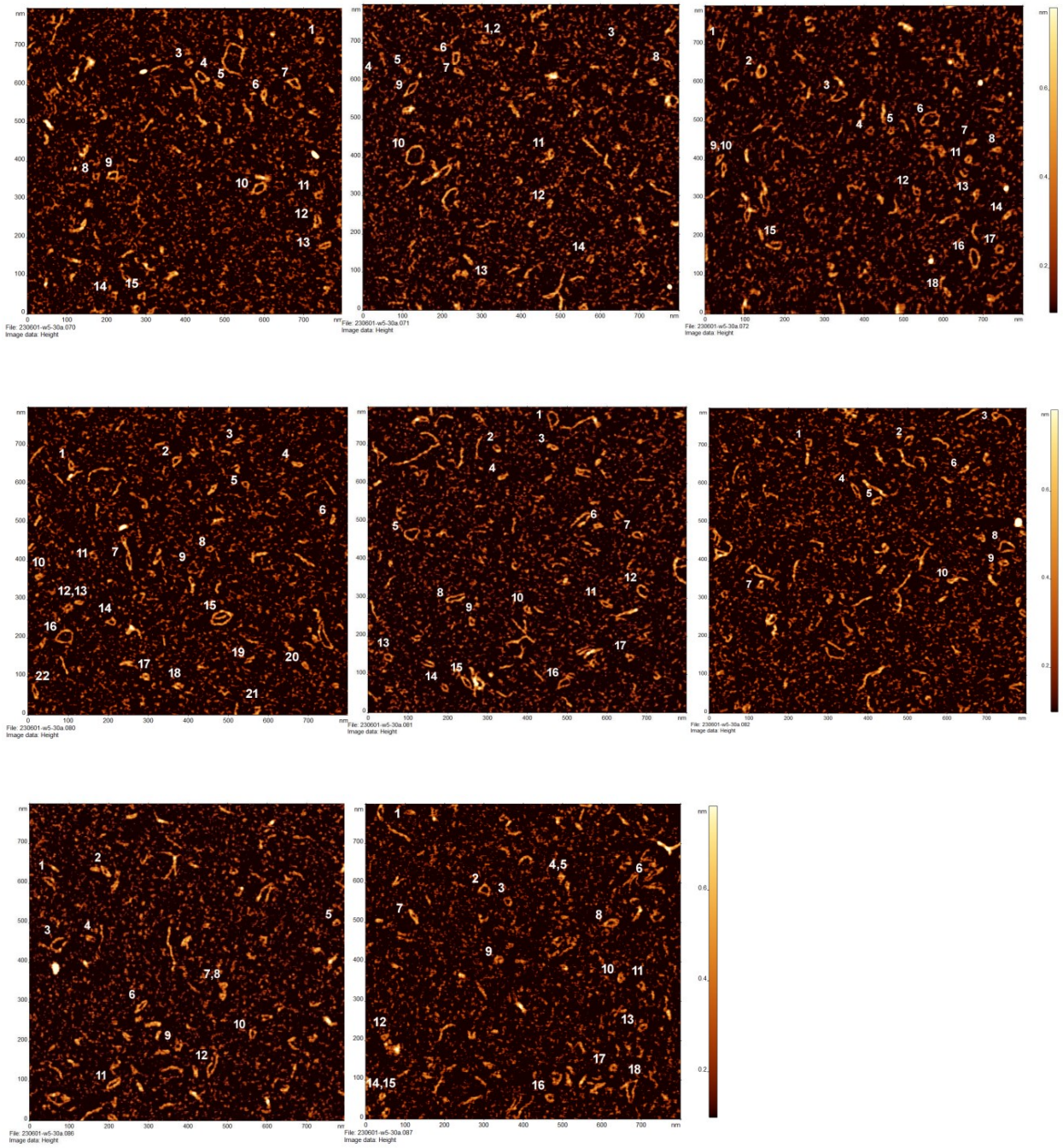

Figure 56. Impossible DNA wheel AFM imaging. Each panel corresponds to the scanning of an 800 x 800 nm area. Numerical labels indicate the identity of each of the structure's contour measurements determined. The circumference values (nm) of 521 structures were analyzed by Gaussian distribution.

LIST OF REFERENCES

(1) Katz, L.; Chen, Y. Y.; Gonzalez, R.; Peterson, T. C.; Zhao, H.; Baltz, R. H. Synthetic Biology Advances and Applications in the Biotechnology Industry: A Perspective. *Journal of Industrial Microbiology and Biotechnology* **2018**, *45* (7), 449–461. https://doi.org/10.1007/s10295-018-2056-y.

(2) Weng, Y.; Huang, Q.; Li, C.; Yang, Y.; Wang, X.; Yu, J.; Huang, Y.; Liang, X.-J. Improved Nucleic Acid Therapy with Advanced Nanoscale Biotechnology. *Molecular Therapy - Nucleic Acids* **2020**, *19*, 581–601. https://doi.org/10.1016/j.omtn.2019.12.004.

(3) Gavrilescu, M.; Chisti, Y. Biotechnology—a Sustainable Alternative for Chemical Industry. *Biotechnology Advances* **2005**, *23* (7), 471–499. https://doi.org/10.1016/j.biotechadv.2005.03.004.

(4) Jesiek, B. K. The Origins and Early History of Computer Engineering in the United States. *IEEE Annals of the History of Computing* **2013**, *35* (3), 6–18. https://doi.org/10.1109/MAHC.2013.2.

(5) Feynman, R. P. There's Plenty of Room at the Bottom. *Engineering and Science* **1960**, *23* (5), 22–36.

(6) Ball, P. Chemistry Meets Computing. *Nature* **2000**, *406* (6792), 118–120. https://doi.org/10.1038/35018259.

(7) de Silva, P. A.; Gunaratne, N. H. Q.; McCoy, C. P. A Molecular Photoionic AND Gate Based on Fluorescent Signalling. *Nature* **1993**, *364* (6432), 42–44. https://doi.org/10.1038/364042a0.

(8) Stojanovic, M. N.; Mitchell, T. E.; Stefanovic, D. Deoxyribozyme-Based Logic Gates. *J. Am. Chem. Soc.* **2002**, *124* (14), 3555–3561. https://doi.org/10.1021/ja016756v.

(9) Stojanović, M. N.; Stefanović, D. Deoxyribozyme-Based Half-Adder. *J. Am. Chem. Soc.* **2003**, *125* (22), 6673–6676. https://doi.org/10.1021/ja0296632.

(10) Okamoto, A.; Tanaka, K.; Saito, I. DNA Logic Gates. *J. Am. Chem. Soc.* **2004**, *126* (30), 9458–9463. https://doi.org/10.1021/ja047628k.

(11) Saghatelian, A.; Völcker, N. H.; Guckian, K. M.; Lin, V. S.-Y.; Ghadiri, M. R. DNA-Based Photonic Logic Gates: AND, NAND, and INHIBIT. *J. Am. Chem. Soc.* **2003**, *125* (2), 346–347. https://doi.org/10.1021/ja029009m.

(12) Seelig, G.; Soloveichik, D.; Zhang, D. Y.; Winfree, E. Enzyme-Free Nucleic Acid Logic Circuits. *Science* **2006**, *314* (5805), 1585–1588. https://doi.org/10.1126/science.1132493.

(13) Qian, L.; Winfree, E. A Simple DNA Gate Motif for Synthesizing Large-Scale Circuits. *J R Soc Interface* **2011**, *8* (62), 1281–1297. https://doi.org/10.1098/rsif.2010.0729.

(14) Hagiya, M.; Yaegashi1, S.; Takahashi, K. Computing with Hairpins and Secondary Structures of DNA. In *Nanotechnology: Science and Computation*; Chen, J., Jonoska, N., Rozenberg, G., Eds.; Natural Computing Series; Springer: Berlin, Heidelberg, 2006; pp 293–308. https://doi.org/10.1007/3-540-30296-4_18.

(15) Katz, E. Enzyme-Based Logic Gates and Networks with Output Signals Analyzed by Various Methods. *ChemPhysChem* **2017**, *18* (13), 1688–1713. https://doi.org/10.1002/cphc.201601402.

(16) Katz, E. Biocomputing — Tools, Aims, Perspectives. *Current Opinion in Biotechnology* **2015**, *34*, 202–208. https://doi.org/10.1016/j.copbio.2015.02.011.

(17) *DNA- and RNA-Based Computing Systems*; Katz, E., Ed.; John Wiley & Sons: Weinheim, Germany, 2021.
(18) Benenson, Y. Complexity from Simple Building Blocks: Engineering Large-Scale Information-Processing Networks from Molecules. *CHIMIA* **2016**, *70* (6), 392–392. https://doi.org/10.2533/chimia.2016.392.
(19) Erbas-Cakmak, S.; Kolemen, S.; Sedgwick, A. C.; Gunnlaugsson, T.; James, T. D.; Yoon, J.; Akkaya, E. U. Molecular Logic Gates: The Past, Present and Future. *Chem. Soc. Rev.* **2018**, *47* (7), 2228–2248. https://doi.org/10.1039/C7CS00491E.
(20) Meiser, L. C.; Nguyen, B. H.; Chen, Y.-J.; Nivala, J.; Strauss, K.; Ceze, L.; Grass, R. N. Synthetic DNA Applications in Information Technology. *Nat Commun* **2022**, *13* (1), 352. https://doi.org/10.1038/s41467-021-27846-9.
(21) Liu, L.; Liu, P.; Ga, L.; Ai, J. Advances in Applications of Molecular Logic Gates. *ACS Omega* **2021**, *6* (45), 30189–30204. https://doi.org/10.1021/acsomega.1c02912.
(22) Malvino, A. P.; Brown, J. A. *Digital Computer Electronics*, 3rd ed.; Glencoe McGraw-Hill, 1999.
(23) Kieffer, C.; Genot, A. J.; Rondelez, Y.; Gines, G. Molecular Computation for Molecular Classification. *Advanced Biology* **2023**, *7* (3), 2200203. https://doi.org/10.1002/adbi.202200203.
(24) *Fundamentals of Biochemistry: Life at the Molecular Level, 5th Edition | Wiley*, 5th ed.; Wiley: United States, 2016.
(25) *DNA- and RNA-Based Computing Systems*; Katz, E., Ed.; John Wiley & Sons: Weinheim, Germany, 2021.
(26) Adleman, L. M. Molecular Computation of Solutions to Combinatorial Problems. *Science* **1994**, *266* (5187), 1021–1024. https://doi.org/10.1126/science.7973651.
(27) Zadegan, R. M.; Jepsen, M. D. E.; Hildebrandt, L. L.; Birkedal, V.; Kjems, J. Construction of a Fuzzy and Boolean Logic Gates Based on DNA. *Small* **2015**, *11* (15), 1811–1817. https://doi.org/10.1002/smll.201402755.
(28) Pei, H.; Liang, L.; Yao, G.; Li, J.; Huang, Q.; Fan, C. Reconfigurable Three-Dimensional DNA Nanostructures for the Construction of Intracellular Logic Sensors. *Angewandte Chemie International Edition* **2012**, *51* (36), 9020–9024. https://doi.org/10.1002/anie.201202356.
(29) Guz, N.; Fedotova, T. A.; Fratto, B. E.; Schlesinger, O.; Alfonta, L.; Kolpashchikov, D. M.; Katz, E. Bioelectronic Interface Connecting Reversible Logic Gates Based on Enzyme and DNA Reactions. *ChemPhysChem* **2016**, *17* (14), 2247–2255. https://doi.org/10.1002/cphc.201600129.
(30) Sarker, A.; Ahmed, T.; Rashid, S. M. M.; Anwar, S.; Jaman, L.; Tara, N.; Alam, Md. M.; Babu, H. Md. H. Realization of Reversible Logic in DNA Computing. In *2011 IEEE 11th International Conference on Bioinformatics and Bioengineering*; 2011; pp 261–265. https://doi.org/10.1109/BIBE.2011.46.
(31) Orbach, R.; Remacle, F.; Levine, R. D.; Willner, I. Logic Reversibility and Thermodynamic Irreversibility Demonstrated by DNAzyme-Based Toffoli and Fredkin Logic Gates. *Proceedings of the National Academy of Sciences* **2012**, *109* (52), 21228–21233. https://doi.org/10.1073/pnas.1219672110.
(32) Yang, C.-N.; Hsu, C.-Y.; Chuang, Y.-C. Molecular Beacon-Based Half-Adder and Half-Subtractor. *Chem. Commun.* **2012**, *48* (1), 112–114. https://doi.org/10.1039/C1CC14518E.

(33) Wu, G.; Seeman, N. C. Multiplying with DNA. *Nat Comput* **2006**, *5* (4), 427–441. https://doi.org/10.1007/s11047-006-9006-8.
(34) Wang, F.; Lv, H.; Li, Q.; Li, J.; Zhang, X.; Shi, J.; Wang, L.; Fan, C. Implementing Digital Computing with DNA-Based Switching Circuits. *Nat Commun* **2020**, *11* (1), 121. https://doi.org/10.1038/s41467-019-13980-y.
(35) Kieffer, C.; Genot, A. J.; Rondelez, Y.; Gines, G. Molecular Computation for Molecular Classification. *Advanced Biology* **2023**, *n/a* (n/a), 2200203. https://doi.org/10.1002/adbi.202200203.
(36) Liu, J.; Liu, S.; Zou, C.; Xu, S.; Zhou, C. Research Progress in Construction and Application of Enzyme-Based DNA Logic Gates. *IEEE Transactions on NanoBioscience* **2023**, *22* (2), 245–258. https://doi.org/10.1109/TNB.2022.3181615.
(37) Stojanovic, M. N.; Stefanovic, D.; Rudchenko, S. Exercises in Molecular Computing. *Acc Chem Res* **2014**, *47* (6), 1845–1852. https://doi.org/10.1021/ar5000538.
(38) Zhang, C.; Ge, L.; Zhuang, Y.; Shen, Z.; Zhong, Z.; Zhang, Z.; You, X. DNA Computing for Combinational Logic. *Sci. China Inf. Sci.* **2018**, *62* (6), 61301. https://doi.org/10.1007/s11432-018-9530-x.
(39) Zhang, Z.; Fan, C.; He, L. Development of Nano-Scale DNA Computing Devices. *Current Nanoscience* **2005**, *1* (1), 89–93. https://doi.org/10.2174/1573413052953138.
(40) Fan, D.; Wang, J.; Wang, E.; Dong, S. Propelling DNA Computing with Materials' Power: Recent Advancements in Innovative DNA Logic Computing Systems and Smart Bio-Applications. *Advanced Science* **2020**, *7* (24), 2001766. https://doi.org/10.1002/advs.202001766.
(41) Polak, R. E.; Keung, A. J. A Molecular Assessment of the Practical Potential of DNA-Based Computation. *Current Opinion in Biotechnology* **2023**, *81*, 102940. https://doi.org/10.1016/j.copbio.2023.102940.
(42) Radamson, H. H.; He, X.; Zhang, Q.; Liu, J.; Cui, H.; Xiang, J.; Kong, Z.; Xiong, W.; Li, J.; Gao, J.; Yang, H.; Gu, S.; Zhao, X.; Du, Y.; Yu, J.; Wang, G. Miniaturization of CMOS. *Micromachines* **2019**, *10* (5), 293. https://doi.org/10.3390/mi10050293.
(43) Ye, S.; Liu, L.; Ma, Y.; Wang, Y. Stacked Lateral Gate-All-Around Metal–Oxide–Semiconductor Field-Effect Transistors and Their Three-Dimensional Integrated Circuits. *Silicon* **2023**, *15* (5), 2467–2478. https://doi.org/10.1007/s12633-022-02190-9.
(44) Vidhya, N.; Seethalakshmi, V.; Suganyadevi, S. Non-Silicon Computing with Quantum Superposition Entanglement Using Qubits. In *Quantum Computing: A Shift from Bits to Qubits*; Pandey, R., Srivastava, N., Singh, N. K., Tyagi, K., Eds.; Studies in Computational Intelligence; Springer Nature: Singapore, 2023; pp 131–150. https://doi.org/10.1007/978-981-19-9530-9_8.
(45) Ruiz, I. M.; Arbona, J.-M.; Lad, A.; Mendoza, O.; Aimé, J.-P.; Elezgaray, J. Connecting Localized DNA Strand Displacement Reactions. *Nanoscale* **2015**, *7* (30), 12970–12978. https://doi.org/10.1039/C5NR02434J.
(46) Mendoza, O.; Mergny, J.-L.; Aimé, J.-P.; Elezgaray, J. G-Quadruplexes Light up Localized DNA Circuits. *Nano Lett.* **2016**, *16* (1), 624–628. https://doi.org/10.1021/acs.nanolett.5b04354.
(47) Chatterjee, G.; Dalchau, N.; Muscat, R. A.; Phillips, A.; Seelig, G. A Spatially Localized Architecture for Fast and Modular DNA Computing. *Nature Nanotech* **2017**, *12* (9), 920–927. https://doi.org/10.1038/nnano.2017.127.

(48) Teichmann, M.; Kopperger, E.; Simmel, F. C. Robustness of Localized DNA Strand Displacement Cascades. *ACS Nano* **2014**, *8* (8), 8487–8496. https://doi.org/10.1021/nn503073p.
(49) You, M.; Zhu, G.; Chen, T.; Donovan, M. J.; Tan, W. Programmable and Multiparameter DNA-Based Logic Platform For Cancer Recognition and Targeted Therapy. *J. Am. Chem. Soc.* **2015**, *137* (2), 667–674. https://doi.org/10.1021/ja509263k.
(50) Lv, H.; Xie, N.; Li, M.; Dong, M.; Sun, C.; Zhang, Q.; Zhao, L.; Li, J.; Zuo, X.; Chen, H.; Wang, F.; Fan, C. DNA-Based Programmable Gate Arrays for General-Purpose DNA Computing. *Nature* **2023**, 1–9. https://doi.org/10.1038/s41586-023-06484-9.
(51) Doricchi, A.; Platnich, C. M.; Gimpel, A.; Horn, F.; Earle, M.; Lanzavecchia, G.; Cortajarena, A. L.; Liz-Marzán, L. M.; Liu, N.; Heckel, R.; Grass, R. N.; Krahne, R.; Keyser, U. F.; Garoli, D. Emerging Approaches to DNA Data Storage: Challenges and Prospects. *ACS Nano* **2022**, *16* (11), 17552–17571. https://doi.org/10.1021/acsnano.2c06748.
(52) Mirzayi, S.; Ravan, H.; Soltanian, S. Borderline Boolean States Improve the Biosensing Applications of DNA Circuits. *International Journal of Biological Macromolecules* **2022**, *207*, 1005–1010. https://doi.org/10.1016/j.ijbiomac.2022.03.197.
(53) Zhao, S.; Yu, L.; Yang, S.; Tang, X.; Chang, K.; Chen, M. Boolean Logic Gate Based on DNA Strand Displacement for Biosensing: Current and Emerging Strategies. *Nanoscale Horiz.* **2021**, *6* (4), 298–310. https://doi.org/10.1039/D0NH00587H.
(54) Romieu, A. "AND" Luminescent "Reactive" Molecular Logic Gates: A Gateway to Multi-Analyte Bioimaging and Biosensing. *Org. Biomol. Chem.* **2015**, *13* (5), 1294–1306. https://doi.org/10.1039/C4OB02076F.
(55) Moerman, P. G.; Schulman, R. DNA Computation Improves Diagnostic Workflows. *Nat. Nanotechnol.* **2020**, *15* (8), 626–627. https://doi.org/10.1038/s41565-020-0710-9.
(56) Wang, C.; Zhang, Z.; Qiu, Y.; Bao, Y.; Song, Q.; Zou, B. In Situ Track-Generated DNA Walker for AND-Gate Logic Imaging of Telomerase and Flap Endonuclease 1 Activities in Living Cells. *Anal. Chem.* **2024**, *96* (2), 756–765. https://doi.org/10.1021/acs.analchem.3c03952.
(57) Chen, J.; Fu, S.; Zhang, C.; Liu, H.; Su, X. DNA Logic Circuits for Cancer Theranostics. *Small* **2022**, *18* (20), 2108008. https://doi.org/10.1002/smll.202108008.
(58) Wang, D.; Li, S.; Zhao, Z.; Zhang, X.; Tan, W. Engineering a Second-Order DNA Logic-Gated Nanorobot to Sense and Release on Live Cell Membranes for Multiplexed Diagnosis and Synergistic Therapy. *Angewandte Chemie International Edition* **2021**, *60* (29), 15816–15820. https://doi.org/10.1002/anie.202103993.
(59) Wang, H.; Zheng, J.; Sun, Y.; Li, T. Cellular Environment-Responsive Intelligent DNA Logic Circuits for Controllable Molecular Sensing. *Biosensors and Bioelectronics* **2018**, *117*, 729–735. https://doi.org/10.1016/j.bios.2018.07.006.
(60) Elbaz, J.; Shlyahovsky, B.; Li, D.; Willner, I. Parallel Analysis of Two Analytes in Solutions or on Surfaces by Using a Bifunctional Aptamer: Applications for Biosensing and Logic Gate Operations. *ChemBioChem* **2008**, *9* (2), 232–239. https://doi.org/10.1002/cbic.200700436.
(61) Li, Y.; Deng, J.; Han, Z.; Liu, C.; Tian, F.; Xu, R.; Han, D.; Zhang, S.; Sun, J. Molecular Identification of Tumor-Derived Extracellular Vesicles Using Thermophoresis-Mediated DNA Computation. *J. Am. Chem. Soc.* **2021**, *143* (3), 1290–1295. https://doi.org/10.1021/jacs.0c12016.

(62) Wu, K.; Qi, C.; Zhu, Z.; Wang, C.; Song, B.; Chang, C. Terahertz Wave Accelerates DNA Unwinding: A Molecular Dynamics Simulation Study. *J. Phys. Chem. Lett.* **2020**, *11* (17), 7002–7008. https://doi.org/10.1021/acs.jpclett.0c01850.
(63) Qi, M.; Shi, P.; Zhang, X.; Cui, S.; Liu, Y.; Zhou, S.; Zhang, Q. Reconfigurable DNA Triplex Structure for pH Responsive Logic Gates. *RSC Adv.* **2023**, *13* (15), 9864–9870. https://doi.org/10.1039/D3RA00536D.
(64) Bui, H.; Garg, S.; Miao, V.; Song, T.; Mokhtar, R.; Reif, J. Design and Analysis of Linear Cascade DNA Hybridization Chain Reactions Using DNA Hairpins. *New J. Phys.* **2017**, *19* (1), 015006. https://doi.org/10.1088/1367-2630/aa53d0.
(65) Stojanovic, M. N.; de Prada, P.; Landry, D. W. Catalytic Molecular Beacons. *ChemBioChem* **2001**, *2* (6), 411–415. https://doi.org/10.1002/1439-7633(20010601)2:6<411::AID-CBIC411>3.0.CO;2-I.
(66) Molden, T. A.; Grillo, M. C.; Kolpashchikov, D. M. Manufacturing Reusable NAND Logic Gates and Their Initial Circuits for DNA Nanoprocessors. *Chemistry – A European Journal* **2021**, *27* (7), 2421–2426. https://doi.org/10.1002/chem.202003959.
(67) Ge, L.; Wang, W.; Sun, X.; Hou, T.; Li, F. Versatile and Programmable DNA Logic Gates on Universal and Label-Free Homogeneous Electrochemical Platform. *Anal. Chem.* **2016**, *88* (19), 9691–9698. https://doi.org/10.1021/acs.analchem.6b02584.
(68) Bai, D.; Zhang, J.; Zhang, Y.; Yu, H.; Zhang, L.; Han, X.; Lv, K.; Wang, L.; Luo, W.; Wu, Y.; Zhou, X.; Wang, W.; Feng, T.; Xie, G. A Spatially Controlled Proximity Split Tweezer Switch for Enhanced DNA Circuit Construction and Multifunctional Transduction. *Small n/a* (n/a), 2307421. https://doi.org/10.1002/smll.202307421.
(69) Stojanovic, M. N.; Stefanovic, D. A Deoxyribozyme-Based Molecular Automaton. *Nat Biotechnol* **2003**, *21* (9), 1069–1074. https://doi.org/10.1038/nbt862.
(70) Su, H.; Xu, J.; Wang, Q.; Wang, F.; Zhou, X. High-Efficiency and Integrable DNA Arithmetic and Logic System Based on Strand Displacement Synthesis. *Nat Commun* **2019**, *10* (1), 5390. https://doi.org/10.1038/s41467-019-13310-2.
(71) Qian, L.; Winfree, E. Scaling Up Digital Circuit Computation with DNA Strand Displacement Cascades. *Science* **2011**, *332* (6034), 1196–1201. https://doi.org/10.1126/science.1200520.
(72) Elbaz, J.; Lioubashevski, O.; Wang, F.; Remacle, F.; Levine, R. D.; Willner, I. DNA Computing Circuits Using Libraries of DNAzyme Subunits. *Nature Nanotech* **2010**, *5* (6), 417–422. https://doi.org/10.1038/nnano.2010.88.
(73) Chandran, H.; Gopalkrishnan, N.; Phillips, A.; Reif, J. Localized Hybridization Circuits. In *DNA Computing and Molecular Programming*; Cardelli, L., Shih, W., Eds.; Lecture Notes in Computer Science; Springer Berlin Heidelberg: Berlin, Heidelberg, 2011; Vol. 6937, pp 64–83. https://doi.org/10.1007/978-3-642-23638-9_8.
(74) Lund, K.; Manzo, A. J.; Dabby, N.; Michelotti, N.; Johnson-Buck, A.; Nangreave, J.; Taylor, S.; Pei, R.; Stojanovic, M. N.; Walter, N. G.; Winfree, E.; Yan, H. Molecular Robots Guided by Prescriptive Landscapes. *Nature* **2010**, *465* (7295), 206–210. https://doi.org/10.1038/nature09012.
(75) Bhattacharyya, R. P.; Reményi, A.; Yeh, B. J.; Lim, W. A. Domains, Motifs, and Scaffolds: The Role of Modular Interactions in the Evolution and Wiring of Cell Signaling Circuits. *Annu Rev Biochem* **2006**, *75*, 655–680. https://doi.org/10.1146/annurev.biochem.75.103004.142710.

(76) Scott, J. D.; Pawson, T. Cell Signaling in Space and Time: Where Proteins Come Together and When They're Apart. *Science* **2009**, *326* (5957), 1220–1224. https://doi.org/10.1126/science.1175668.
(77) Kholodenko, B. N. Cell-Signalling Dynamics in Time and Space. *Nat Rev Mol Cell Biol* **2006**, *7* (3), 165–176. https://doi.org/10.1038/nrm1838.
(78) Zhang, Y.; Chen, W.; Fang, Y.; Zhang, X.; Liu, Y.; Ju, H. Activating a DNA Nanomachine via Computation across Cancer Cell Membranes for Precise Therapy of Solid Tumors. *J. Am. Chem. Soc.* **2021**, *143* (37), 15233–15242. https://doi.org/10.1021/jacs.1c06361.
(79) Yasuga, H.; Inoue, K.; Kawano, R.; Takinoue, M.; Osaki, T.; Kamiya, K.; Miki, N.; Takeuchi, S. Serial DNA Relay in DNA Logic Gates by Electrical Fusion and Mechanical Splitting of Droplets. *PLOS ONE* **2017**, *12* (7), e0180876. https://doi.org/10.1371/journal.pone.0180876.
(80) Engelen, W.; Wijnands, S. P. W.; Merkx, M. Accelerating DNA-Based Computing on a Supramolecular Polymer. *J. Am. Chem. Soc.* **2018**, *140* (30), 9758–9767. https://doi.org/10.1021/jacs.8b06146.
(81) Piranej, S.; Bazrafshan, A.; Salaita, K. Chemical-to-Mechanical Molecular Computation Using DNA-Based Motors with Onboard Logic. *Nat. Nanotechnol.* **2022**, *17* (5), 514–523. https://doi.org/10.1038/s41565-022-01080-w.
(82) Seeman, N. C. Biochemistry and Structural DNA Nanotechnology: An Evolving Symbiotic Relationship. *Biochemistry* **2003**, *42* (24), 7259–7269. https://doi.org/10.1021/bi030079v.
(83) Seeman, N. C. DNA in a Material World. *Nature* **2003**, *421* (6921), 427–431. https://doi.org/10.1038/nature01406.
(84) Muscat, R. A.; Strauss, K.; Ceze, L.; Seelig, G. DNA-Based Molecular Architecture with Spatially Localized Components. **2013**.
(85) Dalchau, N.; Chandran, H.; Gopalkrishnan, N.; Phillips, A.; Reif, J. Probabilistic Analysis of Localized DNA Hybridization Circuits. *ACS Synth. Biol.* **2015**, *4* (8), 898–913. https://doi.org/10.1021/acssynbio.5b00044.
(86) Walsh, A. S.; Yin, H.; Erben, C. M.; Wood, M. J. A.; Turberfield, A. J. DNA Cage Delivery to Mammalian Cells. *ACS Nano* **2011**, *5* (7), 5427–5432. https://doi.org/10.1021/nn2005574.
(87) Zhang, T.; Tian, T.; Zhou, R.; Li, S.; Ma, W.; Zhang, Y.; Liu, N.; Shi, S.; Li, Q.; Xie, X.; Ge, Y.; Liu, M.; Zhang, Q.; Lin, S.; Cai, X.; Lin, Y. Design, Fabrication and Applications of Tetrahedral DNA Nanostructure-Based Multifunctional Complexes in Drug Delivery and Biomedical Treatment. *Nat Protoc* **2020**, *15* (8), 2728–2757. https://doi.org/10.1038/s41596-020-0355-z.
(88) Rothemund, P. W. K. Folding DNA to Create Nanoscale Shapes and Patterns. *Nature* **2006**, *440* (7082), 297–302. https://doi.org/10.1038/nature04586.
(89) Zhan, P.; Peil, A.; Jiang, Q.; Wang, D.; Mousavi, S.; Xiong, Q.; Shen, Q.; Shang, Y.; Ding, B.; Lin, C.; Ke, Y.; Liu, N. Recent Advances in DNA Origami-Engineered Nanomaterials and Applications. *Chem. Rev.* **2023**, *123* (7), 3976–4050. https://doi.org/10.1021/acs.chemrev.3c00028.
(90) Hong, F.; Zhang, F.; Liu, Y.; Yan, H. DNA Origami: Scaffolds for Creating Higher Order Structures. *Chem. Rev.* **2017**, *117* (20), 12584–12640. https://doi.org/10.1021/acs.chemrev.6b00825.
(91) Rajendran, A.; Endo, M.; Katsuda, Y.; Hidaka, K.; Sugiyama, H. Programmed Two-Dimensional Self-Assembly of Multiple DNA Origami Jigsaw Pieces. *ACS Nano* **2011**, *5* (1), 665–671. https://doi.org/10.1021/nn1031627.

(92) Ke, Y.; Douglas, S. M.; Liu, M.; Sharma, J.; Cheng, A.; Leung, A.; Liu, Y.; Shih, W. M.; Yan, H. Multilayer DNA Origami Packed on a Square Lattice. *J. Am. Chem. Soc.* **2009**, *131* (43), 15903–15908. https://doi.org/10.1021/ja906381y.
(93) Woo, S.; Rothemund, P. W. K. Programmable Molecular Recognition Based on the Geometry of DNA Nanostructures. *Nature Chem* **2011**, *3* (8), 620–627. https://doi.org/10.1038/nchem.1070.
(94) Gerasimova, Y. V.; Kolpashchikov, D. M. Towards a DNA Nanoprocessor: Reusable Tile-Integrated DNA Circuits. *Angewandte Chemie International Edition* **2016**, *55* (35), 10244–10247. https://doi.org/10.1002/anie.201603265.
(95) Song, L.; Xiao, M.; Lai, W.; Li, L.; Wan, Y.; Pei, H. Intracellular Logic Computation with Framework Nucleic Acid-Based Circuits for mRNA Imaging†. *Chinese Journal of Chemistry* **2021**, *39* (4), 947–953. https://doi.org/10.1002/cjoc.202000575.
(96) Yang, S.; Luo, J.; Zhang, L.; Feng, L.; He, Y.; Gao, X.; Xie, S.; Gao, M.; Luo, D.; Chang, K.; Chen, M. A Smart Nano-Theranostic Platform Based on Dual-microRNAs Guided Self-Feedback Tetrahedral Entropy-Driven DNA Circuit. *Adv Sci (Weinh)* **2023**, *10* (19), e2301814. https://doi.org/10.1002/advs.202301814.
(97) Goodman, R. P.; Schaap, I. A. T.; Tardin, C. F.; Erben, C. M.; Berry, R. M.; Schmidt, C. F.; Turberfield, A. J. Rapid Chiral Assembly of Rigid DNA Building Blocks for Molecular Nanofabrication. *Science* **2005**, *310* (5754), 1661–1665. https://doi.org/10.1126/science.1120367.
(98) Tian, C.; Li, X.; Liu, Z.; Jiang, W.; Wang, G.; Mao, C. Directed Self-Assembly of DNA Tiles into Complex Nanocages. *Angewandte Chemie International Edition* **2014**, *53* (31), 8041–8044. https://doi.org/10.1002/anie.201400377.
(99) Mo, D.; Lakin, M. R.; Stefanovic, D. Logic Circuits Based on Molecular Spider Systems. *Biosystems* **2016**, *146*, 10–25. https://doi.org/10.1016/j.biosystems.2016.03.008.
(100) Wang, H.; Peng, P.; Wang, Q.; Du, Y.; Tian, Z.; Li, T. Environment-Recognizing DNA-Computation Circuits for the Intracellular Transport of Molecular Payloads for mRNA Imaging. *Angew Chem Int Ed Engl* **2020**, *59* (15), 6099–6107. https://doi.org/10.1002/anie.201916432.
(101) Zhu, D.; Huang, J.; Xia, Y.; Su, S.; Zuo, X.; Li, Q.; Wang, L. DNAzymes-Embedded Framework Nucleic Acids (FNAzymes) for Metal Ions Imaging in Living Cells. *Chemosensors* **2023**, *11* (7), 358. https://doi.org/10.3390/chemosensors11070358.
(102) Du, Y.; Peng, P.; Li, T. DNA Logic Operations in Living Cells Utilizing Lysosome-Recognizing Framework Nucleic Acid Nanodevices for Subcellular Imaging. *ACS Nano* **2019**, *13* (5), 5778–5784. https://doi.org/10.1021/acsnano.9b01324.
(103) Groves, B.; Chen, Y.-J.; Zurla, C.; Pochekailov, S.; Kirschman, J. L.; Santangelo, P. J.; Seelig, G. Computing in Mammalian Cells with Nucleic Acid Strand Exchange. *Nature Nanotech* **2016**, *11* (3), 287–294. https://doi.org/10.1038/nnano.2015.278.
(104) Peng, R.; Zheng, X.; Lyu, Y.; Xu, L.; Zhang, X.; Ke, G.; Liu, Q.; You, C.; Huan, S.; Tan, W. Engineering a 3D DNA-Logic Gate Nanomachine for Bispecific Recognition and Computing on Target Cell Surfaces. *J. Am. Chem. Soc.* **2018**, *140* (31), 9793–9796. https://doi.org/10.1021/jacs.8b04319.
(105) Zhou, Z.; Lin, N.; Ouyang, Y.; Liu, S.; Zhang, Y.; Willner, I. Cascaded, Feedback-Driven, and Spatially Localized Emergence of Constitutional Dynamic Networks Driven by Enzyme-

Free Catalytic DNA Circuits. *J. Am. Chem. Soc.* **2023**, *145* (23), 12617–12629. https://doi.org/10.1021/jacs.3c02083.
(106) Amir, Y.; Ben-Ishay, E.; Levner, D.; Ittah, S.; Abu-Horowitz, A.; Bachelet, I. Universal Computing by DNA Origami Robots in a Living Animal. *Nature Nanotech* **2014**, *9* (5), 353–357. https://doi.org/10.1038/nnano.2014.58.
(107) Weizenmann, N.; Scheidgen-Kleyboldt, G.; Ye, J.; Krause, C. B.; Kauert, D.; Helmi, S.; Rouillon, C.; Seidel, R. Chemical Ligation of an Entire DNA Origami Nanostructure. *Nanoscale* **2021**, *13* (41), 17556–17565. https://doi.org/10.1039/D1NR04225D.
(108) *Sequence-programmable covalent bonding of designed DNA assemblies | Science Advances*. https://www.science.org/doi/10.1126/sciadv.aau1157 (accessed 2024-02-04).
(109) Gerasimova, Y. V.; Kolpashchikov, D. M. Connectable DNA Logic Gates: OR and XOR Logics. *Chemistry – An Asian Journal* **2012**, *7* (3), 534–540. https://doi.org/10.1002/asia.201100664.
(110) Lake, A.; Shang, S.; Kolpashchikov, D. M. Molecular Logic Gates Connected through DNA Four-Way Junctions. *Angewandte Chemie International Edition* **2010**, *49* (26), 4459–4462. https://doi.org/10.1002/anie.200907135.
(111)Tyagi, S.; Kramer, F. R. Molecular Beacons: Probes That Fluoresce upon Hybridization. *Nat Biotechnol* **1996**, *14* (3), 303–308. https://doi.org/10.1038/nbt0396-303.
(112) Ortiz-Lombardía, M.; González, A.; Eritja, R.; Aymamí, J.; Azorín, F.; Coll, M. Crystal Structure of a DNA Holliday Junction. *Nat Struct Mol Biol* **1999**, *6* (10), 913–917. https://doi.org/10.1038/13277.
(113) Wyatt, H. D. M.; West, S. C. Holliday Junction Resolvases. *Cold Spring Harb Perspect Biol* **2014**, *6* (9), a023192. https://doi.org/10.1101/cshperspect.a023192.
(114) Bardales, A. C.; Vo, Q.; Kolpashchikov, D. M. Singleton {NOT} and Doubleton {YES; NOT} Gates Act as Functionally Complete Sets in DNA-Integrated Computational Circuits. *Nanomaterials* **2024**, *14* (7), 600. https://doi.org/10.3390/nano14070600.
(115) Stancescu, M.; Fedotova, T. A.; Hooyberghs, J.; Balaeff, A.; Kolpashchikov, D. M. Nonequilibrium Hybridization Enables Discrimination of a Point Mutation within 5–40 °C. *J. Am. Chem. Soc.* **2016**, *138* (41), 13465–13468. https://doi.org/10.1021/jacs.6b05628.
(116) Frezza, B. M.; Cockroft, S. L.; Ghadiri, M. R. Modular Multi-Level Circuits from Immobilized DNA-Based Logic Gates. *J. Am. Chem. Soc.* **2007**, *129* (48), 14875–14879. https://doi.org/10.1021/ja0710149.
(117) Whitehead, A. N.; Russel, B. *Principia Mathematica*, 2nd ed.; The Syndics of the Cambridge University Press, 1963; Vol. 1.
(118) Borghetti, J.; Snider, G. S.; Kuekes, P. J.; Yang, J. J.; Stewart, D. R.; Williams, R. S. 'Memristive' Switches Enable 'Stateful' Logic Operations via Material Implication. *Nature* **2010**, *464* (7290), 873–876. https://doi.org/10.1038/nature08940.
(119) Prezioso, M.; Riminucci, A.; Graziosi, P.; Bergenti, I.; Rakshit, R.; Cecchini, R.; Vianelli, A.; Borgatti, F.; Haag, N.; Willis, M.; Drew, A. J.; Gillin, W. P.; Dediu, V. A. A Single-Device Universal Logic Gate Based on a Magnetically Enhanced Memristor. *Advanced Materials* **2013**, *25* (4), 534–538. https://doi.org/10.1002/adma.201202031.
(120) *BIO2010: Transforming Undergraduate Education for Future Research Biologists*; National Academies Press: Washington, D.C., 2003. https://doi.org/10.17226/10497.

(121) Woodin, T.; Carter, V. C.; Fletcher, L. Vision and Change in Biology Undergraduate Education, A Call for Action—Initial Responses. *LSE* **2010**, *9* (2), 71–73. https://doi.org/10.1187/cbe.10-03-0044.
(122) Zemke, J. M.; Franz, J. A Biphasic Ligand Exchange Reaction on CdSe Nanoparticles: Introducing Undergraduates to Functionalizing Nanoparticles for Solar Cells. *J. Chem. Educ.* **2016**, *93* (4), 747–752. https://doi.org/10.1021/acs.jchemed.5b00847.
(123) Flynn-Charlebois, A.; Burns, J.; Chapelliquen, S.; Sanmartino, H. An Undergraduate Investigation into the 10-23 DNA Enzyme That Cleaves RNA: DNA Can Cut It in the Biochemistry Laboratory. *J. Chem. Educ.* **2011**, *88* (2), 226–228. https://doi.org/10.1021/ed100607k.
(124) Chandrasekaran, A. R. DNA Nanotechnology in the Undergraduate Laboratory: Electrophoretic Analysis of DNA Nanostructure Biostability. *J. Chem. Educ.* **2023**, *100* (1), 316–320. https://doi.org/10.1021/acs.jchemed.2c00656.
(125) Jones, D. R.; DiScenza, D. J.; Mako, T. L.; Levine, M. Environmental Application of Cyclodextrin Metal–Organic Frameworks in an Undergraduate Teaching Laboratory. *J. Chem. Educ.* **2018**, *95* (9), 1636–1641. https://doi.org/10.1021/acs.jchemed.8b00357.
(126) Rowe, L. Ethics and Systems Thinking in Biochemistry: A CRISPR-Based Activity for Undergraduate Students. *J. Chem. Educ.* **2020**, *97* (7), 1944–1950. https://doi.org/10.1021/acs.jchemed.0c00095.
(127) White, H. B.; Benore, M. A.; Sumter, T. F.; Caldwell, B. D.; Bell, E. What Skills Should Students of Undergraduate Biochemistry and Molecular Biology Programs Have upon Graduation? *Biochemistry and Molecular Biology Education* **2013**, *41* (5), 297–301. https://doi.org/10.1002/bmb.20729.
(128) Fung, F. M.; Watts, S. F. Bridges to the Future: Toward Future Ready Graduates in Chemistry Laboratories. *J. Chem. Educ.* **2019**, *96* (8), 1620–1629. https://doi.org/10.1021/acs.jchemed.8b00771.
(129) Llovet, J. M.; Kelley, R. K.; Villanueva, A.; Singal, A. G.; Pikarsky, E.; Roayaie, S.; Lencioni, R.; Koike, K.; Zucman-Rossi, J.; Finn, R. S. Hepatocellular Carcinoma. *Nat Rev Dis Primers* **2021**, *7* (1), 1–28. https://doi.org/10.1038/s41572-020-00240-3.
(130) Macaulay, J. O.; Van Damme, M.-P.; Walker, K. Z. The Use of Contextual Learning to Teach Biochemistry to Dietetic Students. *Biochemistry and Molecular Biology Education* **2009**, *37* (3), 137–142. https://doi.org/10.1002/bmb.20283.
(131) Rybarczyk, B. J.; Baines, A. T.; McVey, M.; Thompson, J. T.; Wilkins, H. A Case-Based Approach Increases Student Learning Outcomes and Comprehension of Cellular Respiration Concepts. *Biochemistry and Molecular Biology Education* **2007**, *35* (3), 181–186. https://doi.org/10.1002/bmb.40.
(132) Testa, S. M.; Selegue, J. P.; French, A.; Criswell, B. Permanganate Oxidation of DNA Nucleotides: An Introductory Redox Laboratory Framed as a Murder Mystery. *J. Chem. Educ.* **2018**, *95* (10), 1840–1847. https://doi.org/10.1021/acs.jchemed.8b00079.
(133) Ying, S.-Y.; Chang, D. C.; Lin, S.-L. The MicroRNA (miRNA): Overview of the RNA Genes That Modulate Gene Function. *Mol Biotechnol* **2008**, *38* (3), 257–268. https://doi.org/10.1007/s12033-007-9013-8.
(134) Russo, F.; Scoyni, F.; Fatica, A.; Pellegrini, M.; Ferro, A.; Pulvirenti, A.; Giugno, R. Chapter 12 - Circulating Noncoding RNAs as Clinical Biomarkers. In *Epigenetic Biomarkers*

and Diagnostics; García-Giménez, J. L., Ed.; Academic Press: Boston, 2016; pp 239–258. https://doi.org/10.1016/B978-0-12-801899-6.00012-7.
(135) Ghafouri-Fard, S.; Honarmand Tamizkar, K.; Hussen, B. M.; Taheri, M. MicroRNA Signature in Liver Cancer. *Pathology - Research and Practice* **2021**, *219*, 153369. https://doi.org/10.1016/j.prp.2021.153369.
(136) Cui, M.; Wang, H.; Yao, X.; Zhang, D.; Xie, Y.; Cui, R.; Zhang, X. Circulating MicroRNAs in Cancer: Potential and Challenge. *Frontiers in Genetics* **2019**, *10*.
(137) Connelly, R. P.; Morozkin, E. S.; Gerasimova, Y. V. Alphanumerical Visual Display Made of DNA Logic Gates for Drug Susceptibility Testing of Pathogens. *ChemBioChem* **2018**, *19* (3), 203–206. https://doi.org/10.1002/cbic.201700626.
(138) Benenson, Y.; Gil, B.; Ben-Dor, U.; Adar, R.; Shapiro, E. An Autonomous Molecular Computer for Logical Control of Gene Expression. *Nature* **2004**, *429* (6990), 423–429. https://doi.org/10.1038/nature02551.
(139) Wang, D.; Fu, Y.; Yan, J.; Zhao, B.; Dai, B.; Chao, J.; Liu, H.; He, D.; Zhang, Y.; Fan, C.; Song, S. Molecular Logic Gates on DNA Origami Nanostructures for MicroRNA Diagnostics. *Anal. Chem.* **2014**, *86* (4), 1932–1936. https://doi.org/10.1021/ac403661z.
(140) Song, X.; Reif, J. Nucleic Acid Databases and Molecular-Scale Computing. *ACS Nano* **2019**, *13* (6), 6256–6268. https://doi.org/10.1021/acsnano.9b02562.
(141) Wetmur, J. G.; Davidson, N. Kinetics of Renaturation of DNA. *Journal of Molecular Biology* **1968**, *31* (3), 349–370. https://doi.org/10.1016/0022-2836(68)90414-2.
(142) Craig, M. E.; Crothers, D. M.; Doty, P. Relaxation Kinetics of Dimer Formation by Self Complementary Oligonucleotides. *Journal of Molecular Biology* **1971**, *62* (2), 383–401. https://doi.org/10.1016/0022-2836(71)90434-7.
(143) Pörschke, D.; Eigen, M. Co-Operative Non-Enzymatic Base Recognition III. Kinetics of the Helix—Coil Transition of the Oligoribouridylic · Oligoriboadenylic Acid System and of Oligoriboadenylic Acid Alone at Acidic pH. *Journal of Molecular Biology* **1971**, *62* (2), 361–381. https://doi.org/10.1016/0022-2836(71)90433-5.
(144) Wetmur, J. G. HYBRIDIZATION AND RENATURATION KINETICS OF NUCLEIC ACIDS. *Annu. Rev. Biophys. Bioeng.* **1976**, *5* (1), 337–361. https://doi.org/10.1146/annurev.bb.05.060176.002005.
(145) Markegard, C. B.; Gallivan, C. P.; Cheng, D. D.; Nguyen, H. D. Effects of Concentration and Temperature on DNA Hybridization by Two Closely Related Sequences via Large-Scale Coarse-Grained Simulations. *J. Phys. Chem. B* **2016**, *120* (32), 7795–7806. https://doi.org/10.1021/acs.jpcb.6b03937.
(146) Marras, S. A. E. Selection of Fluorophore and Quencher Pairs for Fluorescent Nucleic Acid Hybridization Probes. In *Fluorescent Energy Transfer Nucleic Acid Probes: Designs and Protocols*; Didenko, V. V., Ed.; Methods in Molecular Biology™; Humana Press: Totowa, NJ, 2006; pp 3–16. https://doi.org/10.1385/1-59745-069-3:3.
(147) M. Farzan, V.; L. Markelov, M.; Yu. Skoblov, A.; A. Shipulin, G.; S. Zatsepin, T. Specificity of SNP Detection with Molecular Beacons Is Improved by Stem and Loop Separation with Spacers. *Analyst* **2017**, *142* (6), 945–950. https://doi.org/10.1039/C6AN02441F.
(148) Kolpashchikov, D. M. An Elegant Biosensor Molecular Beacon Probe: Challenges and Recent Solutions. *Scientifica* **2012**, *2012* (1), 928783. https://doi.org/10.6064/2012/928783.

(149) Gerasimova, Y. V.; Kolpashchikov, D. M. Detection of Bacterial 16S rRNA Using a Molecular Beacon-Based X Sensor. *Biosensors and Bioelectronics* **2013**, *41*, 386–390. https://doi.org/10.1016/j.bios.2012.08.058.
(150) Voet, D.; Voet, J. G.; Pratt, C. W. *Fundamentals of Biochemistry: Life at the Molecular Level*; John Wiley & Sons, 2016.
(151) Kanan, M. W.; Rozenman, M. M.; Sakurai, K.; Snyder, T. M.; Liu, D. R. Reaction Discovery Enabled by DNA-Templated Synthesis and in Vitro Selection. *Nature* **2004**, *431* (7008), 545–549. https://doi.org/10.1038/nature02920.
(152) Ma, Z.; Taylor, J.-S. Nucleic Acid-Triggered Catalytic Drug Release. *Proceedings of the National Academy of Sciences* **2000**, *97* (21), 11159–11163. https://doi.org/10.1073/pnas.97.21.11159.
(153) Houska, R.; Stutz, M. B.; Seitz, O. Expanding the Scope of Native Chemical Ligation – Templated Small Molecule Drug Synthesis via Benzanilide Formation. *Chem. Sci.* **2021**, *12* (40), 13450–13457. https://doi.org/10.1039/D1SC00513H.
(154) Kolpashchikov, D. M. Binary Probes for Nucleic Acid Analysis. *Chem. Rev.* **2010**, *110* (8), 4709–4723. https://doi.org/10.1021/cr900323b.
(155) O'Reilly, R. K.; Turberfield, A. J.; Wilks, T. R. The Evolution of DNA-Templated Synthesis as a Tool for Materials Discovery. *Acc. Chem. Res.* **2017**, *50* (10), 2496–2509. https://doi.org/10.1021/acs.accounts.7b00280.
(156) Seeman, N. C.; Kallenbach, N. R. Design of Immobile Nucleic Acid Junctions. *Biophysical Journal* **1983**, *44* (2), 201–209. https://doi.org/10.1016/S0006-3495(83)84292-1.
(157) Zhang, X.; Yan, H.; Shen, Z.; Seeman, N. C. Paranemic Cohesion of Topologically-Closed DNA Molecules. *J. Am. Chem. Soc.* **2002**, *124* (44), 12940–12941. https://doi.org/10.1021/ja026973b.
(158) Liu, D.; Wang, M.; Deng, Z.; Walulu, R.; Mao, C. Tensegrity: Construction of Rigid DNA Triangles with Flexible Four-Arm DNA Junctions. *J. Am. Chem. Soc.* **2004**, *126* (8), 2324–2325. https://doi.org/10.1021/ja031754r.
(159) Jones, M. R.; Seeman, N. C.; Mirkin, C. A. Programmable Materials and the Nature of the DNA Bond. *Science* **2015**, *347* (6224), 1260901. https://doi.org/10.1126/science.1260901.
(160) Bardales, A. C.; Mills, J. R.; Kolpashchikov, D. M. DNA Nanostructures as Catalysts: Double Crossover Tile-Assisted 5′ to 5′ and 3′ to 3′ Chemical Ligation of Oligonucleotides. *Bioconjugate Chem.* **2024**, *35* (1), 28–33. https://doi.org/10.1021/acs.bioconjchem.3c00502.
(161) Fu, T. J.; Seeman, N. C. DNA Double-Crossover Molecules. *Biochemistry* **1993**, *32* (13), 3211–3220. https://doi.org/10.1021/bi00064a003.
(162) Rajendran, A.; Endo, M.; Katsuda, Y.; Hidaka, K.; Sugiyama, H. Photo-Cross-Linking-Assisted Thermal Stability of DNA Origami Structures and Its Application for Higher-Temperature Self-Assembly. *J. Am. Chem. Soc.* **2011**, *133* (37), 14488–14491. https://doi.org/10.1021/ja204546h.
(163) Gerling, T.; Kube, M.; Kick, B.; Dietz, H. Sequence-Programmable Covalent Bonding of Designed DNA Assemblies. *Sci Adv* **2018**, *4* (8), eaau1157. https://doi.org/10.1126/sciadv.aau1157.
(164) Kanaya, E.; Yanagawa, H. Template-Directed Polymerization of Oligoadenylates Using Cyanogen Bromide. *Biochemistry* **1986**, *25* (23), 7423–7430. https://doi.org/10.1021/bi00371a026.

(165) Okita, H.; Kondo, S.; Murayama, K.; Asanuma, H. Rapid Chemical Ligation of DNA and Acyclic Threoninol Nucleic Acid (aTNA) for Effective Nonenzymatic Primer Extension. *J. Am. Chem. Soc.* **2023**, *145* (32), 17872–17880. https://doi.org/10.1021/jacs.3c04979.
(166) Ferris, J. P.; Huang, C.-H.; Hagan, W. J. N-Cyanoimidazole and Diimidazole Imine: Water-Soluble Condensing Agents for the Formation of the Phosphodiester Bond. *Nucleosides and Nucleotides* **1989**, *8* (3), 407–414. https://doi.org/10.1080/07328318908054184.
(167) Chen, H.; Du, F.; Chen, G.; Streckenbach, F.; Yasmeen, A.; Zhao, Y.; Tang, Z. Template-Directed Chemical Ligation to Obtain 3′-3′ and 5′-5′ Phosphodiester DNA Linkages. *Sci Rep* **2014**, *4* (1), 4595. https://doi.org/10.1038/srep04595.
(168) Yi, R.; Hongo, Y.; Fahrenbach, A. C. Synthesis of Imidazole-Activated Ribonucleotides Using Cyanogen Chloride. *Chem. Commun.* **2018**, *54* (5), 511–514. https://doi.org/10.1039/C7CC08489G.
(169) Weizenmann, N.; Scheidgen-Kleyboldt, G.; Ye, J.; Krause, C. B.; Kauert, D.; Helmi, S.; Rouillon, C.; Seidel, R. Chemical Ligation of an Entire DNA Origami Nanostructure. *Nanoscale* **2021**, *13* (41), 17556–17565. https://doi.org/10.1039/D1NR04225D.
(170) Kandimalla, E. R.; Agrawal, S. Hoogsteen DNA Duplexes of 3‘−3‘- and 5‘−5‘-Linked Oligonucleotides and Triplex Formation with RNA and DNA Pyrimidine Single Strands: Experimental and Molecular Modeling Studies. *Biochemistry* **1996**, *35* (48), 15332–15339. https://doi.org/10.1021/bi961505y.
(171) Zhou, T.; Chen, G.; Wang, Y.; Zhang, Q.; Yang, M.; Li, T. Synthesis of Unimolecularly Circular G-Quadruplexes as Prospective Molecular Probes. *Nucleic Acids Research* **2004**, *32* (21), e173. https://doi.org/10.1093/nar/gnh162.
(172) Kandimalla, E. R.; Agrawal, S. ‘Cyclicons’ as Hybridization-Based Fluorescent Primer-Probes: Synthesis, Properties and Application in Real-Time PCR. *Bioorganic & Medicinal Chemistry* **2000**, *8* (8), 1911–1916. https://doi.org/10.1016/S0968-0896(00)00136-X.
(173) Cao, Y.; Ding, P.; Yang, L.; Li, W.; Luo, Y.; Wang, J.; Pei, R. Investigation and Improvement of Catalytic Activity of G-Quadruplex/Hemin DNAzymes Using Designed Terminal G-Tetrads with Deoxyadenosine Caps. *Chem. Sci.* **2020**, *11* (26), 6896–6906. https://doi.org/10.1039/D0SC01905D.
(174) Zagorski, K.; Stormberg, T.; Hashemi, M.; Kolomeisky, A. B.; Lyubchenko, Y. L. Nanorings to Probe Mechanical Stress of Single-Stranded DNA Mediated by the DNA Duplex. *International Journal of Molecular Sciences* **2022**, *23* (21), 12916. https://doi.org/10.3390/ijms232112916.
(175) Winfree, E.; Liu, F.; Wenzler, L. A.; Seeman, N. C. Design and Self-Assembly of Two-Dimensional DNA Crystals. *Nature* **1998**, *394* (6693), 539–544. https://doi.org/10.1038/28998.
(176) Rothemund, P. W. K.; Papadakis, N.; Winfree, E. Algorithmic Self-Assembly of DNA Sierpinski Triangles. *PLOS Biology* **2004**, *2* (12), e424. https://doi.org/10.1371/journal.pbio.0020424.
(177) Yan, H.; LaBean, T. H.; Feng, L.; Reif, J. H. Directed Nucleation Assembly of DNA Tile Complexes for Barcode-Patterned Lattices. *Proceedings of the National Academy of Sciences* **2003**, *100* (14), 8103–8108. https://doi.org/10.1073/pnas.1032954100.
(178) Gu, H.; Yang, W.; Seeman, N. C. DNA Scissors Device Used to Measure MutS Binding to DNA Mis-Pairs. *J. Am. Chem. Soc.* **2010**, *132* (12), 4352–4357. https://doi.org/10.1021/ja910188p.

(179) Naskar, S.; Joshi, H.; Chakraborty, B.; Seeman, N. C.; Maiti, P. K. Atomic Structures of RNA Nanotubes and Their Comparison with DNA Nanotubes. *Nanoscale* **2019**, *11* (31), 14863–14878. https://doi.org/10.1039/C9NR00786E.
(180) Abe, H.; Kool, E. T. Destabilizing Universal Linkers for Signal Amplification in Self-Ligating Probes for RNA. *J. Am. Chem. Soc.* **2004**, *126* (43), 13980–13986. https://doi.org/10.1021/ja046791c.
(181) Kadrmas, J. L.; Ravin, A. J.; Leontis, N. B. Relative Stabilities of DNA Three-Way, Four-Way and Five-Way Junctions (Multi-Helix Junction Loops): Unpaired Nucleotides Can Be Stabilizing or Destabilizing. *Nucleic Acids Research* **1995**, *23* (12), 2212–2222. https://doi.org/10.1093/nar/23.12.2212.
(182) Wang, X.; Seeman, N. C. Assembly and Characterization of 8-Arm and 12-Arm DNA Branched Junctions. *J. Am. Chem. Soc.* **2007**, *129* (26), 8169–8176. https://doi.org/10.1021/ja0693441.